DISCOVERY AND CHARACTERIZATION OF NOVEL REGULATORS OF

MITOCHONDRIAL COPPER HOMEOSTASIS

A Dissertation

by

NATALIE MICHELLE GARZA

Submitted to the Graduate and Professional School of
Texas A&M University
in partial fulfillment of the requirements for the degree of

DOCTOR OF PHILOSOPHY

Chair of Committee,	Vishal M. Gohil
Committee Members,	Lanying Zeng
	Mary Bryk
	Paul A. Lindahl
Head of Department,	Joshua A. Wand

December 2021

Major Subject: Biochemistry

ABSTRACT

Copper is an essential micronutrient that is used as a cofactor for enzymes involved in diverse cellular processes including mitochondrial respiration and iron transport. However, free copper is highly reactive and deleterious for cellular health. Therefore, conserved chaperones and transporters have evolved to carry out intracellular copper transport. Mutations in these proteins result in fatal human pathologies. Despite the importance of copper in cellular health and human disease, we currently do not know the factor(s) required for copper transport to mitochondria. Here, I utilized yeast genetics, biochemistry, and pharmacology to characterize genes and small molecules that impact copper transport to mitochondria.

First, to identify novel genetic regulators of copper trafficking to mitochondria, I performed a genome-wide copper-sensitized screen using *Saccharomyces cerevisiae* deletion mutants. This screen identified many genes required for vacuolar biogenesis as putative regulators of mitochondrial copper homeostasis. Biochemical characterization of these mutants revealed that vacuolar acidity is critical for maintaining the levels of mitochondrial copper. I further show that the activity of cytochrome *c* oxidase (CcO), a mitochondrial cuproenzyme, could be synthetically controlled by altering vacuolar pH or by supplementing media with additional copper. Through this comprehensive genomic study, I identified several novel genetic regulators of mitochondrial copper homeostasis and uncovered a biochemical mechanism that link vacuolar pH to mitochondrial energy metabolism.

Second, I focused my attention on characterizing elesclomol (ES), an investigational anticancer drug, which was recently shown to deliver copper to mitochondrial CcO. Utilizing mass spectrometry and yeast sub-cellular fractionation, I showed that ES treatment leads to a striking increase in cellular and mitochondrial iron levels along with the expected increase in copper levels. I used yeast mutants of iron and copper transport to determine that ES-mediated increase in cellular iron is dependent on Fet3, a component of iron import machinery. Fet3 is a copper-containing oxidase that receives copper in the Golgi compartment. Thus, my work suggests that ES can transport copper to the Golgi lumen as well. Collectively, my work has identified novel regulators of mitochondrial copper levels and provided new insights on the application of ES for the disorders of copper and iron metabolism.

DEDICATION

To my family.

ACKNOWLEDGEMENTS

CONTRIBUTORS AND FUNDING SOURCES

The manuscript describing the work in Chapter III is in preparation for the submission to a journal, for which I am the first author. I performed all experimental work described in this chapter, except for the construction of yeast deletion mutants

NOMENCLATURE

AP-3	Adaptor protein 3 complex
CcO	Cyctochrome c Oxidase
ConcA	Concanamycin A
Cu	Copper
ES	Elesclomol
ES-Cu	Elesclomol-Copper complex
Fe	Iron
ICP-MS	Inductively coupled plasma-mass spectrometry
PAGE	Polyacrylamide gel electrophoresis
PCR	Polymerase chain reaction
SDS	Sodium dodecyl sulphate

TABLE OF CONTENTS

LIST OF FIGURES

LIST OF TABLES

Page

CHAPTER I

INTRODUCTION

Copper as an enzymatic cofactor

Copper is an essential trace element found in all living organisms. It plays a vital role in many biochemical reactions by acting as a catalytic cofactor for evolutionarily conserved enzymes involved in diverse cellular processes such as the cell's response to oxidative stress, iron import, and oxidative phosphorylation (Kim et al., 2008). As a redox-active metal, copper can accept or donate electrons, allowing it to exist in multiple oxidation states. This ability to undergo redox cycling makes copper a critical cofactor for many cuproenzymes as listed in Table 1.1

Table 1.1 Common cuproenzymes

Cuproenzyme	Function
Cytochrome c oxidase	Terminal enzyme of the mitochondrial respiratory chain. Catalyzes the reduction of O_2 to H_2O.
Ferro-O_2-oxidoreductase	Plasma membrane localized multi-copper oxidase in yeast. Catalyzes the oxidation of Fe^{2+} to Fe^{3+} for cellular iron import.
Superoxide dismutase 1	Cytosolic copper-zinc superoxide dismutase. Catalyzes the conversion of O_2^- to H_2O_2 and O_2.
Ceruloplasmin	Multi-copper oxidase produced by liver. Catalyzes oxidation of Fe^{2+} to Fe^{3+} for its transport in the plasma.
Hephaestin	Multi-copper oxidase produced by the enterocytes. Catalyzes oxidation of Fe^{2+} to Fe^{3+} for its transport in the plasma.
Lysyl oxidase	An extracellular enzyme that is required for crosslinking collagen in the connective tissue. Catalyzes the conversion of lysine molecules into highly reactive aldehydes that form cross-links in extracellular matrix proteins.
Dopamine β-hydroxylase	Neurotransmitter synthesizing enzyme in the brain. Catalyzes the conversion of dopamine to norepinephrine.
Peptidylglycine α-amidating mono oxygenase	Biosynthesis of signaling peptides in the brain. Catalyzes the conversion of glycine amides to amides and glyoxylate.
Tyrosinase	Required for melanin biosynthesis in melanosomes. Catalyzes the oxidation of tyrosine to dopaquinone.

Copper as a toxic element

Although the redox properties of copper are essential for its function as an enzymatic cofactor, these same properties make copper deleterious for cellular health. This is because unbound copper reacts with oxygen to generate reactive oxygen species (ROS), such as superoxide, hydrogen peroxide and hydroxyl radicals, as shown in Figure 1.1 (Halliwell, 1992; Jomova et al., 2011). Additionally, the high binding affinity of copper to metalloproteins presents a challenge because many metalloproteins often imperfectly discriminate between different metal ions and copper can outcompete other metals including iron, zinc, etc. (Foster et al., 2014). To avoid mis-metalation, the natural abundance of cellular copper is maintained at very low levels. For example, in the yeast, *Saccharomyces cerevisiae*, copper abundance is approximately ten-fold lower than iron (Holmes-Hampton et al., 2012). The approximate concentration of free copper in the cytoplasm is predicted to be as low as 10^{-18} M, ~one molecule of free Cu^+ per cell (Rae et al., 1999). Therefore, cellular copper pools must be tightly balanced to sustain a sufficient supply for metalation of cuproproteins, while minimizing its toxicity.

$AH_2 + Cu\ (II)$	$\rightarrow$	$AH\cdot + Cu(I) + H^+$
$AH\cdot + O_2$	$\rightarrow$	$A + O_2{}^- + H^+$
$Cu(I) + O_2$	$\rightarrow$	$Cu(II) + O_2{}^-$
$Cu(II) + O_2{}^-$	$\rightarrow$	$Cu(I) + O_2$
$Cu(I) + H_2O_2$	$\rightarrow$	$OH\cdot + OH^- + Cu(II)$
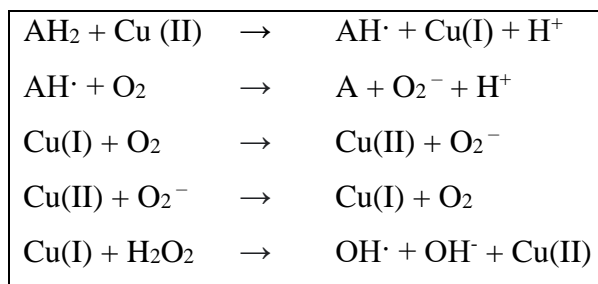
Figure 1.1 Copper-induced production of oxygen radicals
AH_2 represents any divalent reducing compound.

Import and subcellular distribution of copper

Proteins involved in cellular import of copper and its subsequent transport to cuproenzymes in different intracellular compartments are conserved from yeast to humans (Figure 1.2 and Table 1.2). Most extracellular copper ions are in the form of cupric ions (Cu^{2+}). These cupric ions are reduced into cuprous ions (Cu^+) by plasma membrane reductases Fre1 and Fre2 in yeast (Dancis et al., 1990; Georgatsou and Alexandraki 1999; Yun et al. 2001), before their import by plasma membrane copper transporters, Ctr1 or Ctr3 (Dancis et al., 1994; Peña et al., 2000). These transporters selectively transfer copper to the cytoplasm, where copper is immediately bound to either a copper chaperone or to non-proteinaceous ligand(s) (Kim et al., 2008).

Copper chaperones shuttle copper to various cuproenzymes present in different subcellular compartments (Figure 1.2). One such copper chaperone, Ccs1, can associate with the plasma membrane, where it directly interacts with Ctr1 to obtain newly imported Cu^+ (Pope et al., 2013). Ccs1, then escorts Cu^+ to copper-zinc superoxide dismutase, Sod1, in the cytoplasm (Lamb et al., 2000). Similarly, another cytosolic copper metallochaperone, Atx1, delivers copper to Ccc2, an ATP-dependent copper pump on the Golgi membrane (Fu et al., 1995; Lin and Culotta, 1995). Ccc2 and its human homologs, ATP7A and ATP7B, are essential for transporting copper into the lumen of the Golgi to facilitate the metalation of secretory pathway cuproenzymes. One such protein in yeast is Fet3, which is a multi-copper oxidase that gets metalated in the Golgi and is subsequently transported to the plasma membrane, where it is required for the import of extracellular iron. (Figure 1.2).

3
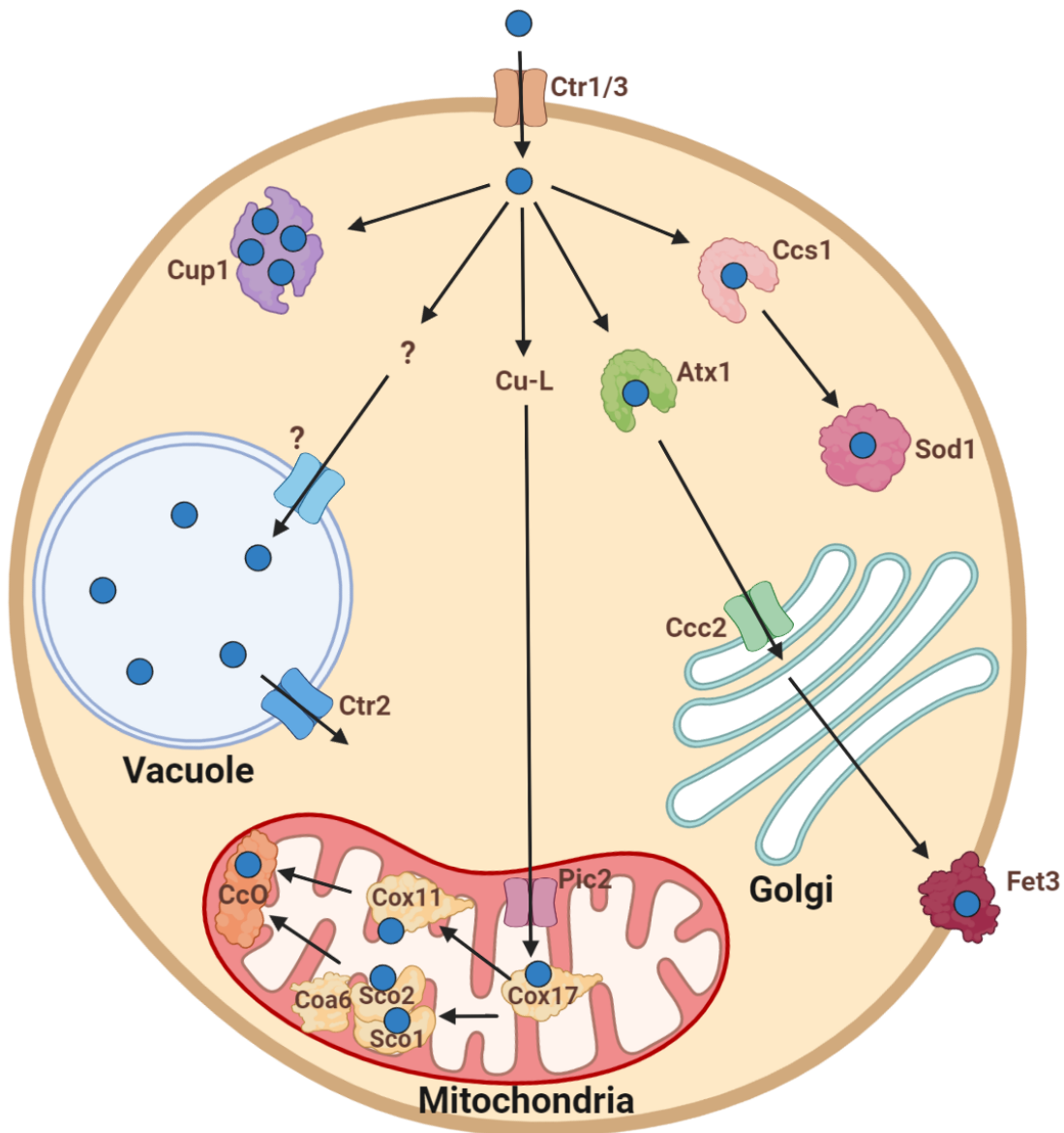
Figure 1.2 Copper trafficking in the yeast cell

Extracellular copper is imported by the copper-transporter Ctr1. Copper is then immediately bound to copper chaperones or copper ligands for its delivery to the various cellular organelles. Ccs1 transports copper to cytosolic antioxidant protein, Sod1. Cytosolic Atx1 delivers copper to Golgi membrane localized Ccc2, which subsequently pumps copper into the Golgi lumen. Copper in the Golgi lumen is used to metalate secretory cuproenzymes such as Fet3. Copper is presumed to be transported to the mitochondria bound to an uncharacterized ligand (L). Copper enters mitochondrial matrix via Pic2. The insertion of copper into CcO is mediated by copper-chaperones Sco1, Cox11 and Cox17 and disulfide reductases Coa6 and Sco2. Excess copper is either stored in the cytoplasm by Cup1, a metallothionein that serves to detoxify the cell from excessive cytosolic copper or is transported to the vacuole via an unknown mechanism. Stored vacuolar copper is released by Ctr2.

Excess copper ions are sequestered in either the vacuole or are bound to metallothioneins, such as Cup1 (Figure 1.2) (Hamer et al., 1985; Chatterjee et al., 2020; Blaby-Haas and Merchant, 2014). Metallothioneins are a family of low molecular weight proteins rich in cysteine residues, which facilitate copper binding via thiol groups (Fogel and Welch 1982; Winge et al., 1985; Calderone et al., 2005; Jensen et al., 1996). Copper ions are also stored in the vacuole; however, the mechanism by which copper is imported into the vacuole remains obscure (Blaby-Haas and Merchant, 2014). Vacuolar copper is proposed to be coordinated to polyphosphate (Nguyen et al., 2019). It is mobilized after reduction by Fre6 and then exported into the cytoplasm by Ctr2, a copper transporter present on the vacuolar membrane (Rees et al., 2004; Rees and Thiele, 2007).

Copper transport to the mitochondria is not well understood. Due to dual localization of copper metallochaperone, Cox17, in cytoplasm and mitochondria, it was mistakenly labeled as a copper shuttle for the mitochondria (Robinson and Winge, 2010). However, experiments showing continued transport of cytosolic copper to the mitochondria when Cox17 is tethered to the mitochondrial membrane argue against the role of Cox17 as a copper shuttle (Cobine et al., 2006). Crucially, import of cytosolic proteins into mitochondria occurs in the unfolded "apo" form, further ruling out Cox17 as a candidate for copper courier to the mitochondria (Banci et al., 2009). According to the current model, copper enters the mitochondria bound to a non-proteinaceous ligand (Figure 1.2) (Cobine et al., 2004). This copper-ligand (Cu-L) is imported to the mitochondrial matrix via Pic2 (Vest et al., 2013; Vest et al., 2016). Indirect experimental

evidence suggests that this matrix localized Cu-L pool is used for both the metalation of

CcO and a fraction of active Sod1 that localizes to the mitochondrial intermembrane

space (Cobine et al., 2006). Once inside the mitochondria, copper is delivered to CcO

subunits in a bucket-brigade fashion by the action of mitochondrial inter-membrane

space localized copper metallochaperones – Cox17, Cox11, and Sco1 (Table 1.2).

Table 1.2 Evolutionarily conserved copper transporting proteins

Yeast Protein	Human homolog	Function
Atx1	ATOX1	A cytosolic copper metallochaperone that delivers copper to Ccc2/ATP7A/ATP7B
Ctr1	CTR1	High-affinity plasma membrane copper transporter
Ccc2	ATP7A	Golgi localized copper transporting P-type ATPase
	ATP7B	
Cox11	COX11	A mitochondrial copper metallochaperone that delivers copper to the Cox1 subunit of CcO
Cox17	COX17	A mitochondrial copper metallochaperone that transfers copper to Sco1 and Cox11 proteins
Ccs1	CCS	A cytosolic and mitochondrial copper metallochaperone that delivers copper to Sod1
Sco1	SCO1	A mitochondrial copper metallochaperone that delivers copper to the Cox2 subunit of CcO
Sco2	SCO2	A mitochondrial copper-dependent thioldisulfide oxidoreductase involved in copper transport to Cox2
Pic2	SLC25A3	Mitochondrial copper importer
Ctr2	SLC31A2	Copper transporter of the vacuolar membrane

Cytochrome *c* oxidase – the mitochondrial cuproenzyme

Cytochrome *c* Oxidase (CcO) is the terminal enzyme of the mitochondrial

respiratory chain and the main site for cellular respiration. CcO catalyzes electron

transfer from reduced cytochrome *c* to molecular oxygen, while simultaneously pumping

protons from the matrix to the intermembrane space to contribute to the proton gradient

that powers mitochondrial ATP synthesis. This multi-subunit complex is localized to the mitochondrial inner membrane and contains copper and heme as cofactors (Tsukihara, 1995) (Figure 1.3). Three copper ions are bound within the catalytic core of CcO as Cu_A and Cu_B sites, which are present in Cox2 and Cox1 subunits, respectively (Maréchal et al., 2012) (Figure 1.3).
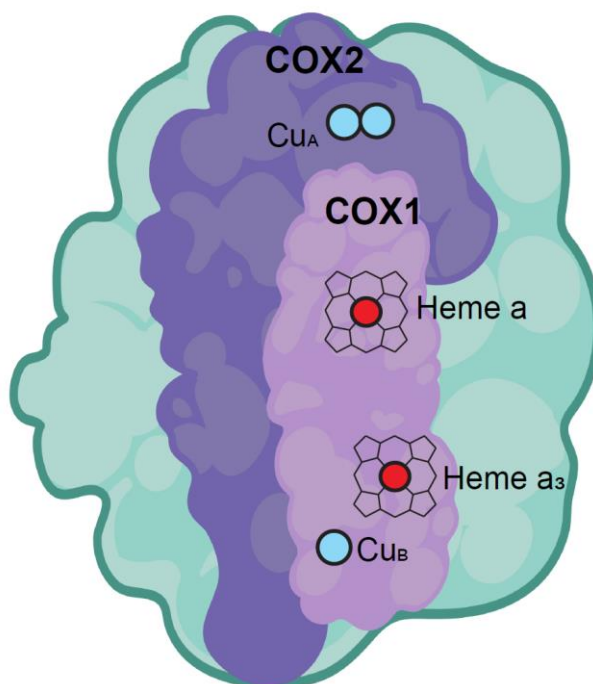
Figure 1.3 Schematic of Cytochrome *c* Oxidase subunits Cox1 and Cox2
CcO contains two catalytic subunits, Cox1 and Cox2. Cox1 contains two heme cofactors (heme a and heme a_3) and one copper cofactor called the Cu_B site. Cox2 contains one binuclear copper site, called the Cu_A site.

Incorporation of Cu^+ into either site requires multiple chaperones, which are present in the mitochondrial intermembrane space. The maturation of Cu_A and Cu_B occurs independently and is facilitated by a sequential transfer of copper from one metallochaperone to the other, in a bucket brigade manner. Specifically, Cox17, Sco1, Sco2, and Coa6 proteins are involved in copper delivery to the Cu_A site, whereas Cox17,

Cox19, and Cox11 are required for the metalation of Cu_B site (Soto et al., 2012). The metalation of these subunits is required for the maturation and stability of CcO holoenzyme. Cu_A is a binuclear copper site, accepting electrons from reduced cytochrome *c* and transferring them to the heme a center on the Cox1 subunit. Electrons from heme a are then transferred to the heme-a_3-Cu_B binuclear center in Cox1 and then to molecular oxygen reducing it to water (Ferguson-Miller and Babcock, 1996). Genetic mutations in any of the proteins involved in copper transport to CcO disrupt its stability and diminish its activity.

Diseases of copper homeostasis

While copper plays an evolutionary conserved role as an essential cofactor for many enzymes involved in vital cellular functions (e.g., mitochondrial respiration, iron acquisition, and ROS scavenging), it has additional functions in higher eukaryotes. For example, enzymes involved in melanin synthesis, neuropeptide maturation, blood coagulation, and connective tissue maturation are all copper-dependent (Kim et al., 2008). The importance of maintaining proper copper trafficking in higher eukaryotes is underscored by the severe clinical pathologies associated with disrupted copper trafficking including, neurodegeneration, mitochondrial myopathies, and metabolic diseases (Kaler et al., 2013; Kaler et al., 2011; Shoubridge et al., 2001).

The daily recommended dose of copper for adult human beings is ~1.5 mg, which most adults acquire through diet (Chambers et al., 2010). Humans absorb dietary copper through CTR1 localized on the apical membrane of intestinal cells (Nose et al., 2006). The absorbed copper is then pumped into the blood circulation by ATP7A, which

localizes to the basolateral membrane of intestinal enterocytes (Monty et al., 2005). Mutations resulting in the loss or reduction in function of ATP7A result in Menkes disease, which is characterized by copper accumulation in enterocytes and copper deficiency in nearly all other tissues (Danks et al., 1972). Due to this copper deficiency, Menkes patients exhibit decreased activity of cuproenzymes such as CcO (Maehara et al., 1983). This is particularly devastating for high energy demanding tissues such as the brain, skeletal muscle, and the heart (Maehara et al., 1983; Kodama et al., 1989). Menkes patients often suffer from neurological abnormalities and mental retardation (Kodama et al., 1999). Due to progressive neurological impairments, Menke's patients typically do not live past early childhood and die by the age of 5 (Tümer and Møller, 2010).

ATP7A has a paralog, ATP7B which is also essential for maintaining copper homeostasis in humans. ATP7B is primarily expressed in hepatocytes, where it performs two functions - exporting excess copper in the bile and metalating secretory pathway cuproenzymes such as ceruloplasmin (Prohaska, 2008; Bingham et al., 1998). Ceruloplasmin is a cuproenzyme secreted into the blood and is essential for the proper absorption of iron from the blood into the various tissues (Vashchenko and MacGillivray, 2013). Loss of function mutations in the *ATP7B* gene result in Wilson's disease. Wilson's disease is characterized by excessive accumulation of copper in the liver and alterations in systemic iron homeostasis (Gow et al., 2000). Clinical presentations of this disorder include neurological, psychiatric, ophthalmological and hepatic manifestations (Mulligan and Bronstein, 2020).

In addition to the Menkes and Wilson's diseases, mutations in proteins involved in the delivery of copper to CcO, result in mitochondrial disorders (Baertling et al., 2015; Papadopoulou et al., 1999; Valnot et al., 2000). Patients suffering from mutations in the *SCO1* gene exhibit mitochondrial disease symptoms due to CcO deficiency (Valnot et al., 2000). Symptoms include neurological disorders, hypertrophic cardiomyopathy, encephalopathy, and lactic acidosis (Valnot et al., 2000; Leary et al., 2013). Similarly, patients with mutations in the *SCO2* display mitochondrial dysfunction. *SCO2* patients have a life expectancy of < 1 year due to infantile cardioencephalomyopathy (Papadopoulou et al., 1999; Jaksch et al., 2000). Mutations in *COA6* has been shown to cause hypertrophic cardiomyopathy (Calvo et al., 2010; Baertling et al., 2015)
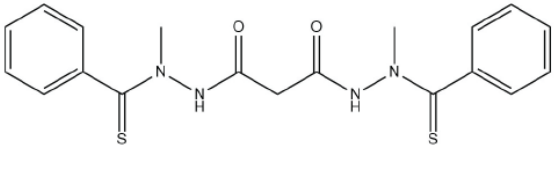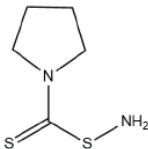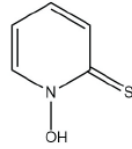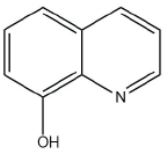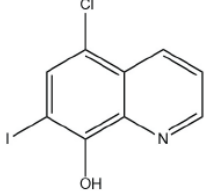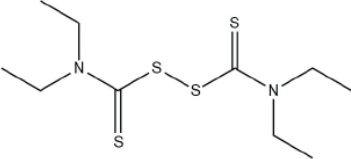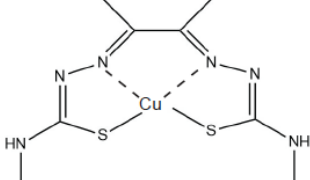
Therapeutic approaches for the treatment of copper deficiency disorders

In *in vitro* systems, copper supplementation can restore copper delivery to CcO, bypassing the need for certain mitochondrial copper chaperones (Jaksch et al., 2001; Baertling et al., 2015; Ghosh et al., 2014). However, the use of direct subcutaneous injections of copper-histidine as a therapeutic agent has not been successful in ameliorating disease pathology in most cases (Freisinger et al., 2004; Desai and Kaler, 2008). This is likely due to the downregulation of Ctr1 after repeated exposure to high concentrations of copper-histidine. Therefore, there is an unmet need for pharmacological agents that can deliver copper into cells independent of copper transporting machinery.

Currently, the US Food and Drug Administration has approved the use of metal binding agents for the chelation of excess metals for disorders of heavy metal overload (Franz, 2013). However, depending on the dose and the form these compounds are administered in, they can also be utilized for the delivery of metals (Franz, 2013; Duncan and White, 2012). Due to the physiological importance of copper and its unique redox activity, many different copper binding compounds have been synthesized and investigated for their therapeutic potential in treating human diseases (Figure 1.3). As the chemistry of these compounds differs, it is likely that their biological implications will also differ. They have been investigated for their unique biological actions and have strong potential for applications.

Through a targeted screen focused on these copper-binding molecules, Soma et al., showed that low doses of elesclomol (ES) can safely and effectively deliver copper to CcO, thereby restoring mitochondrial function in genetic models of copper deficiency (Soma et al., 2018). In a subsequent study, it was shown that ES-Cu complex can ameliorate disease pathology and dramatically extend lifespan of Menkes-affected mice (Guthrie et al., 2020). ES is a bis(thiohydrazide) amide compound that binds copper(II) in the extracellular environment and forms a membrane permeable complex, which upon entering the mitochondria releases copper (Gohil, 2021). The released copper is bioavailable for the metalation of CcO. However, administration of high dosages of ES leads to the generation of unmanageable levels of reactive oxygen species leading to oxidative stress and ultimately apoptotic death of cells (Nagai et al., 2012).

Table 1.3 Structures of potentially therapeutic inorganic copper-complexes

Compound	Therapeutic use	Chemical structure
Elesclomol	•Cancer	
Ammonium pyrrolidine dithiocarbamate	•Alzheimer's disease •Cancer	
Pyrithione	•Antifungal	
8-Hydroxy quinoline	•Antifungal	
Clioquinol	•Alzheimer's disease •Huntington's disease •Cancer	
Disulfiram	•Cancer	
Cu-ATSM	•Cancer	

<u>Yeast as a model system to study copper trafficking</u>

The yeast *Saccharomyces cerevisiae* has been widely employed to investigate copper trafficking and mitochondrial function, allowing for numerous breakthroughs in these fields (De Freitas et al., 2003; Lasserre et al., 2015). This single-celled organism is the simplest eukaryote that shares many characteristics with multi-cellular organisms in terms of the cellular metal homeostasis. For example, CcO and all previously identified copper-chaperones are evolutionarily conserved (Table 1.2).

Importantly, yeast can utilize either glycolysis or aerobic respiration for the generation of cellular energy. This is particularly useful for studying mitochondrial copper regulatory pathways because yeast can tolerate mutations that inactivate mitochondrial respiration by surviving on glycolysis (Lasserre et al., 2015). Thereby mutations expected to result in defective aerobic energy generation could be studied in yeast (Diaz-Ruiz et al., 2009). Importantly, a library of yeast knockouts of all nonessential genes is commercially available, which allows for the fast and unbiased means for identifying novel regulators of mitochondrial copper metabolism. In particular the common laboratory-used BY4741 strain provides a powerful tool for detecting disruption in copper homeostasis because one of the copper transporter, Ctr3, is disabled in this strain (Knight et al., 1996). Thus, under basal conditions these cells are mildly copper deficient, making cuproenzymes more sensitive to disruptions of intracellular copper trafficking. Therefore, I have extensively used the yeast model system in my dissertation research focused on discovering novel regulators of mitochondrial copper homeostasis.

CHAPTER II

A GENOME-WIDE COPPER-SENSITIZED SCREEN IDENTIFIES NOVEL

REGULATORS OF MITOCHONDRIAL CYTOCHROME *C* OXIDASE ACTIVITY *

Summary

       Copper is essential for the activity and stability of cytochrome *c* oxidase (CcO), the terminal enzyme of the mitochondrial respiratory chain. Loss-of-function mutations in genes required for copper transport to CcO result in fatal human disorders. Despite the fundamental importance of copper in mitochondrial and organismal physiology, systematic identification of genes that regulate mitochondrial copper homeostasis is lacking. To discover these genes, we performed a genome-wide screen using a library of DNA-barcoded yeast deletion mutants grown in copper-supplemented media. Our screen recovered a number of genes known to be involved in cellular copper homeostasis as well as genes previously not linked to mitochondrial copper biology. These newly

identified genes include the subunits of the adaptor protein 3 complex (AP-3) and components of the cellular pH-sensing pathway Rim20 and Rim21, both of which are known to affect vacuolar function. We find that AP-3 and Rim mutants exhibit decreased vacuolar acidity, which in turn perturbs mitochondrial copper homeostasis and CcO function. CcO activity of these mutants could be rescued by either restoring vacuolar pH or supplementing growth media with additional copper. Consistent with these genetic data, pharmacological inhibition of the vacuolar proton pump leads to decreased mitochondrial copper content and a concomitant decrease in CcO abundance and activity. Taken together, our study uncovered novel genetic regulators of mitochondrial copper homeostasis and provided a mechanism by which vacuolar pH impacts mitochondrial respiration through copper homeostasis.

Introduction

Copper is an essential trace metal that serves as a cofactor for a number of enzymes in various biochemical processes, including mitochondrial bioenergetics (Kim et al., 2008). For example, copper is essential for the activity of cytochrome *c* oxidase (CcO), the evolutionarily conserved terminal enzyme of the mitochondrial respiratory chain and the main site of cellular respiration (Little et al., 2018). CcO metalation requires transport of copper to mitochondria followed by its insertion into Cox1 and Cox2, the two copper-containing subunits of CcO (Cobine et al., 2020). Genetic defects that prevent copper delivery to CcO disrupt its assembly and activity resulting in rare but fatal infantile disorders (Baertling et al., 2015; Papdopoulou et al., 1999; Valnot et al., 2000).

Intracellular trafficking of copper poses a challenge because of the high reactivity of this transition metal. Copper in an aqueous environment of the cell can generate deleterious reactive oxygen species *via* Fenton chemistry (Halliwell and Gutteridge 1984) and can inactivate other metalloproteins by mismetallation (Foster et al., 2014). Consequently, organisms must tightly control copper import and trafficking to subcellular compartments to ensure proper cuproprotein biogenesis while preventing toxicity. Indeed, aerobic organisms have evolved highly conserved proteins to import and distribute copper to cuproenzymes in cells (Nevitt et al., 2012). Extracellular copper is imported by plasma membrane copper transporters and is immediately bound to metallochaperones Atx1 and Ccs1 for its delivery to different cuproenzymes residing in the Golgi and cytosol, respectively (Robinson and Winge, 2010).

However, copper transport to the mitochondria is not well understood. A nonproteinaceous ligand, whose molecular identity remains unknown, has been proposed to transport cytosolic copper to the mitochondria (Cobine et al., 2020), where it is stored in the matrix (Cobine et al., 2004). This mitochondrial matrix pool of copper is the main source of copper ions that are delivered to CcO subunits in a particularly complex process requiring multiple metallochaperones and thiol reductases (Cobine et al., 2020; Cobine et al., 2006; Timón-Gómez et al., 2018). Specifically, copper from the mitochondrial matrix is exported to the intermembrane space via a yet unidentified transporter, where it is inserted into the CcO subunits by metallochaperones Cox17, Sco1, and Cox11 that operate in a bucket-brigade manner (Timón-Gómez et al., 2018). The copper-transporting function of metallochaperones requires disulfide reductase activities of Sco2 and Coa6, respectively (Leary et al., 2009; Soma et al., 2019).

In addition to the mitochondria, vacuoles in yeast and vacuole-like lysosomes in higher eukaryotes have been identified as critical storage sites and regulators of cellular copper homeostasis (Blaby-Haas and Merchant, 2014; Polishchuk and Polishchuck, 2016; Portney et al., 2001). Copper enters the vacuole by an unknown mechanism and is proposed to be stored as Cu(II) coordinated to polyphosphate (Nguyen et al., 2019). Depending on the cellular requirement, vacuolar copper is reduced to Cu(I), allowing its mobilization and export through Ctr2 (Rees et al., 2004; Rees and Thiele, 2007). Currently, the complete set of factors regulating the intracellular distribution of copper and its transport to the mitochondria remains unknown.

Here, we sought to identify regulators of mitochondrial copper homeostasis by exploiting the copper requirement of CcO in a genome-wide screen using a DNA-barcoded yeast deletion library. Our screen was motivated by prior observations that respiratory growth of yeast mutants such as *coa6Δ* can be rescued by copper supplementation in the media (Wu et al., 2016; Ghosh et al., 2014; Glerum et al., 1996). Thus, we designed a copper-sensitized screen to identify yeast mutants whose growth can be rescued by addition of copper in the media. Our screen recovered Coa6 and other genes with known roles in copper metabolism while uncovering genes involved in vacuolar function as regulators of mitochondrial copper homeostasis. Here, we have highlighted the roles of two cellular pathways—adaptor protein 3 complex (AP-3) and the pH-sensing pathway Rim101—that converge on vacuolar function, as important factors regulating CcO biogenesis by maintaining mitochondrial copper levels.

Results

A genome-wide copper-sensitized screen using a DNA-barcoded yeast deletion mutant library

We chose the yeast, *Saccharomyces cerevisiae*, to screen for genes that impact mitochondrial copper homeostasis because it can tolerate mutations that inactivate mitochondrial respiration by surviving on glycolysis. This enables the discovery of novel regulators of mitochondrial copper metabolism whose knockout is expected to result in a defect in aerobic energy generation (Diaz-Ruiz et al., 2009). Yeast cultured in glucose-containing media (YPD) uses glycolytic fermentation as the primary source for cellular energy; however in glycerol/ethanol-containing nonfermentable media (YPGE), yeast

must utilize the mitochondrial respiratory chain and its terminal cuproenzyme, CcO, for energy production. Based on the nutrient-dependent utilization of different energy-generating pathways, we expect that deletion of genes required for respiratory growth will specifically reduce growth in nonfermentable (YPGE) medium, but will not impair growth of those mutants in fermentable (YPD) medium. Moreover, if respiratory deficiency in yeast mutants is caused by defective copper delivery to mitochondria, then these mutants may be amenable to rescue *via* copper supplementation in YPGE respiratory growth media (Figure 2.1). Therefore, to identify genes required for copper-dependent respiratory growth, we cultured the yeast deletion mutants in YPD and YPGE with or without 5 µM $CuCl_2$ supplementation (Figure 2.1). Our genome-wide yeast deletion mutant library was derived from the variomics library reported previously (Huang et al., 2013); it is composed of viable haploid yeast mutants, where each mutant has one gene replaced with the selection marker *kanMX4* and two unique flanking sequences (Figure 2.1). These flanking sequences labeled "UP" and "DN" contain universal priming sites as well as a 20-bp barcode sequence that is specific to each deletion strain. This unique barcode sequence allows for the quantification of the relative abundance of individual strains within a pool of competitively grown strains by DNA barcode sequencing (Smith et al., 2009). Here, we utilized this DNA barcode sequencing approach to quantify the relative fitness of each mutant grown in YPD and YPGE ± Cu to early stationary phase (Figure 2.1).
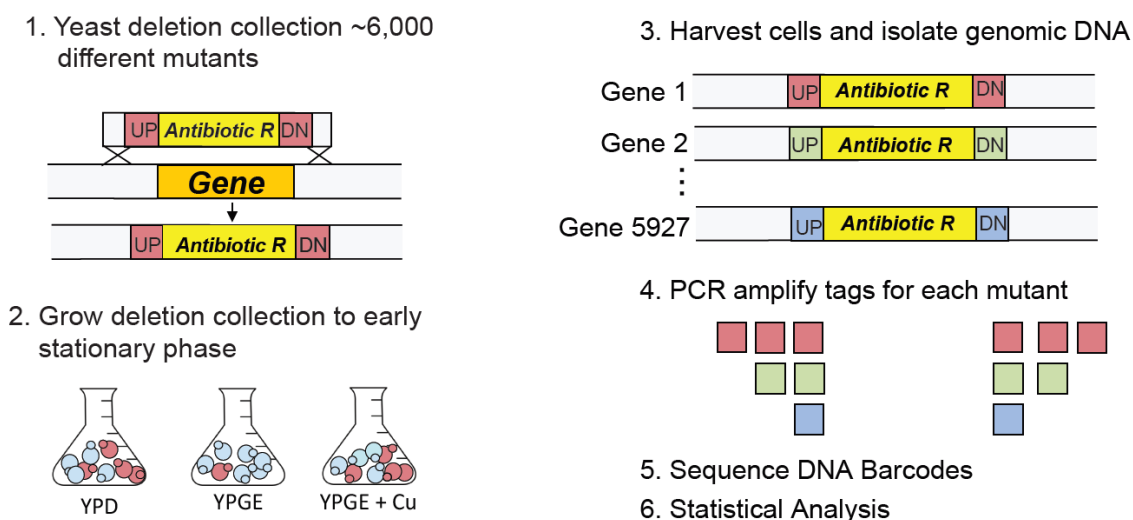
Figure 2.1 Schematic of genome-wide copper-sensitized screen
The yeast deletion library is a collection of 6000 mutants, where each mutant has a gene replaced with *kanMX4* cassette that is flanked by a unique UP tag (UP) and DOWN tag (DN) sequences. The deletion mutant pool was grown in fermentable (YPD) and nonfermentable (YPGE) medium with and without 5 μM CuCl$_2$ supplementation till cells reached an optical density of 5.0. The genomic DNA was isolated from harvested cells and was used as template to amplify UP and DN tag DNA barcode sequences using universal primers. PCR products were then sequenced and the resulting data analyzed. The mutants with deletion in genes required for respiratory growth are expected to grow poorly in nonfermentable medium resulting in reduced barcode reads for that particular gene(s). However, if the same gene(s) function is supported by copper supplementation, then we expect increased barcode reads for that gene(s) in copper-supplemented nonfermentable growth medium. (Figure reprinted from Garza et al., 2021).

Genes required for respiratory growth

We began the screen by identifying mutant strains with respiratory deficiency since perturbation of mitochondrial copper metabolism is expected to compromise aerobic energy metabolism. To identify mutants with this growth phenotype, we compared the relative abundance of each barcode in YPD with that of YPGE using a T-score based on Welch's two-sample *t* test. The T-score provides a quantitative measure of the difference in the abundance of a given mutant in two growth conditions. A negative T-score identifies mutants that grow poorly in respiratory conditions;

conversely, a positive T-score identifies mutants with better competitive growth in respiratory conditions. We rank-ordered all mutants from negative to positive T-scores and found that the lower tail of the distribution was enriched in genes with known roles in mitochondrial respiratory chain function, confirming the fidelity of the screening conditions and the knockout strains (Figure 2.2A; Supplementary table 1). The top "hits" representing mutants with the most negative T-score included *COQ3*, *COX5A*, *RCF2*, *COA4*, and *PET54,* genes that are involved in coenzyme Q and respiratory complex IV function (Figure 2.2A). To more systematically identify cellular pathways that were enriched for reduced respiratory growth, we performed gene ontology analysis using an online tool—*Gene Ontology enRichment anaLysis and visuaLizAtion* (GOrilla) (Eden et al., 2009). The gene ontology (GO) analysis identified *mitochondrial respiratory chain complex assembly* (p-value: 7.73e-23) and *cytochrome c oxidase assembly* (p-value: 5.09e-22) as the top-scoring biological process categories (Figure 2.2B) and *mitochondrial part* (p-value: 1.40e-25) and *mitochondrial inner membrane* (p-value: 1.48e-20) as the top-scoring cellular component category (Figure 2.2C). This unbiased analysis identified the expected pathways and processes validating our screening results. We further benchmarked the performance of our screen by determining the enrichment of genes encoding for mitochondria-localized and oxidative phosphorylation (OXPHOS) proteins at three different p-value thresholds ($p < 0.05$, $p < 0.025$, and $p < 0.01$) (Figure 2.3). We observed that at a p-value of <0.05, ∼25% of the genes encoded for mitochondrially localized proteins, of which ∼40% are OXPHOS proteins (Figure 2.3; Supplementary

table 2). The percentage of mitochondria-localized and OXPHOS genes increased progressively as we increased the stringency of our analysis by decreasing the significance cutoff from p-value of 0.05 to 0.01 (Figure 2.3). A total of 370 genes were identified to have respiratory deficient growth at $p < 0.01$, of which 116 are known to encode mitochondrial proteins (Vögtle et al., 2017), nearly half of these are OXPHOS proteins from a total of 137 known OXPHOS genes in yeast (Figure 2.3; Supplementary table 2). Expectedly, the respiratory deficient mutants included genes required for mitochondrial NADH dehydrogenase (*NDI1*) and OXPHOS complex II, III, IV, and V as well as genes involved in cytochrome *c* and ubiquinone biogenesis, which together form mitochondrial energy-generating machinery (Figure 2.2D; Supplementary table 2). Additionally, genes encoding TCA cycle enzymes and mitochondrial DNA expression were also scored as hits (Figure 2.4). Surprisingly, a large fraction of genes required for respiratory growth encoded nonmitochondrial proteins involved in vesicle-mediated transport (Figure 2.4).

B

Gene Set - Process	P-Value	ES
Mitochondrial respiratory chain complex assembly	7.73e-23	16.80
Cytochrome *c* oxidase assembly	5.09e-22	17.26
Respiratory chain complex IV assembly	3.33e-14	17.40
Mitochondrial respiratory chain complex IV assembly	3.33e-14	17.40
Cellular respiration	2.26e-13	9.61

C

Gene Set - Component	P-Value	ES
Mitochondrial part	1.40e-25	4.33
Mitochondrial inner membrane	1.48e-20	6.14
Mitochondrial membrane	5.10e-20	4.58
Organelle inner membrane	4.17e-19	5.67
Mitochondrial membrane part	7.02e-9	4.23

Figure 2.2 Genes required for respiratory growth

(A) growth of each mutant in the deletion collection cultured in YPGE and YPD media was measured by BarSeq and analyzed by T-score. T(YPGE-YPD) scores are plotted for the top and bottom 500 mutants. Known mitochondrial respiratory genes are highlighted in *red*. (B) and (C),

23

gene ontology analysis was used to identify the top five cellular processes (B) and cellular components (C) that were significantly enriched among our top-scoring hits from a rank ordered list, where ranking was done from the lowest to highest T-score. (D) a schematic of mitochondrial OXPHOS subunits and assembly factors, where genes depicted in red were "hits" in the screen with their T-scores values below –2.35 (p-value $\leq$ 0.05). ES, enrichment score. (Figure reprinted from Garza et al., 2021).
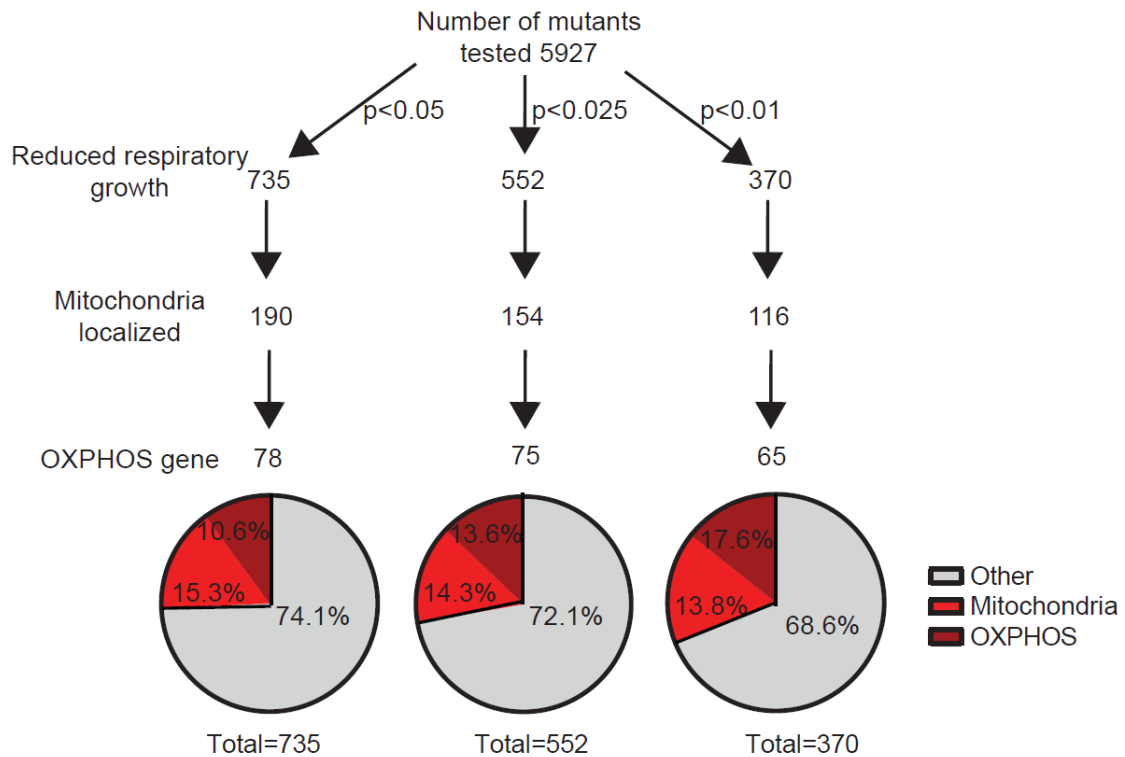
Figure 2.3 Enrichment of OXPHOS and other mitochondrial genes increases with increased stringency of p-value threshold

Illustration of the number of respiratory deficient strains identified at each p-value threshold. The distribution of hits between known OXPHOS protein encoding genes (maroon), other mitochondrial protein encoding genes (red), and non-mitochondrial protein encoding genes (grey) is shown. (Figure reprinted from Garza et al., 2021).

Other genes encoding mitochondrial proteins

TCA Cycle
Fum1, Idh1, Kgd1, Kgd2, Mdh1

Additional mitochondrial hits
Aat1, Aim17, Aim24, Aim26, Ald4, Apj1, Cym1, Ddl1, Gep7, Gut2, Iai11, Mcp2, Mfm1, Mgr1, Mic60, Mrs2, Nfu1, Num1, Pis1, Puf3, Put1, Rrg7, Sap185, Sod2, Tim21, Uth1, Yhm2, Ysc83

Mitochondrial DNA expression
Aim23, Mba1, Mod5, Mrp49, Mrpl1, Mrpl39, Mrx6, Msc6, Oms1, Pet20, Ppe1, Pth2, Pth4, Qri7

Glutathione biosynthesis
Gsh1, Gsh2

Rim101 pathway
Dfg16, Rim8, Rim9, Rim13, Rim20, Rim21, Rim101

AP-3 Complex
Apl5, Apl6, Apm3, Aps3

Other vesicle mediated transport
Age2, Apl2, Apl4, Apm1, Aps1, Arf2, Arl3, Avl9, Bmh2, Ccz1, Did4, Gcs1, Get1, Get2, Gyp1, Inp53, Irc6, Mon1, Pep8, Ras2, Ric1, Rtt10, Rvs167, Shr3, Snf8, Svp26, Swa2, Sys1, Tda3, Vab2, Vam7, Vam10, Vps5, Vps17, Vps29

Other vesicle mediated transport continued
Vps35, Vps41, Vps51, Vps63, Yck3, Yip4, Ypt7

Ion and other transport
Ant1, Atx1, Avt5, Ccc1, Erc1, Flc1, Flc2, Flc3, Fre7, Ftr1, Gdt1, Gef1, Hxt8, Kha1, Mch5, Nhx1, Osh3, Rav1, Rav2, Sam3, Stl1, Stv1, Vtc5, YDL199C, YGR125W, YOL162W

Other hits

Aht1	Jnm1	Rim11	YDR048C
Adh6	Kns1	Rmd1	YDR269C
Apt2	Ktr2	Rmd8	YDR271C
Arg80	Ldb18	Rot2	YDR391C
Asi3	Lug1	Rpl16B	YDR455C
Azf1	Mak10	Rrd2	YER097W
Ber1	Mbr1	Rtc1	YGL199C
Bmh1	Mdh2	Rvs167	YGL235W
Bye1	Mds3	Sas3	Ygp1
Car1	Met16	Scs22	YHL005C
Car2	Mft1	Sds3	YJR087W
Cat8	Mnl2	Ser3	YJR120W
Cnn1	Mrk1	Sgn1	YKL136W
Cti6	Mth1	Ski7	YLL020C
Ctt1	Msc6	Sko1	YLR169W
Cub1	Msn1	Smi1	YLR202C
Cys4	Nab6	Snf3	YLR269C
Dat1	Nbp2	Snf4	YLR345W
Dbr1	Ndl1	Sok1	YML082W
Dcs1	Ngl2	Sok2	YML089W
Ddr48	Nis1	Spg3	YML090W
Eaf7	Npr1	Spo7	YMR057C
Edc3	Npr2	Ssa1	YMR315W
Erv2	Nsi1	Ste20	Yng1
Far10	Ntg2	Syh1	Ynk1
Fbp1	Nto1	Toh1	YNL140C
Fbp26	Nut1	Tor1	YNL179C
Fsh1	Opi1	Trm10	YNR042W
Fyv8	Orm2	Ubr1	YOL036W
Gal11	Par32	Ume1	YOR139C
Gal7	Pcl6	Ura4	YOR333C
Gal80	Pcl8	Vba4	YPL150W
Gal83	Pho2	Vhs1	YPL182C
Gdh1	Pho4	Vms1	YPR012W
Glc8	Pph21	Vps61	YPR039W
Gzf3	Ppm1	YAL004W	YPR050C
Hap4	Ppq1	Yap5	YPR114W
Hap5	Psp2	YBL044W	YPR123C
Hda2	Psy2	YBL055C	Yps7
Hda3	Ptk1	YBL096C	Yta7
Hel2	Ptp3	YBR224W	
Hir1	Pub1	YBR225W	
Hir2	Pus1	YBR226C	
Irc14	Pyc1	YDL068W	
Isw2	Rck2	YDL172C	

Figure 2.4 Respiratory deficient mutants of non-OXPHOS related proteins
Non-OXPHOS associated proteins with a p-value ≤ 0.01 for T-score (YPGE-YPD) were grouped into different functional categories. (Figure reprinted from Garza et al., 2021).

Pathway analysis for copper-based rescue

Next, we focused on identifying mutants in which copper supplementation improved their fitness in respiratory growth conditions by comparing their frequency in YPGE +5 µM CuCl$_2$ *versus* YPGE growth conditions. We rank-ordered the genes from positive to negative T-scores. Mutants with positive T-scores are present in the upper tail of the distribution that displayed improved respiratory growth upon copper

supplementation (Figure 2.5A, Supplementary table 3). Notably, several genes known to be involved in copper homeostasis were recovered as high-scoring "hits" in our screen and were present as expected in the upper tail of distribution (Figure 2.5A). For example, we recovered *CTR1*, which encodes the plasma membrane copper transporter (Dancis et al., 1994), *ATX1*, which encodes a metallochaperone involved in copper trafficking to the Golgi body (Lin and Culotta, 1995), *GEF1* and *KHA1*, which encode proteins involved in copper loading into the cuproproteins in the Golgi compartment (Wu et al., 2016; Gaxiola et al., 1998), *GSH1* and *GSH2*, which are required for biosynthesis of copper-binding molecule glutathione, and *COA6*, which encodes a mitochondrial protein that we previously discovered to have a role in copper delivery to the mitochondrial CcO (Soma et al., 2019; Ghosh et al., 2014; Ghosh et al., 2016) (Figure 2.5A). Nevertheless, for many of our other top-scoring hits, evidence supporting their role in mitochondrial copper homeostasis was either limited or lacking entirely.
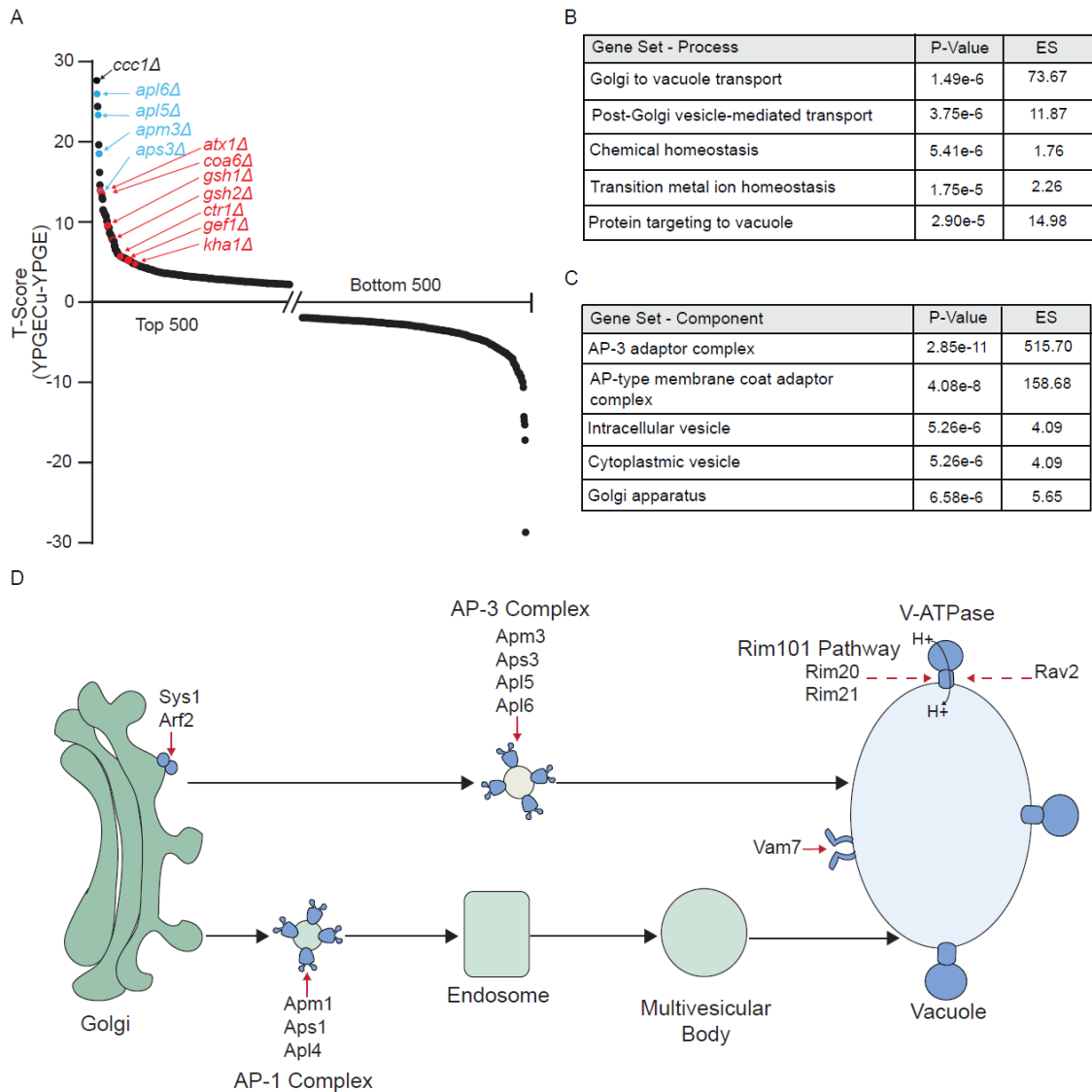
Figure 2.5 Genes required for copper homeostasis
(A)T(YPGECu-YPGE) score is plotted for top and bottom 500 mutants. Known copper homeostasis genes are highlighted in red. AP-3 subunits are highlighted in blue. (B-C) Gene ontology analysis was used to identify the top five cellular processes (B) and cellular components (C) that were significantly enriched in our top scoring hits. ES indicates enrichment score. (D) Secretory pathway mutants that displayed significantly improved growth in YPGE+Cu are displayed in blue. A dashed arrow indicates that the proteins listed are not a subunit of the complex but are involved in the maintenance of listed complex. (Figure reprinted from Garza et al., 2021).

To determine which cellular pathways are essential for maintaining copper homeostasis, we performed GO analysis using GOrilla. GO analysis identified biological processes—*Golgi to vacuole transport* (*p*-value: 1.49e-6), and *post-Golgi vesicle-mediated transport*, (*p*-value: 3.75e-6) as the most significantly enriched pathways (Figure 2.5B). Additionally, GO category *transition metal ion homeostasis* was also in the top five significantly enriched pathways, (*p*-value: 1.75e-5) (Figure 2.5B). GO analysis for cellular component categories identified adaptor protein 3 complex (AP-3), which is known to transport vesicles from the Golgi body to vacuole, as the top-scoring cellular component (*p*-value: 2.85e-11) (Figure 2.5C). All four subunits of AP-3 complex (*APL6*, *APM3*, *APL5*, *APS3*) complex were in the top ten of our rank-sorted list (Figure 2.5A, Figure 2.4) (Bagh et al., 2017; Dell'Angelica, 2009). Additionally, two subunits of the Rim101 pathway (*RIM20* and *RIM21*), both of which are linked to vacuolar function (Lamb et al., 2001), were also in our list of top-scoring genes (Figure 2.4). Of note, the seven major components of the Rim101 pathway were identified as top-scoring hits for respiratory deficient growth (Figure 2.4). Placing the hits from our screen on cellular pathways revealed a number of hits that were either involved in Golgi bud formation (Sys1, Arf2), vesicle coating (AP-3 and AP-1 complex subunits), tethering and fusion of Golgi vesicle cargo to the vacuole (Vam7), and vacuolar ATPase expression and assembly (Rim20, Rim21, Rav2) (Figure 2.5D). We reasoned that these biological processes and cellular components were likely high scoring due to the role of the vacuole as a major storage site of intracellular metals (Blaby-Haas and Merchant, 2014). We decided to focus on AP-3 and Rim mutants, as these cellular components

were not previously linked to mitochondrial respiration or mitochondrial copper homeostasis.

AP-3 mutants exhibit reduced abundance of CcO and VATPase subunits

To validate our screening results and to determine the specificity of the copper-based rescue of AP-3 mutants, we compared the respiratory growth of AP-3 deletion strains, *aps3Δ*, *apl5Δ*, and *apl6Δ* on YPD and YPGE media with or without Cu, Mg, or Zn supplementation. Each of the AP-3 mutants exhibited reduced respiratory growth in YPGE media at 37°C, which was fully restored by copper, but not by magnesium or zinc (Figure 2.6A), indicating that the primary defect in these cells is dysregulated copper homeostasis. Here we used 37°C for growth measurement as an additional stressor to fully uncover growth defect on solid media. The *coa6Δ* mutant was used as a positive control because we have previously shown that respiratory growth deficiency of *coa6Δ* can be rescued by Cu supplementation (Ghosh et al., 2014). Since recent work has identified the role of the yeast vacuole in mitochondrial iron homeostasis (Chen et al., 2020, Hughes et al., 2020) we asked if iron supplementation could also rescue the respiratory growth of AP-3 mutants. Unlike copper, which rescued respiratory growth of AP-3 mutants at 5 μM concentration, low concentrations of iron (≤20 μM) did not rescue respiratory growth; but we did find that high iron supplementation (100 μM) improved their respiratory growth (Figure 2.7). To uncover the biochemical basis of reduced respiratory growth, we focused on Cox2, a copper-containing subunit of CcO, whose stability is dependent on copper availability and whose levels serve as a reliable proxy

29

for mitochondrial copper content. The steady-state levels of Cox2 were modestly but consistently reduced in all four AP-3 mutants tested (Figure 2.6B).
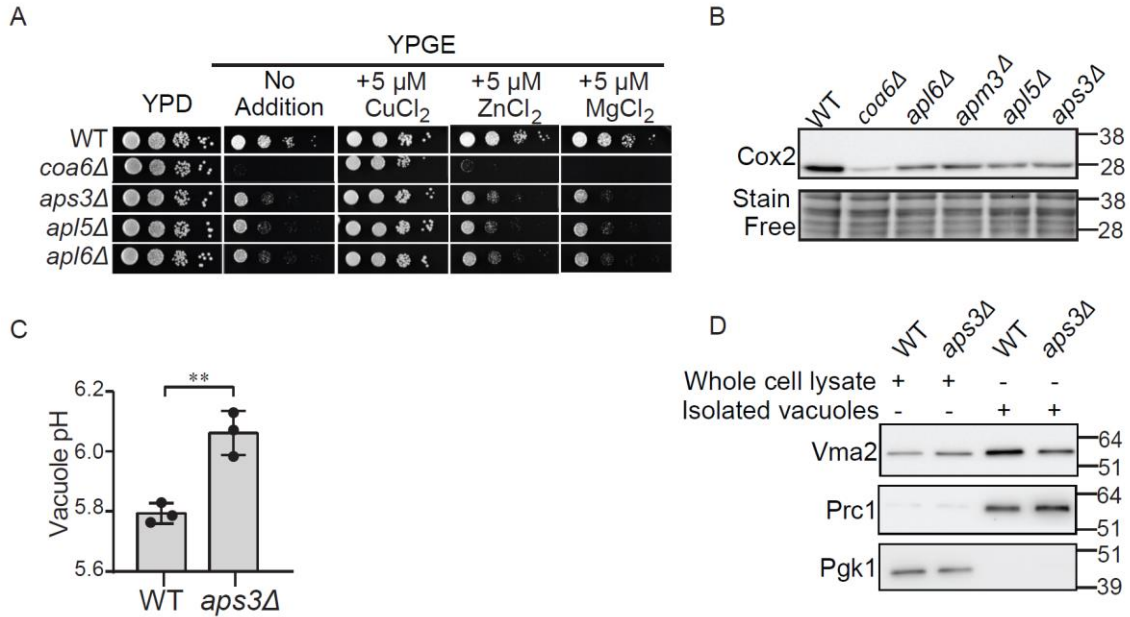
Figure 2.6 Loss of AP-3 results in reduced vacuolar and mitochondrial function
(A)Serial dilutions of WT and the indicated mutants were seeded onto YPD and YPGE plates with and without 5 μM $CuCl_2$, $MgCl_2$ and $ZnCl_2$ and grown at 37°C for two (YPD) or four days (YPGE). *coa6Δ* cells, which have been previously shown to be rescued by $CuCl_2$, were used as a control. (B) Whole cell protein lysate was analyzed by SDSPAGE/western blot using a Cox2-specific antibody to detect CcO abundance. Stain free imaging served as a loading control. *coa6Δ* cell lysate was used as control for decreased Cox2 levels. (C) Vacuolar pH of WT and *aps3Δ* cells was measured by using BCECF-AM dye. Data is expressed as mean ± SD; (n = 3), **$p = 0.0046$. Each data point represents a biological replicate. (D) Whole cell lysate and isolated vacuole fractions were analyzed by SDSPAGE/western blot. Vma2 was used to determine V-ATPase abundance. Prc1 and Pgk1 served as loading controls for vacuole and whole cell protein lysate, respectively. (Figure reprinted from Garza et al., 2021).

AP-3 complex function has not been directly linked to mitochondria but is linked to the trafficking of proteins from the Golgi body to the vacuole. Therefore, the decreased abundance of Cox2 in AP-3 mutants could be due to an indirect effect involving the vesicular trafficking role of the AP-3 complex. A previous study has shown that the AP-3 complex interacts with a subunit of the V-ATPase in human cells

(Bagh et al., 2017). As perturbations in V-ATPase function had been linked to defective respiratory growth (Chen et al., 2020; Hughes et al., 2020; Ohya et al., 1991; Eide et al., 1993; Hughes and Gottschling, 2012), we sought to determine if AP-3 impacts mitochondrial function *via* trafficking V-ATPase subunit(s) to the vacuole. We first measured vacuolar acidification and found that the AP-3 mutant, *aps3Δ*, exhibited significantly increased vacuolar pH (Figure 2.6C). We hypothesized that the elevated vacuolar pH of *aps3Δ* cells could be due to a perturbation in the trafficking of V-ATPase subunit(s). To test this possibility, we measured the levels of V-ATPase subunit Vma2, in wild type (WT) and *aps3Δ* cells, by western blotting and found that Vma2 levels were indeed reduced in the isolated vacuolar fractions of *aps3Δ* cells but were unaffected in the whole cells (Figure 2.6D). The decreased abundance of Vma2 in vacuoles of yeast AP-3 mutant explains decreased vacuolar acidification because Vma2 is an essential subunit of V-ATPase. Taken together, these results suggest that the AP-3 complex is required for maintaining vacuolar acidification, which in turn could impact mitochondrial copper homeostasis.
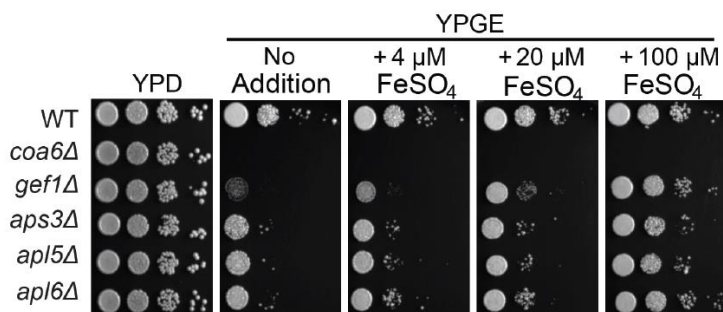
Figure 2.7 Respiratory growth of AP-3 mutants is restored by high iron supplementation
Serial dilutions of WT and the indicated mutants were seeded onto YPD and YPGE plates with and without 4, 20 or 100 μM FeSO₄ at 37°C and grown for two (YPD) or four days (YPGE).

Here *gef1Δ* cells were used as a positive control for iron-based rescue. (Figure reprinted from Garza et al., 2021).

Genetic defects in Rim101 pathway perturb mitochondrial copper homeostasis

Next, we focused on two other hits from the screen, Rim20 and Rim21, which are the members of the Rim101 pathway that has been previously linked to the V-ATPase expression (Maeda, 2012; Pérez-Sampietro and Herrero, 2014; Read et al., 2016; Xu et al., 2004). The loss of Rim101 results in the decreased expression of V-ATPase subunits (Pérez-Sampietro and Herrero, 2014; Read et al., 2016). Consistently, we found elevated vacuolar pH in *rim20Δ* cells (Figure 2.8A). We then compared the respiratory growth of *rim20Δ* and *rim21Δ* on YPD and YPGE media with or without Cu, Zn, or Mg supplementation. Consistent with our screening results, these mutants exhibited reduced respiratory growth that was fully restored by copper but not magnesium or zinc (Figure 2.8B). To directly test the roles of these genes in cellular copper homeostasis, we measured the whole-cell copper levels of *rim20Δ* by inductively coupled plasma–mass spectrometry (ICP-MS). The intracellular copper levels under basal or copper-supplemented conditions in *rim20Δ* cells were comparable to WT cells, suggesting that the copper import or sensing machinery is not defective in this mutant (Figure 2.8C). In contrast to the total cellular copper levels, *rim20Δ* did exhibit significantly reduced mitochondrial copper levels, which were restored by copper supplementation (Figure 2.8D).

Figure 2.8 Normalization of vacuolar pH in *rim20Δ* cells restores mitochondrial copper homeostasis

(A)Vacuolar pH of WT and *rim20Δ* cells was measured by BCECF-AM dye, **$p = 0.0012$. (B) Serial dilutions of WT and the indicated mutants were seeded onto YPD and YPGE plates with or without 5 μM $CuCl_2$, $MgCl_2$, or $ZnCl_2$ and grown at 37°C for two (YPD) or four days
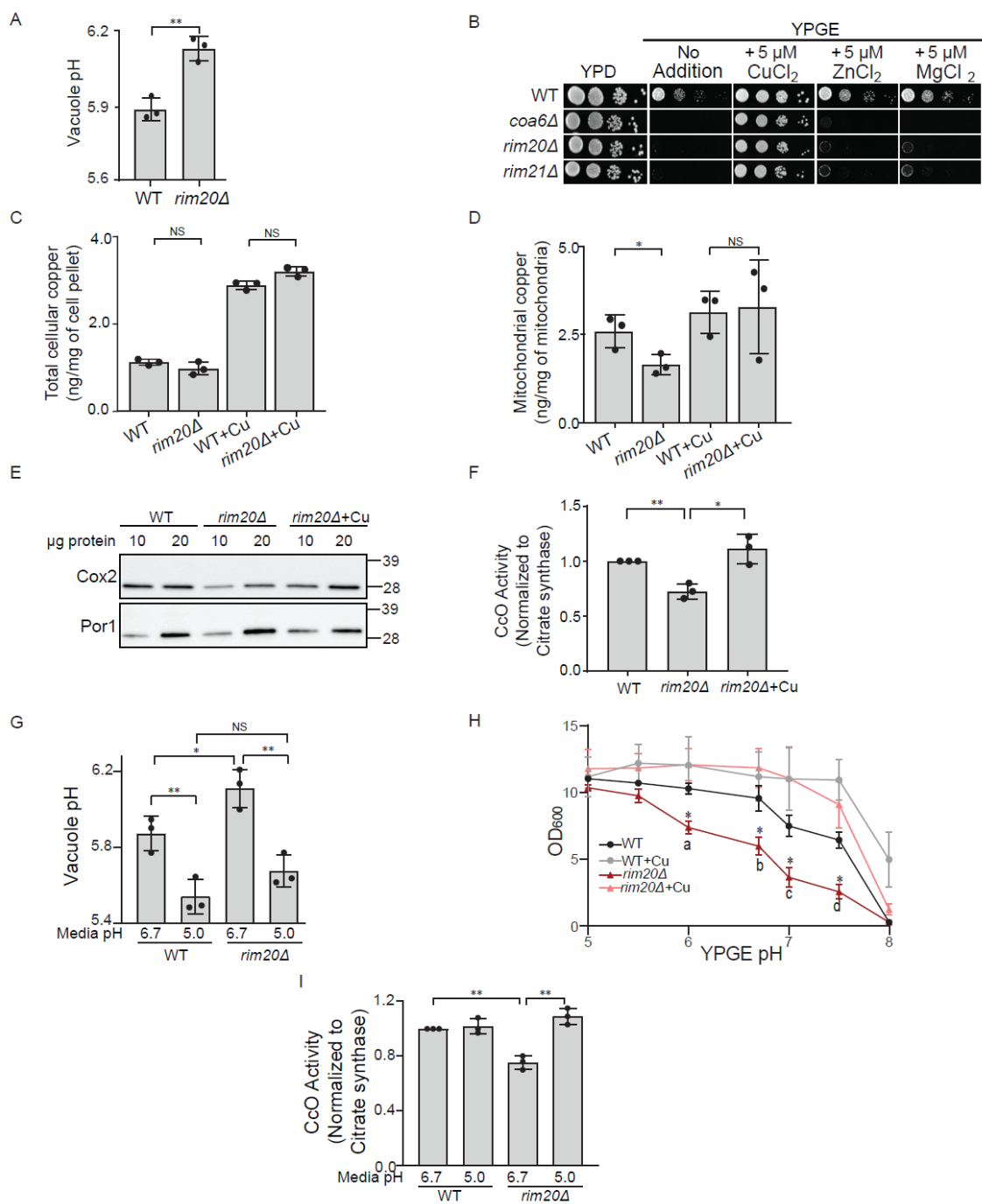
(YPGE). (C) Cellular and (D) mitochondrial copper levels were measured by ICP-MS, $*p = 0.0399$ (E) Mitochondrial proteins were analyzed by SDS-PAGE/western blot. Cox2 served as a marker for CcO levels, and Por1 served as a loading control. (F) CcO activity was measured spectrophotometrically and normalized to the citrate synthase activity, $*p = 0.0194$, $**p = 0.0023$. (G) Vacuolar pH of WT and *rim20Δ* cultured in standard (pH 6.7) or acidified (pH 5.0) YPGE medium was measured by BCECF-AM dye, (WT 6.7 vs WT 5.0, $**p = 0.0098$), (WT 6.7 vs *rim20Δ* 6.7, $*p = 0.0388$), (*rim20Δ* 6.7 vs *rim20Δ* 5.0, $**p = 0.0045$). (H) The optical density of WT and *rim20Δ* cultures after 42 hours growth in YPGE medium at the indicated pH values with or without 5 μM CuCl$_2$. a-d indicate minimum significance values between *rim20Δ* and the other tested conditions. a ($p = 0.0290$), b ($p = 0.0268$), c ($p = 0.0245$), d ($p = 0.0167$). (I) CcO activity of WT and *rim20Δ* cultured in standard or acidified YPGE was normalized to citrate synthase activity, (WT 6.7 vs *rim20Δ* 6.7, $**p = 0.0011$), (*rim20Δ* 6.7 vs *rim20Δ* 5.0, $**p = 0.0017$). Data are expressed as mean ± SD; NS = not significant, (n = 3). Each data point represents a biological replicate. (Figure reprinted from Garza et al., 2021).

The decrease in mitochondrial copper levels is expected to perturb the biogenesis of CcO in *rim20Δ* cells. Therefore, we measured the abundance and activity of this complex by western blot analysis and enzymatic assay, respectively. Consistent with the decrease in mitochondrial copper levels, *rim20Δ* cells exhibited a reduction in the abundance of Cox2 along with a decrease in CcO activity, both of which were rescued by copper supplementation (Figure 2.8 E and F). To further dissect the compartment-specific effect by which Rim20 impacts cellular copper homeostasis, we measured the abundance and activity of Sod1, a mainly cytosolic cuproenzyme. We found that unlike CcO, Sod1 abundance and activity remain unchanged in *rim20Δ* cells (Figure 2.9).

To determine if the decrease in CcO activity in the absence of Rim20 was due to its role in maintaining vacuolar pH, we manipulated vacuolar pH by changing the pH of the growth media. Previously, it has been shown that vacuolar pH is influenced by the pH of the growth media through endocytosis (Brett et al., 2011; Orij et al., 2012). Indeed, acidifying growth media to pH 5.0 from the basal pH of 6.7 normalized vacuolar pH of *rim20Δ* to the WT levels and both strains exhibited lower vacuolar pH when

grown in acidified media (Figure 2.8G). Under these conditions of reduced vacuolar pH, the respiratory growth of *rim20Δ* was restored to WT levels (Figure 2.8H). Notably, alkaline media also reduced the respiratory growth of WT cells, though the extent of growth reduction was lower than *rim20Δ*, which is likely because of a fully functional V-ATPase in WT cells (Figure 2.8H). The restoration of respiratory growth by copper supplementation was independent of growth media pH (Figure 2.8H). To uncover the biochemical basis of the restoration of respiratory growth of *rim20Δ* by acidified media, we measured CcO enzymatic activity in WT and *rim20Δ* cells grown in either basal or acidified growth medium (pH 6.7 and 5.0), respectively. Consistent with the respiratory growth rescue, the CcO activity was also restored in cells grown at an ambient pH of 5.0 (Figure 2.8I). Taken together, these findings causally link vacuolar pH to CcO activity *via* mitochondrial copper homeostasis.
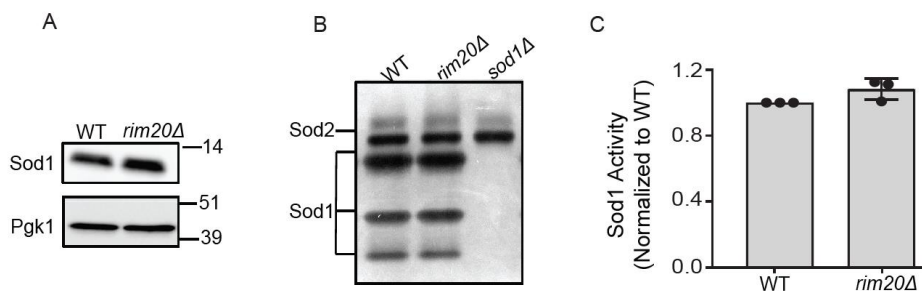
Figure 2.9 Activity of cytosolic cuproenzyme Sod1 is not altered in *rim20Δ* cells
(A)Crude cytosolic fraction was analyzed by SDSPAGE/western blot to detect Sod1 abundance in the indicated strains. Pgk1 was used as a loading control. (B) Sod activity in isolated crude cytosolic fraction from the indicated strains was measured by in-gel assay as described in Methods. (C) For quantification of the Sod1 activity in (B), the images were digitalized and densitometry analysis was performed using the Image Lab software. (Figure reprinted from Garza et al., 2021).

Pharmacological inhibition of the V-ATPase results in decreased mitochondrial copper

        To directly assess the role of vacuolar pH in maintaining mitochondrial copper homeostasis, we utilized Concanamycin A (ConcA), a small-molecule inhibitor of V-ATPase. Treating WT cells with increasing concentrations of ConcA led to progressively increased vacuolar pH (Figure 2.10A). Notably, the increase in vacuolar pH with pharmacological inhibition of V-ATPase by ConcA was much more pronounced (Figure 2.10A) than *via* genetic perturbation in *aps3Δ* or *rim20Δ* cells (Figure 2.6C And 2.8A). Correspondingly, we observed a pronounced decrease in CcO abundance and activity in ConcA-treated cells (Figure 2.10 B and C). This decrease in abundance of CcO is likely due to a reduction in mitochondrial copper levels (Figure 2.10D). This data establishes the role of the vacuole in regulating mitochondrial copper homeostasis and CcO function.
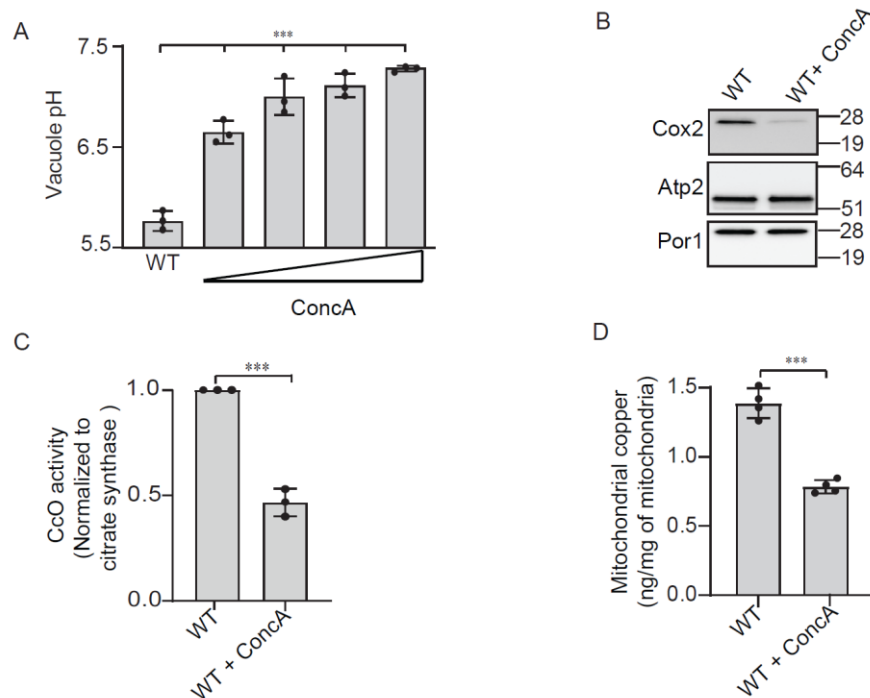
Figure 2.10 Pharmacological inhibition of V-ATPase decreases mitochondrial copper content
(A)Vacuolar pH of WT cells grown in the presence of either DMSO or 125, 250, 500, 1000 nM ConcA, (WT vs WT + 125 nM ConcA, $p = 0.0005$), (WT vs WT + 250 nM ConcA, $p = 0.0005$), (WT vs WT + 500 nM ConcA, $p = 0.0001$), (WT vs WT + 1000 nM ConcA, $p < 0.0001$). (B) Mitochondrial proteins in WT cells treated with DMSO or 500 nM ConcA were analyzed by SDSPAGE/western blot. Cox2 served as a marker for CcO abundance, Atp2 and Por1 were used as loading controls. (C) CcO activity in WT cells treated with DMSO or 500 nM ConcA is shown after normalization with citrate synthase activity, ***$p = 0.0001$. (D) Mitochondria copper levels in WT cells treated with DMSO or 500 nM ConcA were determined by ICP-MS, ***$p < 0.0001$. Data are expressed as mean ± SD; (n = 3 or 4). Each data point represents a biological replicate. (Figure reprinted from Garza et al., 2021).

Discussion

Mitochondria are the major intracellular copper storage sites that harbor important cuproenzymes like CcO. When faced with copper deficiency, cells prioritize mitochondrial copper homeostasis suggesting its critical requirement for this organelle (Dodani et al., 2011). However, the complete set of factors required for mitochondrial copper homeostasis has not been identified. Here, we report a number of novel genetic

regulators of mitochondrial copper homeostasis that link mitochondrial bioenergetic function with vacuolar pH. Specifically, we show that when vacuolar pH is perturbed by genetic, environmental, or pharmacological factors, copper availability to the mitochondria is subsequently limited, which in turn reduces CcO function and impairs aerobic growth and mitochondrial respiration.

It has been known for a long time that V-ATPase mutants have severely reduced respiratory growth (Ohya et al., 1991; Eide et al., 1993) and more recent high-throughput studies have corroborated these observations (Merz and Westermann, 2009; Schlecht et al., 2014; Stenger et al., 2020). However, the molecular mechanisms underlying this observation have remained obscure. Recent studies have shown that a decrease in vacuolar acidity (*i.e.*, increased vacuolar pH) perturbs cellular and mitochondrial iron homeostasis, which impairs mitochondrial respiration, as iron is also required for electron transport through the mitochondrial respiratory chain due to its role in iron–sulfur cluster biogenesis and heme biosynthesis (Chen et al., 2020; Hughes et al., 2020; Weber et al., 2020; Yambire et al., 2019). In an elegant series of experiments, Hughes *et al.* (Hughes et al., 2020) showed that when V-ATPase activity is compromised, there is an elevation in cytosolic amino acids because vacuoles with defective acidification are unable to import and store amino acids. The resulting elevation in cytosolic amino acids, particularly cysteine, disrupts cellular iron homeostasis and iron-dependent mitochondrial respiration. Although this exciting study took us a step closer to our understanding of V-ATPase-dependent mitochondrial function, the mechanism by which elevated cysteine perturbs iron homeostasis is still

unclear. Since cysteine can strongly bind copper (Giles et al., 2003; Rigo et al., 2004) its sequestration in cytosol by cysteine would decrease its availability to Fet3, a multicopper oxidase (Taylor et al., 2005) required for the uptake of extracellular iron, which in turn would aggravate iron deficiency. Thus, a defect in cellular copper homeostasis could cause a secondary defect in iron homeostasis. Consistent with this idea, we observed a rescue of AP-3 mutants' respiratory growth with high iron supplementation (Figure 2.7). Interestingly, AP-3 has also been previously linked to vacuolar cysteine homeostasis (Llinares et al., 2015).

Our results showing diminished CcO activity and/or Cox2 levels in AP-3, Rim20, and ConcA-treated cells (Figure 2.6B, Figure 2.8, E and F, and Figure 2.10, B and C) connect vacuolar pH to mitochondrial copper biology. However, a modest decrease in CcO activity may not be sufficient to reduce respiratory growth. Therefore, it is very likely that the decreased respiratory growth we have observed is a result of a defect not only in copper but also in iron homeostasis. Consistent with this idea, previous high-throughput studies reported sensitivity of AP-3 and Rim101 pathway mutants in conditions of iron deficiency and overload (Jo et al., 2008; Jo et al., 2009). Moreover, Rim20 and Rim101 mutants have been shown to display sensitivity to copper starvation in *Cryptococcus neoformans*, an opportunistic fungal pathogen (Chun et al., 2010) and partial knockdown of Ap3s1, a subunit of AP-3 complex in zebrafish, sensitized developing melanocytes to hypopigmentation in low-copper environmental conditions (Ishizaki et al., 2010). Thus, the Rim pathway and the AP-3 pathway are linked to copper homeostasis in multiple organisms. Our discovery of AP-3 pathway

mutants and other mutants involved in the Golgi-to-vacuole transport (Figure 2.5) is also consistent with a previous genome-wide study, which identified the involvement of these genes in Cu-dependent growth of yeast *S. cerevisiae* (Schlecht et al., 2014); however, the biochemical mechanism underlying the functional connection between the vacuole and mitochondrial CcO was not previously elucidated. Thus, the results from our study are not only consistent with previous studies but also provide a biochemical mechanism elucidating how disruption in vacuolar pH perturbs mitochondrial respiratory function *via* copper dependence of CcO. Interestingly, in both the genetic and pharmacological models of reduced V-ATPase function, mitochondrial copper levels were reduced (Figure 2.8D and Figure 2.10D) but were not absent, suggesting that the vacuole may only partially contribute to mitochondrial Cu homeostasis. Supporting this hypothesis, rescue of respiratory growth by copper supplementation was successful irrespective of vacuolar pH (Figure 2.8H).

The results of this study could also provide insights into mechanisms underlying the pathogenesis of human diseases associated with aberrant copper metabolism and/or decreased V-ATPase function including Alzheimer's disease, amyotrophic lateral sclerosis (ALS), and Parkinson's disease (Colacurcio and Nixon et al., 2016; Corrionero and Horvitz, 2018; Desai and Kaler, 2008; Kaler, 2013; Nixon et al., 2008; Nguyen et al., 2019; Stepien et al., 2020). Although multiple factors are known to contribute to the pathogenesis of these diseases, our study suggests that disrupted mitochondrial copper homeostasis may also be an important contributing factor. In contrast to these multifactorial diseases, pathogenic mutations in AP-3 subunits are known to cause

Hermansky–Pudlak syndrome (HPS), a rare autosomal disorder, which is often associated with high morbidity (Ammann et al., 2016; Dell'Angelica et al., 1999; El-Chemaly and Young, 2016). Just as in yeast, AP-3 in humans is required for the transport of vesicles to the lysosome, which is evolutionarily and functionally related to the yeast vacuole. Our study linking AP-3 to mitochondrial function suggests that decreased mitochondrial function could contribute to HPS pathology. More generally, decreased activity of V-ATPase has been linked to age-related decrease in lysosomal function (Bagh et al., 2017; Korvatska et al., 2013; Lee et al., 2010) and impaired acidification of yeast vacuole has been shown to cause accelerated aging (Hughes and Gottschling 2012). Therefore, in addition to uncovering the fundamental aspects of cell biology of metal transport and distribution, our study suggests a possible role of mitochondrial copper in multiple human disorders.

Experimental procedures

Yeast strains and growth conditions

Individual yeast *S. cerevisiae* mutants used in this study were obtained from Open Biosystems or were constructed by one-step gene disruption using a hygromycin cassette (Janke et al., 2004). All strains used in this study are listed in Table 2.1. Authenticity of yeast strains was confirmed by polymerase chain reaction (PCR)-based genotyping. Yeast cells were cultured in either YPD (1% yeast extract, 2% peptone, and 2% dextrose [w/v]) or YPGE (3% glycerol +1% ethanol [w/v]) medium. Solid YPD and YPGE media were prepared by addition of 2% (w/v) agar. For metal supplementation experiments,

growth medium was supplemented with divalent chloride salts of Cu, Mn, Mg, Zn, or FeSO$_4$. For growth on solid media, 3 µl of tenfold serial dilutions of precultures was seeded onto YPD or YPGE plates and incubated at 37 °C for the indicated period. For growth in the liquid medium, yeast cells were precultured in YPD and inoculated into YPGE and grown to mid-log phase. To acidify or alkalinize liquid YPGE, equivalents of HCl or NaOH were added, respectively. Liquid growth assays in acidified or alkalinized YPGE cultures involved growth for 42 h. For growth in the presence of concanamycin A (ConcA), cells were first cultured in YPD, transferred to YPGE and allowed to grow for 24 h, then ConcA was added and allowed to grow further for 20 h. Growth in liquid media was monitored spectrophotometrically by measuring optical density at 600 nm.

Construction of yeast deletion pool

The yeast deletion collection for Bar-Seq analysis was derived from the Variomics library constructed previously (Huang et al., 2013) and was a kind gift of Xuewen Pan. The heterozygous diploid deletion library was sporulated and selected in liquid haploid selection medium (SC-Arg-His-Leu+G418+Canavanine) to obtain haploid cells containing gene deletions. To do this, we followed previously described protocol (Huang et al., 2013) with the following modification of adding uracil to allow the growth of deletion library lacking *URA3*. Prior to sporulation, the library pool was grown under conditions to first allow loss of *URA3* plasmids and then subsequent selection for cells lacking *URA3* plasmids. Original deletion libraries were initially constructed where each yeast open reading frame (ORF) was replaced with *kanMX4* cassette containing two

gene-specific barcode sequences referred to as the UP tag and the DN tag since they are located upstream and downstream of the cassette (Pan et al., 2004), respectively.

Pooled growth assays

A stored glycerol stock of the haploid deletion pool containing 1.5×10^8 cells/ml (equivalent of 3.94 optical density/ml) was thawed and approximately 60 µl was used to inoculate 6 ml of YPD, YPGE or YPGE +5 µM CuCl$_2$ media in quadruplicates in 50 ml falcon tubes at a starting optical density of 0.04, which corresponded to ∼1.5×10^6 cells/ml. The cells were grown at 30 °C in an incubator shaker at 225 rpm until they reached an optical density of ∼5.0 before harvesting. Cells were pelleted by centrifugation at 3000g for 5 min and washed once with sterile water and stored at –80 °C. Frozen cell pellets were thawed and resuspended in sterile nanopure water and counted. Genomic DNA was extracted from 5×10^7 cells using YeaStar Genomic DNA kit (Catalog No.D2002) from Zymo Research. The extracted DNA was used as a template to amplify barcode sequence by PCR, followed by purification of amplified DNA by QIAquick PCR purification kit from Qiagen. The number of PCR cycles used for amplification was determined by quantitative real-time PCR such that barcode sequence amplification did not exit the exponential portion of the PCR reaction. The amplified UP and DN barcode DNA were purified by gel electrophoresis and sequenced on Illumina HiSeq 2500 with 50 base pair, paired-end sequencing at Genomics and Bioinformatics Service of Texas A&M AgriLife Research.

Assessing fitness of barcoded yeast strains by DNA sequencing

The sequencing reads were aligned to the barcode sequences using Bowtie2 (version 2.2.4) with the -N flag set to 0. Bowtie2 outputs were processed and counted using Samtools (version 1.3.1). Barcode sequences shorter than 15 nts or mapped to multiple reference barcodes were discarded. We noted that the DN tag sequences were missing for many genes and therefore we only used UP tag sequences to calculate the fitness score using T statistics. At a sequencing depth of 500,000 reads, UP tag sequences could be detected at the final timepoint in the YPD media for 82.7% (3984/4817) of nonessential yeast ORFs and 27.5% (305/1110) of essential yeast ORFs for a total genomic coverage of 72.5% (4927/5927) of all yeast ORFs.

Gene ontology analysis

To identify enriched gene ontology terms, we generated a rank-ordered list based on T-Scores (Supplementary tables 1 and 3) and used the reference genome for *S. cerevisiae* in GOrilla (http://cbl-gorilla.cs.technion.ac.il/).

Cellular and mitochondrial copper measurements

Cellular and mitochondrial copper levels were measured by ICP-MS using NexION 300D instrument from PerkinElmer Inc. Briefly, intact yeast cells were washed twice with ultrapure metal-free water containing 100 μM EDTA (TraceSELECT; Sigma) followed by two more washes with ultrapure water to eliminate EDTA. For mitochondrial samples, the same procedure was performed using 300 mM mannitol (TraceSELECT; Sigma) to maintain mitochondrial integrity. After washing, samples were weighed, digested with 40% (w/v) nitric acid (TraceSELECT; Sigma) at 90 °C for

18 h, followed by 6 h digestion with 0.75% H$_2$O$_2$ (Sigma-Supelco), then diluted in ultrapure water, and analyzed. Copper standard solutions were prepared by diluting commercially available mixed metal standards (BDH Aristar Plus).

Subcellular fractionation

Whole-cell lysates were prepared by resuspending ~100 mg of yeast cells in 350 µl SUMEB buffer (1.0% [w/v] sodium dodecyl sulfate, 8 M urea, 10 mM MOPS, pH 6.8, 10 mM EDTA, 1 mM Phenylmethanesulfonyl fluoride [PMSF], and 1X EDTA-free protease inhibitor cocktail from Roche) containing 350 mg of acid-washed glass beads (Sigma-Aldrich). Samples were then placed in a bead beater (mini bead beater from Biospec products), which was set at maximum speed. The bead beating protocol involved five rounds, where each round lasted for 50 s followed by 50 s incubation on ice. Lysed cells were kept on ice for 10 min, then heated at 70°C for 10 min. Cell debris and glass beads were spun down at 14,000g for 10 min at 4°C. The supernatant was transferred to a separate tube and was used to perform SDS-PAGE/western blotting.

Mitochondria were isolated as described previously (Meisinger et al., 2006). Briefly, 0.5–2.5 g of cell pellet was incubated in DTT buffer (0.1 M Tris-HCl, pH 9.4, 10 mM DTT) at 30°C for 20 min. The cells were then pelleted by centrifugation at 3000g for 5 min, resuspended in spheroplasting buffer (1.2 M sorbitol, 20 mM potassium phosphate, pH 7.4) at 7 ml/g, and treated with 3 mg zymolyase (US Biological Life Sciences) per gram of cell pellet for 45 min at 30°C. Spheroplasts were pelleted by centrifugation at 3000g for 5 min, then homogenized in homogenization buffer (0.6 M sorbitol, 10 mM Tris-HCl, pH 7.4, 1 mM EDTA, 1 mM PMSF, 0.2% [w/v] bovine

serum albumin (BSA) [essentially fatty acid-free, Sigma-Aldrich]) with 15 strokes using a glass Teflon homogenizer with pestle B. After two centrifugation steps for 5 min at 1500g and 4000g, the final supernatant was centrifuged at 12,000g for 15 min to pellet mitochondria. Mitochondria were resuspended in SEM buffer (250 mM sucrose, 1 mM EDTA, 10 mM MOPS-KOH, pH 7.2, containing 1X protease inhibitor cocktail from Roche).

Isolation of pure vacuoles was performed as previously described (Haas, 1995). Yeast spheroplasts were pelleted at 3000g at 4°C for 5 min. Dextran-mediated spheroplast lysis of 1 g of yeast cells was performed by gently resuspending the pellet in 2.5 ml of 15% (w/v) Ficoll400 in Ficoll Buffer (10 mM PIPES/KOH, 200 mM sorbitol, pH 6.8, 1 mM PMSF, 1X protease inhibitor cocktail) followed by addition of 200 μl of 0.4 mg/ml dextran in Ficoll buffer. The mixture was incubated on ice for 2 min followed by heating at 30 °C for 75 s and returning the samples to ice. A step-Ficoll gradient was constructed on top of the lysate with 3 ml each of 8%, 4%, and 0% (w/v) Ficoll400 in Ficoll Buffer. The step gradient was centrifuged at 110,000g for 90 min at 4°C. Vacuoles were removed from the 0%/4% Ficoll interface.

Crude cytosolic fractions used to quantify Sod1 activity and abundance were isolated as described previously (Horn et al., 2008). Briefly, ∼70 mg of yeast cells were resuspended in 100 μl of solubilization buffer (20 mM potassium phosphate, pH 7.4, 4 mM PMSF, 1 mM EDTA, 1X protease inhibitor cocktail, 1% [w/v] Triton X-100) for 10 min on ice. The lysate was extracted by centrifugation at 21,000g for 15 min at 4°C,

to remove the insoluble fraction. Protein concentrations for all cellular fractions were determined by the BCA assay (Thermo Scientific).

SDS-PAGE and western blotting

For SDS–polyacrylamide gel electrophoresis (SDS-PAGE)/western blotting experiments, 20 µg of protein was loaded for either whole cell lysate or mitochondrial samples, while 30 µg of protein was used for cytosolic and vacuolar fractions. Proteins were separated on 4–20% stain-free gels (Bio-Rad) or 12% NuPAGE Bis-Tris mini protein gels (Thermo Fisher Scientific) and blotted onto a polyvinylidene difluoride membranes. Membranes were blocked for 1 h in 5% (w/v) nonfat milk dissolved in Tris-buffered saline with 0.1% (w/v) Tween 20 (TBST-milk), followed by overnight incubation with a primary antibody in TBST-milk or TBST- 5% (w/v) BSA at 4°C. Primary antibodies were used at the following dilutions: Cox2, 1:50,000 (Abcam 110271); Por1, 1:100,000 (Abcam 110326); Pgk1, 1:50,000 (Life Technologies 459250), Sod1, 1:5000, and Vma2, 1:10,000 (Sigma H9658). Secondary antibodies (GE Healthcare) were used at 1:5000 for 1 h at room temperature. Membranes were developed using Western Lightning Plus-ECL (PerkinElmer) or SuperSignal West Femto (Thermo Fisher Scientific).

Enzymatic activities

To measure Sod1 activity, we used an in-gel assay as described previously, (Flohe and Otting, 1984). Twenty-five micrograms of cytosolic protein was diluted in NativePAGE sample buffer (Thermo Fisher Scientific) and separated onto a 4–16% NativePAGE gel (Thermo Fisher Scientific) at 4°C. The gel was then stained with 0.025% (w/v) nitroblue

tetrazolium, 0.010% (w/v) riboflavin for 20 min in the dark. This solution was then replaced by 1% (w/v) tetramethylethylenediamine for 20 min and developed under a bright light. The gel was imaged by Bio-Rad ChemiDoc MP Imaging System and densitometric analysis was performed using Image Lab software.

CcO and citrate synthase enzymatic activities were measured as described previously (Spinazzi et al., 2012) using a BioTek's Synergy Mx Microplate Reader in a clear 96-well plate (Falcon). To measure CcO activity, 15 µg of mitochondria was resuspended in 115 µl of CcO buffer (250 mM sucrose, 10 mM potassium phosphate, pH 6.5, 1 mg/ml BSA) and allowed to incubate for 5 min. The reaction was started by the addition of 60 µl of 200 µM reduced cytochrome c (equine heart, Sigma) and 25.5 µl of 1% (w/v) N-Dodecyl-Beta-D-Maltoside. Oxidation of cytochrome c was monitored at 550 nm for 3 min, then the reaction was inhibited by the addition of 7 µl of 7 mM KCN. To measure citrate synthase activity, 10 µg of mitochondria was resuspended in 100 µl of citrate synthase buffer (10 mM Tris-HCl pH 7.5, 0.2% [w/v] Triton X-100, 200 µM 5,5′-dithio-bis-[2-nitrobenzoic acid]) and 50 µl of 2 mM acetyl-CoA and incubated for 5 min. To start the reaction, 50 µl of 2 mM oxaloacetate was added and turnover of acetyl-CoA was monitored at 412 nm for 10 min. Enzyme activity was normalized to that of WT for each replicate.

Measuring vacuolar pH

Vacuolar pH was measured using a ratiometric pH indicator dye, BCECF-AM (2′,7′-bis-(2-carboxyethyl)-5-(and-6)-carboxyfluorescein [Life Technologies]) as described by (Diakov et al., 2013) using a BioTek's Synergy Mx Microplate Reader. Briefly, 100 mg

of cells were resuspended in 100 μl of YPGE containing 50 μM BCECF-AM for 30 min shaking at 30°C. To remove extracellular BCECF-AM, cells were washed twice and resuspended in 100 μl of fresh YPGE. In total, 25 μl of this cell culture was added to 2 ml of 1 mM MES buffer, pH 6.7 or 5.0. The fluorescence emission intensity at 535 nm was monitored by using the excitation wavelengths 450 and 490 nm in a clear bottom black 96-well plate, (Falcon). A calibration curve of the fluorescence intensity in response to pH was carried out as described (Diakov et al., 2013).

Statistics

T-scores for each pairwise media comparison (*e.g.*, YPD *versus* YPGE) were calculated using Welch's two-sample *t* test for yeast knockout barcode abundance values normalized for sample sequencing depth (*i.e.*, counts per million). Statistical analysis on bar charts was conducted using two-sided Student's *t* test. Experiments were performed in three or four biological replicates, where biological replicates are defined as experiments performed on different days and different starting preculture. Error bars represent the standard deviation.

Table 2.1 *Saccharomyces cerevisiae* strains used in this study
Table reprinted from Garza et al., 2021.

Yeast Strains	Genotype	Source
BY4741 WT	*MATa, his3Δ1, leu2Δ0, met15Δ0, ura3Δ0*	Greenberg, M.L.
BY4741 *coa6Δ*	*MATa, his3Δ1, leu2Δ0, met15Δ0, ura3Δ0, coa6Δ::kanMX4*	Open Biosystems
BY4741 *gef1Δ*	*MATa, his3Δ1, leu2Δ0, met15Δ0, ura3Δ0, gef1Δ::kanMX4*	Open Biosystems
BY4741 *aps3Δ*	*MATa, his3Δ1, leu2Δ0, met15Δ0, ura3Δ0, aps3Δ::kanMX4*	Open Biosystems
BY4741 *aps3Δ*-NMG	*MATa, his3Δ1, leu2Δ0, met15Δ0, ura3Δ0, aps3Δ::hphMX4*	This study
BY4741 *apm3Δ*	*MATa, his3Δ1, leu2Δ0, met15Δ0, ura3Δ0, apm3Δ::kanMX4*	Open Biosystems
BY4741 *apl5Δ*	*MATa, his3Δ1, leu2Δ0, met15Δ0, ura3Δ0, apl5Δ::kanMX4*	Open Biosystems
BY4741 *apl6Δ*	*MATa, his3Δ1, leu2Δ0, met15Δ0, ura3Δ0, apl6Δ::hphMX4*	Open Biosystems
BY4741 *rim20Δ*	*MATa, his3Δ1, leu2Δ0, met15Δ0, ura3Δ0, rim20Δ::kanMX4, grx1Δ:: hphMX4*	Open Biosystems
BY4741 *rim20Δ* - NMG	*MATa, his3Δ1, leu2Δ0, met15Δ0, ura3Δ0, rim20Δ::hphMX4*	This study
BY4741 *rim21Δ*	*MATa, his3Δ1, leu2Δ0, met15Δ0, ura3Δ0, rim21Δ::kanMX4,*	Open Biosystems

Data Availability

The data presented in this chapter is published by the Journal of Biological Chemistry and available in the supplementary files. Supplementary table 1 is a ranked list of the genes with the smallest to largest T-score in respiratory media compared to fermentable media (YPGE-YPD). Supplementary table 2 contains a list of yeast genes encoding OXPHOS proteins and OXPHOS assembly factors. Supplementary table 3 is a ranked list of the genes with the smallest to largest T-score in copper containing respiratory media compared to respiratory media not supplemented with copper (YPGECu-YPGE).

CHAPTER III

ELESCLOMOL ELEVATES CELLULAR AND MITOCHONDRIAL IRON

CONTENT IN YEAST BY DELIVERING COPPER TO IRON IMPORT

MACHINERY

Summary

Copper and iron are redox active metals that act as cofactors for many essential
cellular enzymes. Disruption in the intracellular homeostasis of either of these metals
results in debilitating and fatal human disorders. Recently, we reported that an
investigational anticancer drug, elesclomol (ES), can deliver copper to critical
mitochondrial cuproenzymes and has the potential to be repurposed for the treatment of
copper deficiency disorders. Here, we sought to determine the specificity of ES and ES-
Cu complex in intracellular metal homeostasis. Using a combination of yeast genetics
and ICP-MS based intracellular metal measurements, we showed that ES and ES-Cu
treatment results in a striking increase in cellular and mitochondrial Fe content, along
with copper. By utilizing yeast mutants of copper and iron transporters, we demonstrate

that ES-based elevation in cellular iron levels is independent of the major cellular copper importer but is dependent on the Fe importer Ftr1 and its partner Fet3, a multicopper-oxidase. As Fet3 is metalated in the Golgi lumen, we sought to uncover the mechanism by which Fet3 receives copper via ES. Using yeast knockouts of genes that encode proteins involved in copper delivery to Fet3, we determined that ES can bypass Atx1 and Grx1, proteins involved in copper delivery to Ccc2, a Golgi membrane localized ATPase that pumps copper from cytosol into the Golgi lumen. In contrast, Ccc2 is essential for ES-mediated increase in cellular iron. Taken together, our study provides a mechanism by which ES distributes copper in cells and impacts cellular and mitochondrial iron homeostasis.

Introduction

Copper is an essential micronutrient that is utilized as a cofactor for a diverse array of enzymes involved different physiological processes (Festa and Thiele 2011). For example, copper plays an essential and evolutionarily conserved role in mitochondrial energy generation, free radical detoxication and iron import. In addition to these fundamental cellular processes, the redox properties of copper are harnessed into more specialized functions such as melanin production, collagen formation, and catecholamine synthesis in evolutionarily advanced organisms like humans (Festa and Thiele 2011). However, copper is also highly reactive and can generate deleterious reactive oxygen species (ROS) (Halliwell et al., 1984). Therefore, copper transporters and chaperones control copper ion levels and bioavailability to ensure proper subcellular and systemic copper distribution while avoiding toxicity (Nevitt et al., 2012; Kim et al., 2008).

Genetic mutations that impair copper absorption or its transport to copper-containing enzymes (cuproenzymes) often manifest in fatal disorders (Tümer et al., 2010; Kodama et al., 2012; Gupta and Lutsenko, 2009; Kaler, 2013; Papadopoulou et al., 199; Valnot et al., 2000; Baertling et al., 2015). For example, mutations in copper chaperones that are required for copper delivery to a mitochondrial cuproenzyme, cytochrome *c* oxidase (CcO), result in mitochondrial disorders that typically present as fatal neurological and cardiac defects in infants (DiMauro et al., 2012; Papdopoulou et al., 1999; Valnot et al., 2000; Baertling et al., 2015). Loss-of-function mutations in

ATP7A, a protein required for dietary copper absorption and its transport through the blood-brain barrier, result in a fatal neurological disorder called Menkes disease (Tümer et al., 2010; Kodama et al., 2012; Gupta and Lutsenko, 2009; Kaler, 2013; Vulpe et al., 1993; Mercer et al., 1993; Kaler, 2011). Currently, no FDA-approved treatment is available for these disorders (Horn et al., 2019).

Recently we showed that elesclomol (ES), a copper-binding investigational oncology drug, can traverse through cellular membranes and deliver copper to cuproenzymes such as mitochondrial CcO and rescue copper-deficient phenotypes in yeast, zebrafish, and murine models (Soma et al., 2018; Guthrie et al., 2020). This exciting finding has raised the possibility of repurposing this cancer drug for the treatment of copper deficiency disorders (Gohil, 2021). ES is a bis(thiohydrazide) amide compound that was originally developed as an anticancer drug. Mechanistically, ES binds Cu(II) in 1:1 ratio in the extracellular environment (Yadav et al., 2013), forming a membrane permeable complex (ES-Cu), which upon entering the mitochondria, releases copper by an unknown mechanism (Nagai et al., 2012). In this manner, ES selectively kills cancer cells by transporting excess copper to mitochondria and thereby inducing the mitochondrial apoptosis pathway (Chen et al., 2013; Nagai et al., 2012; Kirshner et al., 2008).

Although previous work has established the copper-specific role of ES (Nagai et al., 2012), we currently do not know how ES treatment impacts the levels of other metals in cells. A genome-wide study has shown that the homeostatic mechanisms that control

54

the levels of different elements are interconnected (Eide et al., 2005). Moreover, ligands that bind Cu(II) can often bind iron. Indeed, a mass spectrometry study reported that ES can also bind Fe(II). Therefore, in order to fully realize the therapeutic potential of ES as a copper-delivery agent, it is necessary to characterize its impact on cellular metallome. Here, by using a combination of yeast genetics, sub-cellular fractionation, and ICP-MS based metal measurements, we show that in additional to expected elevation in cellular and mitochondrial copper content, ES also indirectly increases cellular iron content by stimulating copper-dependent iron import machinery.

Results

Preformed ES-Cu complex is more efficient than ES in transporting copper

Previous studies have established that cytotoxic effects of ES are dependent on the availability of copper in the growth media, which implies that ES transports external copper into the cells (Nagai et al., 2012; Blackman et al., 2012). As both ES and ES-Cu are promising therapeutics for treating inborn errors of copper metabolism (Soma et al., 2018; Guthrie et al., 2020), we first aimed to compare and quantify the toxicity and efficiency of these compounds as copper couriers. We observed that the growth of wild type (WT) yeast grown in glucose-containing (YPD) media was minimally affected by the presence of either $CuCl_2$ or ES at 5 µM, the highest concentration tested (Figure 3.1A). However, preformed ES-Cu complex or when ES was co-supplemented with $CuCl_2$ in the growth media, we observed growth inhibition at concentrations above 0.25 µM, with IC_{50} values of ES-Cu being 0.57 µM and ES co-supplemented with equimolar $CuCl_2$ being 0.82 µM (Figure 3.1A). Notably, when increasing concentrations of ES

55

were supplemented in the presence of excess copper in the media, we observed the most severe growth inhibition with an IC_{50} of 0.32 µM (Figure 3.1A), a finding consistent with the idea that ES shuttles in and out of the cells to continuously bring extracellular copper into the cells. These results are consistent with previous studies (Nagai et al., 2012; Blackman et al., 2012) and revealed that yeast can tolerate 0.25 µM of ES-Cu without any negative effects on growth, whereas free ES is tolerated at much higher concentrations.
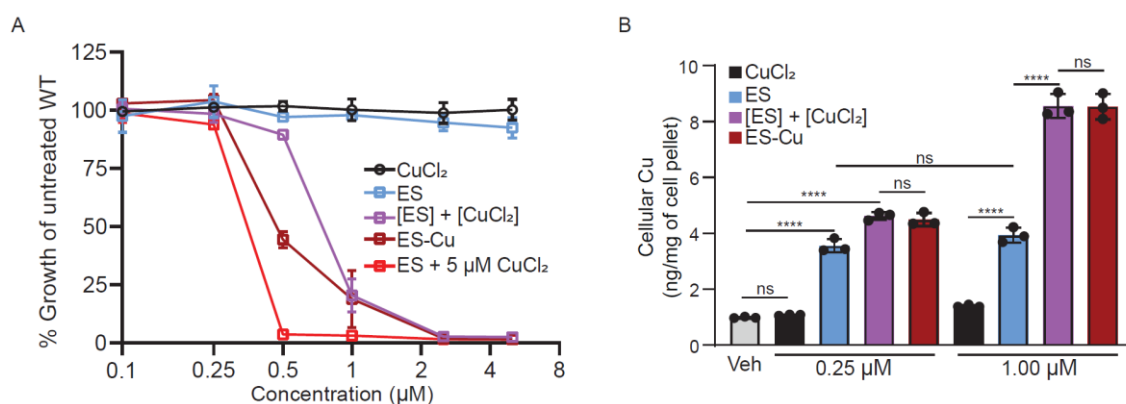

Figure 3.1 Determination of the maximal tolerable dose of ES when supplemented with or without additional copper
(A)BY4741 WT yeast cells were cultured in YPD medium at 30°C in the presence of increasing concentrations (0.0125 to 5 µM) of the indicated chemical species. The cell density was measured spectrophotometrically after 12 hours of growth at 600nm. Percent of growth was calculated by comparing the optical density of each culture to that of WT with vehicle alone. (B) Cu levels in BY4741 WT yeast cells treated with the indicated chemical species were measured by ICP-MS. The data represent the average ± SD; (n=3), ****$p < 0.0001$, ns = not significant.

Next, we wanted to determine the intracellular copper concentration that is detrimental to yeast growth. Supplementation of either 0.25 µM or 1 µM $CuCl_2$, only marginally increased intracellular copper abundance (Figure 3.1B). This could be due to reduced expression of Ctr1, the major copper importer, in copper replete conditions (Dancis et al., 1994). In contrast to $CuCl_2$, supplementation of 0.25 µM of ES, ES +

CuCl$_2$ (each added separately in the media) or preformed ES-Cu complex increased intracellular Cu content by ~4 fold (Figure 3.1B). Furthermore, we found that treatment with ES-Cu or ES+CuCl$_2$ increased cellular Cu content in a dose-dependent manner, but ES alone did not (Figure 3.1B), which is likely due to limited bioavailable copper in the media. These data suggest that yeast growth is not impaired with a ~4-fold increase in intracellular copper levels but an 8-fold increase in copper levels inhibits cellular growth.

Effect of ES-Cu on cellular metallome

Since perturbation in the homeostasis of one metal often results in widespread changes in the cellular metallome (Eide et al., 2005), we sought to determine if ES-Cu supplementation alters the cellular abundance of other metals. For accurate measurements of intracellular metal contents, samples were serially diluted, and tailored calibration curves were generated by inductively-coupled plasma mass spectrometry (ICP-MS) (Figure 3.2). By using this method, we were able to detect cellular metal levels spanning over four orders of magnitude, demonstrating the powerful advantage of this technique (Figure 3.2). ES-Cu treatment led to an expected increase in intracellular copper levels (Figure 3.3A). In addition to copper, we found a striking increase in intracellular iron levels (Figure 3.3B). The abundance of intracellular zinc, magnesium, calcium, selenium, and nickel were unaltered by treatment with ES-Cu (Figure 3.3 C-G), although we did observe a small but significant increase in manganese levels (Figure 3.3H). Notably, the increase in copper and iron levels upon ES-Cu treatment is independent of yeast strain because we observed a similar increase in the levels of both

these metals in W303 background upon ES and ES-Cu treatment (Figure 3.4). Together,

these data suggest that both ES and ES-Cu impacts both copper and iron homeostasis.
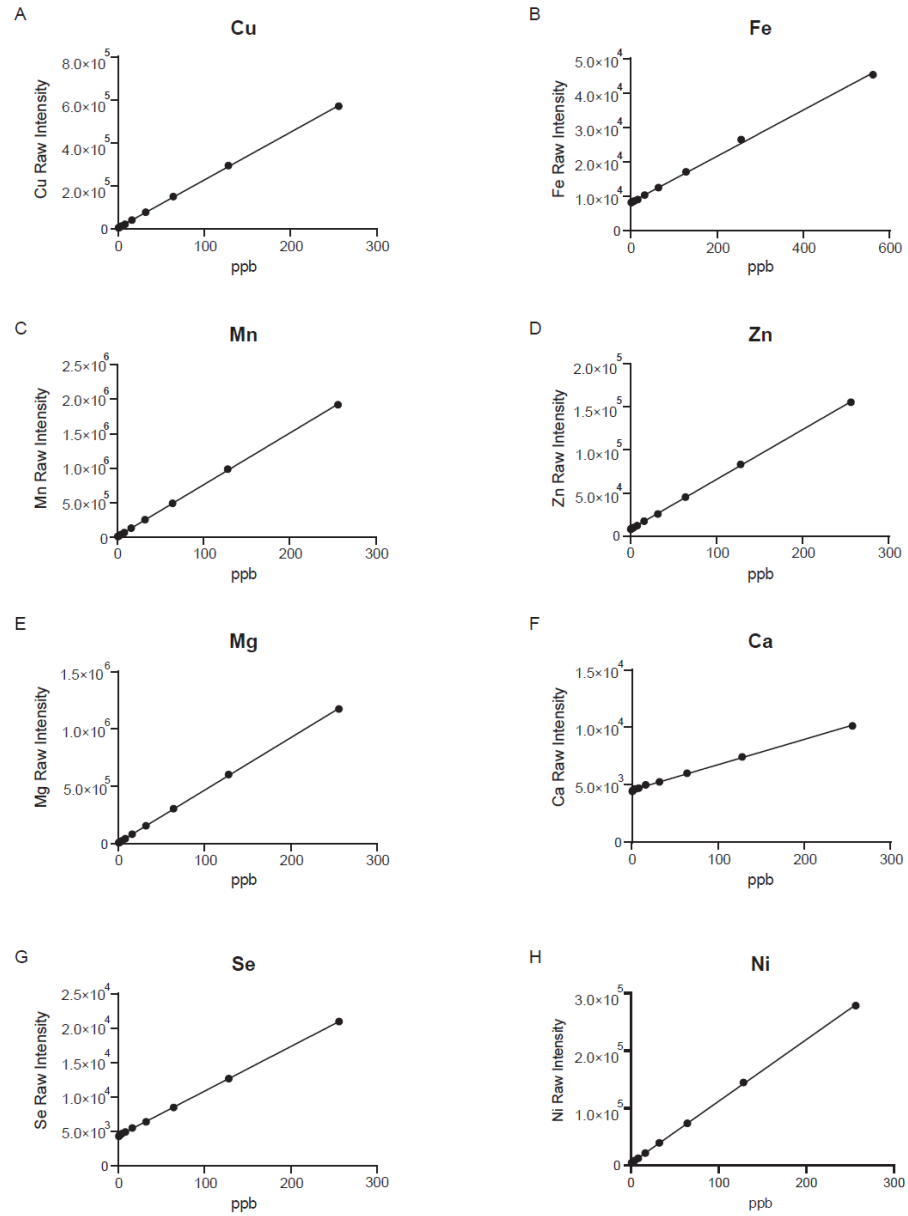
Figure 3.2 ICP-MS calibration curves for different metals
Calibration curves were generated by measuring the raw intensity of the signal generated by each of the indicated ions, at given concentrations. These calibration curves were utilized to calculate the concentrations of cellular metals reported in Figure 3.3.
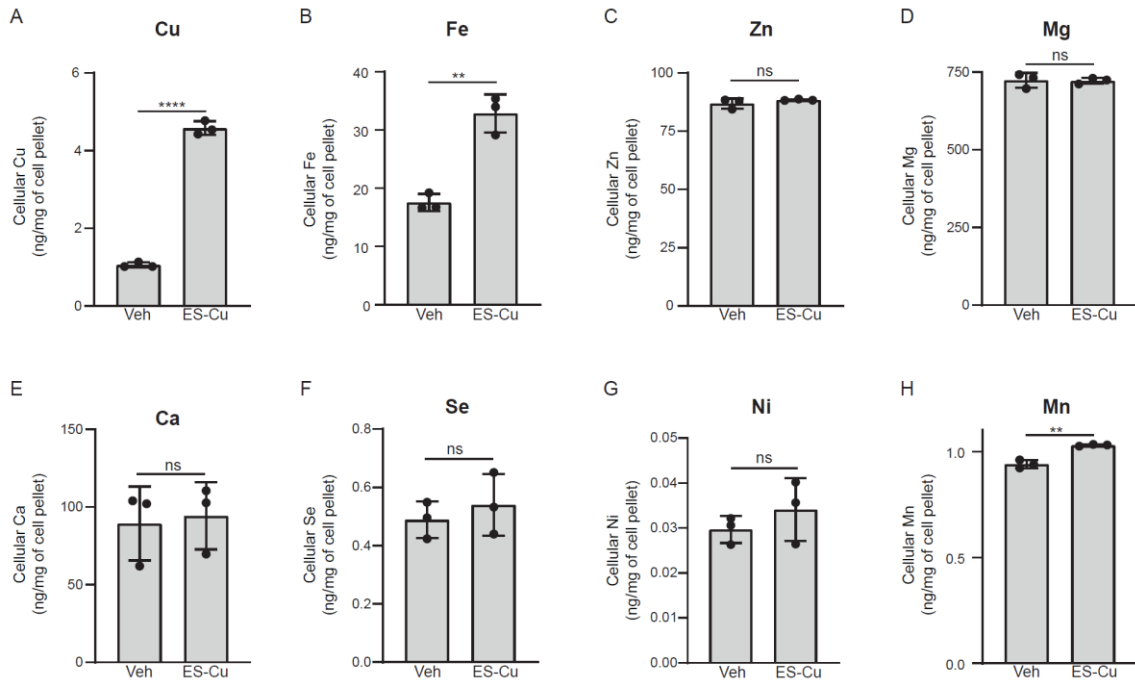
Figure 3.3 ES-Cu elevates cellular Cu, Fe and Mn levels
(A-H) BY4741 WT cells were grown in YPD $\pm$ 250 nM ES-Cu for 10 hours before measuring the cellular content of the indicated metals by ICP-MS. The data represent the average $\pm$ SD; (n=3), ****$p < 0.0001$, **$p < 0.001$, ns = not significant.
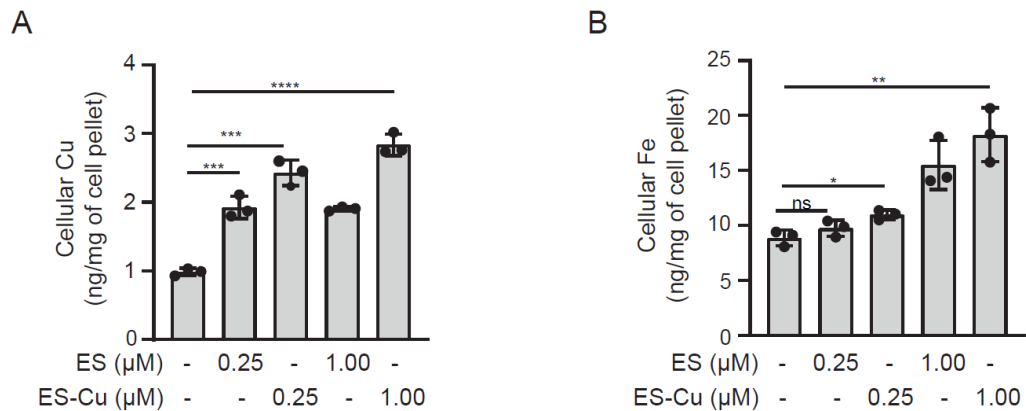
Figure 3.4 ES-Cu stimulates increase in cellular iron levels in yeast strain W303-1A
W303-1A WT cells were grown in YPD $\pm$ 250 nM ES-Cu for 20 hours before measuring cellular (A) Cu and (B) Fe levels by ICP-MS. The data represent the average $\pm$ SD; (n=3). ****$p < 0.0001$, ***$p < 0.001$ **$p < 0.01$, *$p < 0.05$.

ES and ES-Cu treatment elevates mitochondrial iron

Since mitochondria contain many iron-dependent enzymes, we wanted to determine whether ES and ES-Cu treatment could increase iron levels in mitochondria. We performed these experiments using non-fermentable growth media (YPGE), which is known to derepress mitochondrial biogenesis genes (Kayikci and Nielsen, 2015). As in YPD, cells cultured in YPGE were more sensitive to ES-Cu than ES alone, with IC_{50} of ES-Cu mediated growth inhibition being 0.74 µM (Figure 3.5A). We were able to ascribe increased toxicity of ES-Cu to elevated levels of intracellular copper (Figure 3.5B). Both ES and ES-Cu treatment increased intracellular copper and iron levels albeit to a different degree (Figure 3.5B and C). Similar to an increase in cellular copper and iron, ES and ES-Cu also led to an increase in their levels in mitochondria (Figure 3.5D and E). This result shows that iron imported in an ES and ES-Cu dependent manner is being transported to the mitochondria (Figure 3.5E).
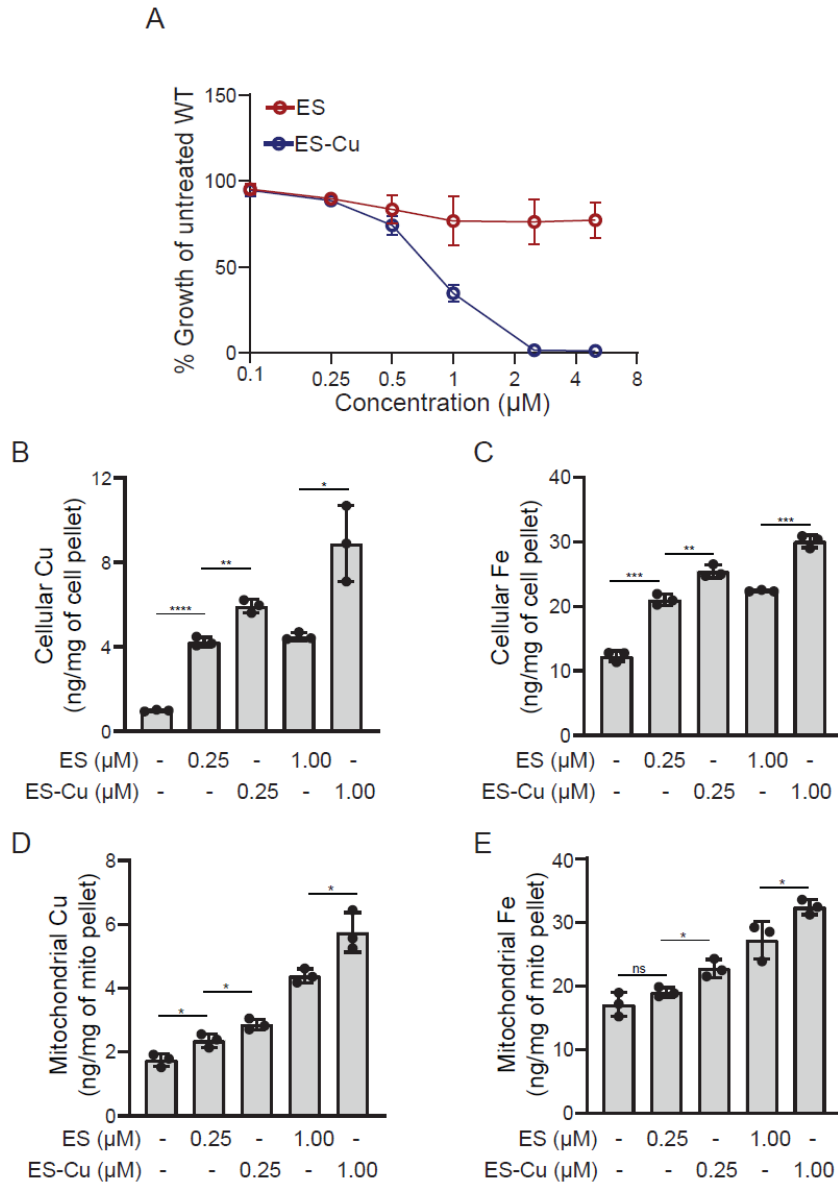
Figure 3.5 ES and ES-Cu treatment elevates mitochondrial copper and iron content
(A)BY4741 WT yeast cells were cultured in YPGE medium at 30°C in the presence of increasing concentrations (0.0125 to 5 μM) of either ES or ES-Cu. The cell density was measured spectrophotometrically after 24 hours of growth at 600 nm. Percent of growth was calculated by comparing the optical density of each culture to that of WT with vehicle alone. Cellular (B) Cu and (C) Fe levels, and mitochondrial (D) Cu and (E) Fe levels of cells grown in YPGE ± ES or ES-Cu. The data represent the average ± SD; (n=3), *p < 0.05, ** p < 0.01, ***p < 0.001, ****p < 0.0001, ns = not significant.

ES-Cu mediated increase in iron levels is dependent on high affinity Fe import machinery

Next, we wanted to determine the mechanism of ES-Cu-mediated elevation in cellular iron levels. We considered two possibilities: First, ES is able to exchange copper with extracellular iron and transport it into the cells in a manner similar to copper. Second, ES-Cu elevates cellular iron by stimulating iron import. To distinguish between these possibilities, we measured the iron and cellular content of ES-Cu treated *ctr1Δ* and *ftr1Δ* yeast mutants that are devoid of major copper and iron importers, respectively (Dancis et al., 1994; Stearman et al., 1996) (Figure 3.6A). As expected *ctr1Δ* cells exhibited reduced copper levels and treatment with ES-Cu elevated copper levels in this mutant to the same extent as WT (Figure 3.6B). Similar levels of copper accumulation were observed in ES-Cu treated *ftr1Δ* cells. These data demonstrate that increase in cellular copper by ES is independent of copper or iron import machinery. In contrast, we found that ES-Cu treatment increased iron levels only in WT and *ctr1Δ* cells but not in *ftr1Δ* cells (Figure 3.6C). These data argue against direct transport of extracellular iron by ES and indicate that the ES-Cu mediated increase in cellular iron levels is dependent on Ftr1, the primary iron importer. Notably, the loss of the low affinity iron importer, Fet4 (Hasset et al., 2000; Dix et al., 1994) did not impact ES-Cu mediated increase copper and iron levels (Figure 3.6 D and E). Together, this data shows that Ftr1 is essential for ES-Cu-mediated increase intracellular iron.
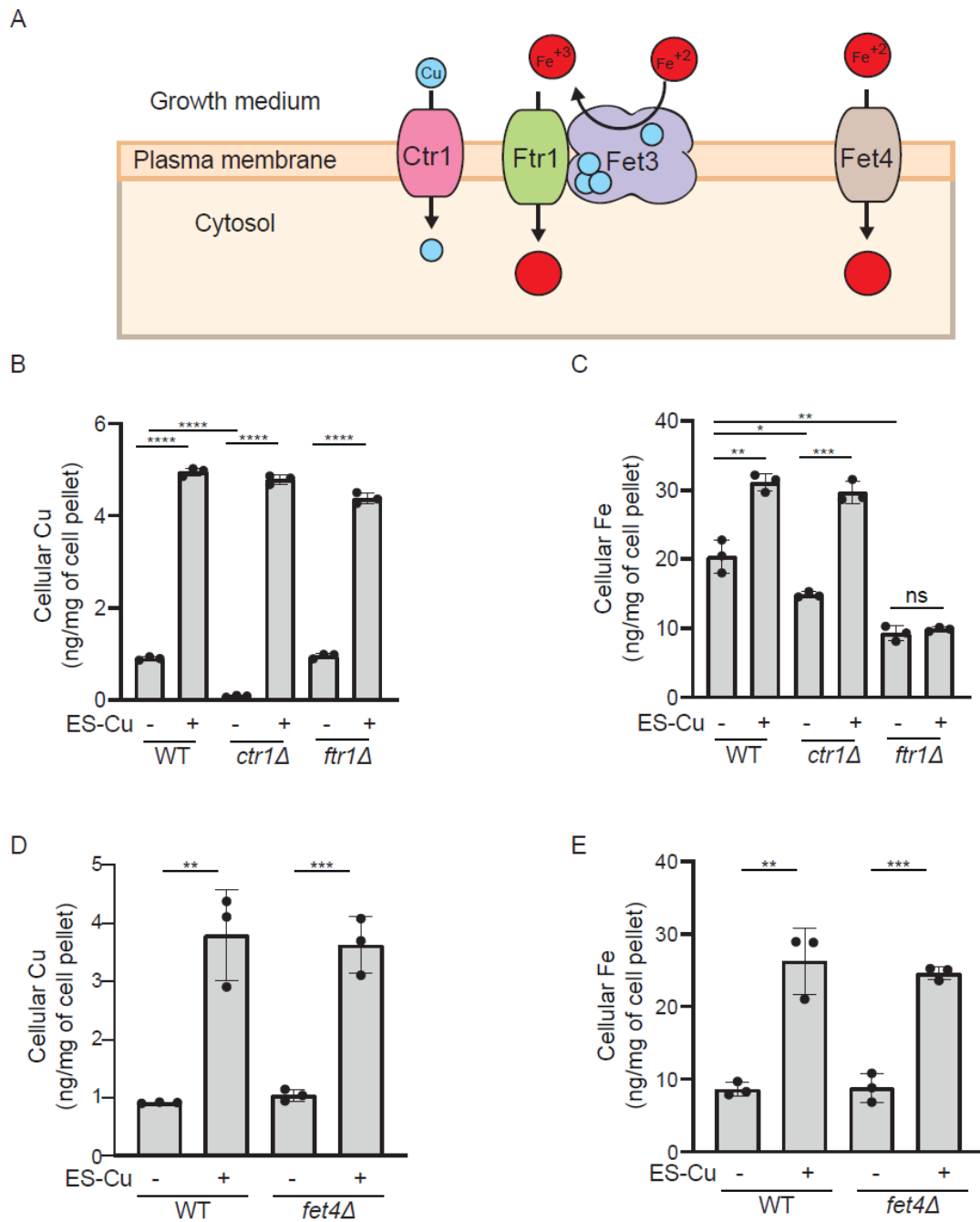
Figure 3.6 ES-Cu mediated increase in iron is dependent on high affinity iron import machinery

(A)Schematic of cellular copper and iron import machinery. Ctr1 and Ftr1 represent high affinity import machinery for copper and iron, respectively. Fet3 is a multi-copper oxidase that oxidizes Fe^{+2} to Fe^{3+} for Ftr1 mediated iron import. Fet3 is essential for Ftr1-dependent iron import. Fet4 is a low affinity iron importer. Copper and iron are depicted as blue and red circles, respectively.

(B) and (C) BY4741 WT, *ctr1Δ* and *ftr1Δ* cells were grown in YPD ± 250 nM ES-Cu for 10 hours before measuring B) Cu and C) Fe by ICP-MS. (D and E) BY4741 WT and *fet4Δ* cells were grown in (YPD + 1 µM $CuCl_2$) ± 250 nM ES-Cu for 10 hours before measuring D) Cu and E) Fe levels by ICP-MS. The data represent the average ± SD; (n=3). ** $p < 0.01$, *** $p < 0.001$, **** $p < 0.0001$

Fet3 and Ccc2 are essential for ES-mediated increase in iron import

Fet3 is a plasma membrane localized multi-copper oxidase that oxidizes Fe^{2+} to Fe^{3+} for its subsequent cellular uptake by Ftr1 (Askwith et al., 1994). Insertion of copper into Fet3 occurs in the Golgi lumen and is essential for its activity (Pena et al., 1999) (Figure 3.7A). Cytosolic copper is pumped into the Golgi lumen by Ccc2, a P-type ATPase, which itself receives copper from Atx1, a cytosolic copper metallochaperone (Figure 3.7A) (Fu et al., 1995; Lin and Culotta, 1995). To test if ES mediated iron import is dependent on these proteins (Atx1, Ccc2, and Fet3), we measured the iron levels in cells lacking these proteins. As expected, treatment with ES-Cu led to a pronounced increase in intracellular copper levels for each of these mutants (Figure 3.7B). However, the increase in iron levels was disrupted in *fet3Δ* and *ccc2Δ* mutants. In contrast, we found that Atx1 is dispensable for ES-Cu-mediated elevation in cellular iron levels (Figure 3.7C). These data demonstrate that ES can bypass Atx1 but not Ccc2 in delivering copper to Fet3 and suggest a possibility that another protein may compensate for the lack of Atx1.

Recently, an *in vitro* study showed that human glutaredoxin-1 (hGrx1) can deliver copper to one of the human homologs of Ccc2, ATP7B (Maghool et al., 2020). This transfer of copper was independent of Atox1, the human homolog of Atx1. These findings suggested that hGrx1 can substitute for Atox1 function in copper delivery to

64

ATP7B. We therefore wondered if the yeast homolog of hGrx1, can substitute for Atx1 in delivering copper to Ccc2 *in vivo*. To test this hypothesis, we constructed yeast mutants *grx1Δ* and *atx1Δgrx1Δ*. ICP-MS-based cellular metal measurements showed that the copper levels of all mutants were comparable to WT under basal or ES-Cu supplemented conditions (Figure 3.7D). However, iron levels of these mutants varied under basal conditions, with *atx1Δ* and *atx1Δgrx1Δ* exhibiting reduced levels of intracellular iron, whereas the iron content of *grx1Δ* cells were comparable to that of WT (Figure 3.7E). These results suggest that *in vivo*, Atx1 plays a critical role in supplying copper to Golgi, but Grx1 does not. Since ES-Cu treatment was able to bypass the requirement of Atx1, we expected an increase in iron levels in *atx1Δgrx1Δ* cells. Indeed, ES-Cu treatment led to an increase in iron levels in both *grx1Δ* and *atx1Δgrx1Δ* cells (Figure 3.7E). Together, these data demonstrate ES-Cu can bypass both Atx1 and Grx1 in delivering copper to Ccc2 *in vivo*.
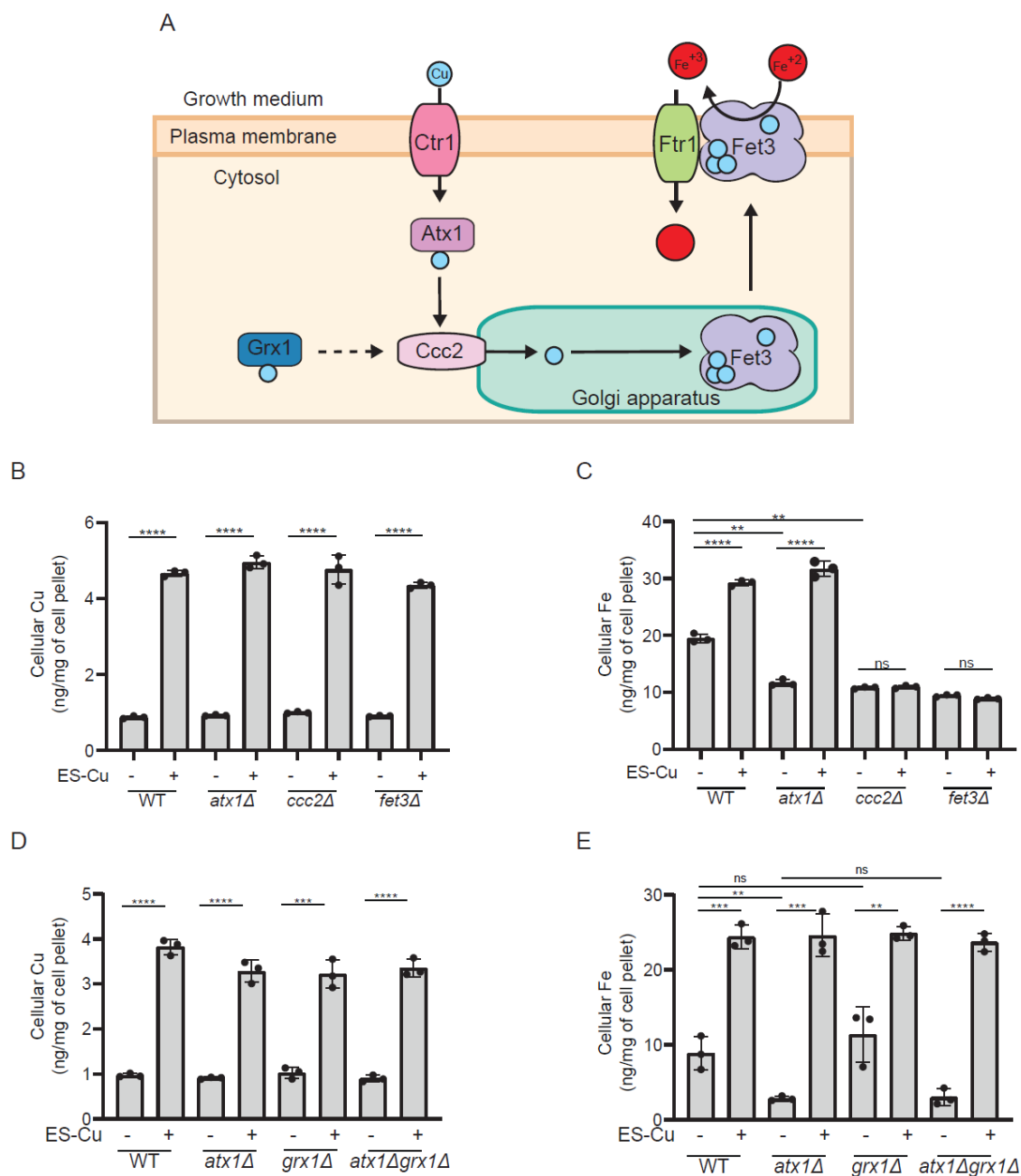
Figure 3.7 ES-Cu trafficked copper is bioavailable for Ccc2 mediated insertion into Fet3

(A) Schematic of copper transport to Fet3. Copper is imported via high affinity copper transporter Ctr1. Once inside the cell copper is bound by the Cu-metallochaperone Atx1, which transporters copper to Ccc2. Ccc2 is a P-type ATPase present on the Golgi membrane that pumps copper into the Golgi lumen where Fet3 metalation takes place. (B) and (C) BY4741 WT, *atx1Δ*, *ccc2Δ* and *fet3Δ* were grown in YPD ± 250 nM ES-Cu for 10 hours before measuring (B)

Cu and (C) Fe levels by ICP-MS. (D) and (E) BY4741 WT, *atx1Δ*, *grx1Δ* and *atx1Δgrx1Δ* cells were grown in (YPD 1 μM CuCl$_2$) ± 250 nM ES-Cu for 10 hours before measuring (A) Cu and (B) Fe levels by ICP-MS. The data represent the average ± SD; (n=3). ****p < 0.0001, ***p < 0.001, **p < 0.01, ns = not significant.

<u>Discussion</u>

As currently no effective therapy exists for copper deficiency disorders, there is a dire need for the identification, characterization, and optimization of copper therapeutics. Our recent studies have highlighted the potential of ES, an investigational cancer drug as a therapeutic for disorders of copper metabolism (Gohil, 2021; Guthrie et al., 2020; Soma et al., 2018). In order to translate these promising pre-clinical studies into repurposing ES or ES-Cu for the treatment of copper deficiency disorders, it is critical to determine its specificity, toxicity, and impact on the overall cellular metallome. Here using a yeast model system, we show that in addition to the expected effect of ES-Cu on cellular levels of copper, it also elevates cellular and mitochondrial iron levels by stimulating copper-dependent iron import machinery.

Since ES has been used in clinical trials for the treatment of cancer, its toxicity profile has been established (Berkenblit et al., 2007; O'Day et al., 2009; O'Day et al., 2013). However, no such information is available for ES-Cu complex. As shown in our recent study, administration of preformed ES-Cu complex is essential for treating copper deficiency disorders such as Menkes disease. Therefore, we compared the tolerability of ES and ES-Cu in parallel and found that that the toxicity of ES is potentiated by the availability of copper, with pre-loaded ES-Cu complex exhibiting much higher toxicity then ES alone (Figure 3.1A). Interestingly, we find that when ES treatment was given in the presence of excess (5 μM) copper, the toxicity was much higher (Figure 3.1A). This

67

finding has an important implication for future therapeutic use of ES-Cu. For instance, in diseases like Menkes, the affected patients are given daily injections of Cu-histidinate (Kaler, 2014). Thus, availability of excess copper in the body may potentiate the toxicity of ES-Cu if it is administered post Cu-histidinate treatment.

By utilizing the more efficient copper courier, ES-Cu, at its maximal tolerable dosage (250 nM) we sought to amplify any ES-Cu triggered alterations in the homeostasis of cellular metals. In this manner, we found that ES-Cu supplementation not only increased copper content but also doubled iron content (Figure 3.3). The effect of ES-Cu on iron levels was indirect, as it acted through the activity of Ftr1-Fet3, a copper dependent high affinity system. This observation allowed us to dissect the mechanism by which ES distributes copper in the intracellular compartments, specifically the Golgi lumen where Fet3 metalation takes place (Yuan et al., 1997). Our study showed that copper delivered by ES is available to Ccc2 in order to pump copper in the Golgi lumen (Figure 3.8). Although it was surprising that Atx1 function was dispensable for ES-mediated copper delivery to Ccc2, there are prior studies that are consistent with this finding. For example, under the conditions of copper excess, the Atox1 binding domain of ATP7A is not required for Golgi copper import (Voskoboinik et al., 1999). In two separate studies using yeast model systems, it was shown excess copper can overcome Atx1 deficiency (Serrano et al., 2004; Lin et al., 1997). Under these conditions, it is possible that glutathione or another Cu-metallochaperone may facilitate transport of copper to Ccc2. In this regard, we tested the role of Grx1, which has recently been shown to transfer copper to ATP7B *in vitro* (Maghool et al., 2020). Our *in vivo* data

using *grx1Δ* and *atx1Δgrx1Δ* double mutant demonstrate that Grx1 is not essential for copper to transport to Ccc2.

The essential requirement of Ccc2 for ES-mediated copper delivery to the Golgi compartment is at odds with our previously reported observations that ES-Cu partially rescue pigmentation defects in the Menkes-affected *mo-br* mice (Guthrie et al., 2020). This is because pigmentation is mediated by a secretory pathway enzyme tyrosinase that receives copper in the Golgi and melanosomes via the action of Ccc2 homolog ATP7A (Setty et al., 2008), which is mutated in these *mo-br* mice. A complete loss of ATP7A function should prevent ES-mediated copper delivery to tyrosinase, which would prevent melanin production. However, ES-Cu treatment did stimulate pigmentation in *mo-br* mice, which could be due to the presence of residual activity of ATP7A (Grimes et al., 1997).

Our findings have implications for possible future applications of ES-Cu in correcting defects in iron homeostasis. This is because Fet3 has two homologs in humans, ceruloplasmin and hephaestin that play a critical role in cellular and systemic iron metabolism (de Silva et al., 1997; Li et al., 2003; Vashchenko and MacGillivary, 2013). ATP7A-related disease, including Menkes, Occipital horn syndrome, and X-linked distal hereditary motor neuropathy, are expected to have defects in iron homeostasis due to disrupted metalation of Golgi cuproenzymes. The role of ES-Cu in correcting this defect should be investigated.
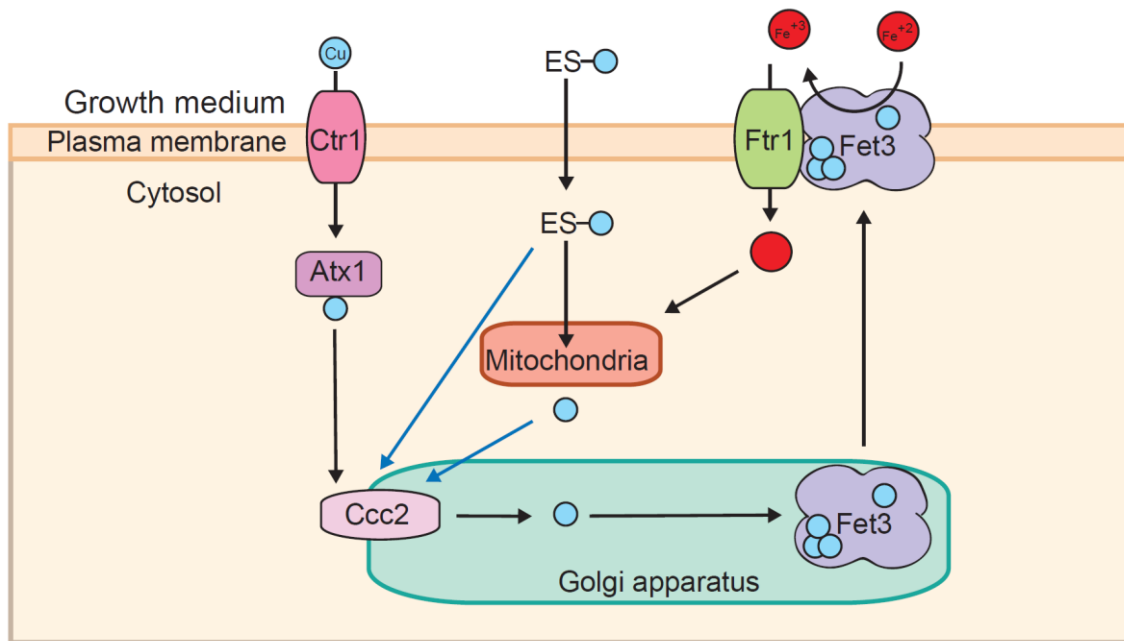
Figure 3.8 Model of ES-Cu stimulated increase in cellular iron abundance
ES-Cu enters the cell and releases copper in a form that is bioavailable to Ccc2. ES coordinated copper may be directly transported to the Golgi apparatus or it may be released in the mitochondria prior to its transport to Ccc2 (indicated by blue arrows). Copper imported by Ccc2 is utilized for the metalation of the multicopper oxidase, Fet3 in the Golgi apparatus. This metalated Fet3 is then localized to the plasma membrane where it oxidizes Fe^{2+} to Fe^{3+} for Ftr1 mediated Fe import. This Ftr1 imported Fe can be trafficked to the mitochondria.

Experimental procedures

Yeast growth conditions

Yeast cells were cultured in either liquid YPD (1% yeast extract, 2% peptone, and 2% dextrose) or YPGE (3% glycerol + 1% ethanol) medium. For growth in liquid medium, yeast cells were precultured in YPD and then inoculated into either YPD or YPGE and grown to mid-log phase. ES, ES-Cu or $CuCl_2$ or vehicle (DMSO) was added to growth media at the listed concentrations. Growth in liquid media was monitored spectrophotometrically at 600 nm.

Construction of yeast knockouts

Individual yeast *Saccharomyces cerevisiae* mutants used in this study were obtained from Open Biosystems or were constructed by one-step gene disruption using a hygromycin cassette (Janke et al., 2004). All yeast strains used in this study are listed in Table 3.1. Authenticity of all yeast strains was confirmed by polymerase chain reaction (PCR)-based genotyping. The primers used to disrupt Grx1 and the primers used to confirm *grx1Δ* and *atx1Δgrx1Δ* mutants are listed in Table 3.2.

Measuring yeast growth

Cultures of WT with and without treatment were grown in YPD or YPGE for 12 or 24 hrs, respectively. The optical density of each culture at 600 nm was measured. The OD_{600} of each culture was divided by the OD_{600} of WT + vehicle. This was then displayed as a percentage.

Mitochondria isolation

Mitochondria were isolated as described previously (Meisinger et al., 2006). Briefly, 0.5-2.5 g of cell pellet was incubated in dithiothreitol (DTT) buffer (0.1 M Tris-HCl, pH 9.4, 10 mM DTT) at 30°C for 20 min. The cells were then pelleted by centrifugation at 3,000×*g* for 5 min, resuspended in spheroplasting buffer (1.2 M sorbitol, 20 mM potassium phosphate, pH 7.4) at 7 mL/g and treated with 3 mg zymolyase (US Biological Life Sciences) per gram of cell pellet for 45 min at 30°C. Spheroplasts were pelleted by centrifugation at 3,000×*g* for 5 min then homogenized in homogenization buffer (0.6 M sorbitol, 10 mM Tris-HCl, pH 7.4, 1 mM EDTA, 1 mM PMSF, 0.2% [w/v] BSA [essentially fatty acid-free, Sigma-Aldrich]) with 15 strokes using a glass

71

Teflon homogenizer with pestle B. After two centrifugation steps of 5 min at 1,500×g and 4,000×g, the final supernatant was centrifuged at 12,000×g for 15 min to pellet mitochondria. Mitochondria were resuspended in Sucrose–EDTA-MOPS (SEM) mitochondria isolation buffer (250 mM sucrose, 1 mM EDTA, 10 mM MOPS-KOH, pH 7.2, containing 1X protease inhibitor cocktail from Roche).

ICP-MS

Cellular and mitochondrial copper and iron levels were measured by inductively coupled plasma (ICP) mass spectrometry using NexION 300D instrument from PerkinElmer Inc. Briefly, 80-300 mg of intact yeast cells were washed twice with 1 mL of ultrapure metal-free water containing 100 μM EDTA (TraceSELECT; Sigma) followed by two more washes with ultrapure water to eliminate EDTA. For mitochondrial samples, the same procedure was performed using 300 mM mannitol (TraceSELECT; Sigma) to maintain mitochondrial integrity. After washing, samples were weighed, digested with 40% (w/v) nitric acid (TraceSELECT; Sigma) at 90°C for 18 h, followed by 6 h digestion with 0.75% H_2O_2 (Sigma-Supelco), then diluted in ultrapure water. For zing, magnesium and calcium, digested samples were further diluted by 10-100-fold to ensure the concentration of these ions were within linear range of the calibration curve. Calibration curves were generating by serially diluting a premixed standard solution (BDH Alistar plus or Milipore sigma ICP multi-element standard solution VIII).

Statistical Analyses

Statistical analysis on bar charts was conducted using two-sided students *t*-Test. Experiments were performed in three biological replicates, where biological replicates

are defined as experiments performed on different starting pre-culture. Error bars represent the standard deviation, *(P<0.05), **(P<0.01), ***(P<0.001) and ****(P < 0.0001).

Table 3.1 *Saccharomyces cerevisiae* **strains used in this study**

Yeast Strains	Genotype	Source
BY4741 WT	*MAT*a, *his3Δ1, leu2Δ0, met15Δ0, ura3Δ0*	Greenberg, M.L.
BY4741 *ctr1Δ*	*MAT*a, *his3Δ1, leu2Δ0, met15Δ0, ura3Δ0, ctr1Δ::kanMX4*	Open Biosystems
BY4741 *ftr1Δ*	*MAT*a, *his3Δ1, leu2Δ0, met15Δ0, ura3Δ0, ftr1Δ::kanMX4*	Open Biosystems
BY4741 *fet4Δ*	*MAT*a, *his3Δ1, leu2Δ0, met15Δ0, ura3Δ0, fet4Δ:: kanMX4*	Open Biosystems
BY4741 *fet3Δ*	*MAT*a, *his3Δ1, leu2Δ0, met15Δ0, ura3Δ0, fet3Δ:: kanMX4*	Open Biosystems
BY4741 *ccc2Δ*	*MAT*a, *his3Δ1, leu2Δ0, met15Δ0, ura3Δ0, ccc2Δ::kanMX4*	Open Biosystems
BY4741 *atx1Δ*	*MAT*a, *his3Δ1, leu2Δ0, met15Δ0, ura3Δ0, atx1Δ:: kanMX4*	Open Biosystems
BY4741 *grx1Δ*	*MAT*a, *his3Δ1, leu2Δ0, met15Δ0, ura3Δ0, grx1Δ:: hphMX4*	This study
BY4741 *atx1Δgrx1Δ*	*MAT*a, *his3Δ1, leu2Δ0, met15Δ0, ura3Δ0, atx1Δ:: kanMX4, grx1Δ::hphMX4*	This study
W303-1A WT	*MAT*a, *leu2-3, 112 trp1-1, can1-100, ura3-1, ade2-1, his3-11,15*	Greenberg, M.L.

Table 3.2 Oligonucleotides used in this study

Oligonucleotide	Sequence (5'-3')
Generation of knockout mutant	AGTGAGCTGTCTACAGATAACGAGC
	TCTTAAAGTAATGGGCCAAGTAAAA
Confirmation of knockout mutant	ATAATTATACAAATAGACAAAACCTCAGAAGGAAAAAAAT GCGTACGCTGCAGGTCGAC
	TTATAAACCTGTGTGCATGGAAAAAACTTTGTCTGCCCTTAAT CGATGAATTCGAGCTCG

CHAPTER IV

CONCLUSIONS

The work described in this thesis was motivated by a longstanding mystery in the field of intracellular copper transport – how is copper transported to the mitochondria? To address this question, I utilized an unbiased yeast genomic screen and characterized the mechanism of intracellular metal transport by a copper-binding compound, elesclomol (ES), which has been previously shown to transport copper to the mitochondria (Nagai et al., 2012). Through these approaches, I discovered a number of novel genetic regulators of mitochondrial copper homeostasis and determined that ES can indirectly increase cellular and mitochondrial iron levels by delivering copper to the Golgi compartment.

I began my investigations on mitochondrial copper homeostasis by searching for novel genetic regulators of copper transport to the mitochondria. Given that the activity and abundance of cytochrome c oxidase (CcO), a mitochondrial cuproenzyme, is dependent on mitochondrial copper abundance, I utilized this enzyme as a proxy for mitochondrial copper levels. Specifically, we designed a genome-wide copper-sensitized screen, which was based on the idea that deletion of genes required for copper delivery to mitochondria would reduce CcO activity, which would impair respiratory growth. Since redundant pathways are expected for intracellular copper trafficking, we expected that the addition of copper salts in the media would rescue respiratory growth of a subset of mutants. Through an unbiased gene ontology analysis of hits from this screen, I

identified genes involved in vacuolar biogenesis as the major regulators of mitochondrial copper homeostasis. I specifically focused on the AP-3 complex and Rim proteins, which have been previously shown to be required for vacuolar biogenesis and V-ATPase expression, respectively.

By utilizing yeast mutants of AP-3, Rim proteins and ConcA, an inhibitor of the V-ATPase, I demonstrated that vacuolar pH is an important physiological regulator of mitochondrial copper homeostasis. Defective V-ATPase function could be bypassed by acidifying the pH of the vacuole, a finding that clearly demonstrated the importance of vacuolar pH but not the enzymatic activity of the V-ATPase in mitochondrial copper homeostasis. Importantly, defective vacuolar pH did not perturb CcO function when copper was supplemented to the growth media. These data suggest that under conditions of copper excess, there must also be a mechanism of copper mobilization to the mitochondria that is independent of V-ATPase function. These were exciting discoveries as the requirement of vacuolar function in maintaining mitochondrial respiration has been known for a long time (Eide et al., 1993; Ohya et al., 1991) but the precise biochemical basis for this requirement remained elusive for many decades.

In addition to uncovering a fundamental link between the functions of two cellular organelles, my study has implications for human health. Defective V-ATPase function has been reported in multiple human diseases including, Alzheimer's, amylotrophic lateral sclerosis, Parkinson's and even aging (Colacurcio and Nixon et al., 2016; Corrionero and Horvitz, 2018; Desai and Kaler, 2008; Kaler, 2013; Nixon et al.,

2008; Nguyen et al., 2019; Stepien et al., 2020). Though these aliments are characterized by defects in multiple different cellular processes, our study implicating the V-ATPase in mitochondrial function suggests that dysfunctional mitochondrial bioenergetics may contribute to the pathology of these conditions. Our findings regarding AP-3 also have important biomedical implications because mutations in AP-3 subunits have been shown to cause Hermansky–Pudlak syndrome (HPS). This disorder is pleiotropic, making it difficult to treat and HPS patients experience early mortality (Ammann et al., 2016; Dell'Angelica et al., 1999; El-Chemaly and Young, 2016). Currently, the mechanism of HPS disease pathogenesis is not well understood. My study identifying the role of AP-3 in mitochondrial function, suggests an unexpected role of mitochondria in HPS disease pathology.

Since no effective therapy currently exists for copper deficiency disorders, there is a dire need for the discovery, characterization, and optimization of copper therapeutics. Recent studies from our lab have uncovered therapeutic potential of ES in copper deficiency disorders such as the Menkes disease and a subset of mitochondrial disorders (Guthrie et al., 2020; Soma et al., 2018). Specifically, we showed that either ES or ES pre-conjugated with copper (ES-Cu), could restore mitochondrial function by delivering copper to the mitochondrial CcO. ES has been studied for almost fifteen years and a wealth of information is available in terms of its toxicity, pharmacokinetics, and metabolism but such information is lacking for ES-Cu. It is important to generate similar information for ES-Cu because this form of ES is essential for the treatment of Menkes

disease, where whole body copper levels are profoundly reduced. Therefore, I sought to compare the efficiencies and specificities of ES and ES-Cu.

Consistent with previous studies, the toxicity of ES was directly correlated to the abundance of copper in the extracellular media (Blackman et al., 2012; Nagai et al., 2012). By treating cells with non-toxic and growth inhibiting concentrations of ES and ES-Cu, I was able to identify the concentration of ES-trafficked copper that was detrimental to cell proliferation. Of note, when ES was administered with excess free $CuCl_2$ as opposed to ES alone, ES-Cu, or free ES and equimolar $CuCl_2$, the toxicity increased. This is likely due to the repeated cycling of ES to the extracellular media to bind and subsequently traffic more copper inside the cells (Nagai et al., 2012). This observation is of significant biomedical relevance as Menkes affected patients are given daily injections of Cu-histidinate (Kaler, 2014) and are expected to have high serum copper levels, which could potentiate the toxicity of ES.

Besides the expected effect of ES and ES-Cu on cellular levels of copper, these compounds, surprisingly, also elevated cellular and mitochondrial iron levels. Utilizing yeast deletion mutants, I showed that ES-Cu stimulated increase in iron levels is mediated by the high-affinity iron import machinery, Ftr1 and Fet3. My results show that ES is able to deliver copper to the Golgi compartment in a Ccc2-dependent manner, stimulating the metalation of Fet3, a multi-copper oxidase required for iron import. Furthermore, I found that increased cellular iron was capable of being transported to the mitochondria. This discovery, if replicated in mammalian system, could open a potential new application of ES/ES-Cu in treating disorders of both copper and iron deficiencies.

77

The human homologs of Fet3, ceruloplasmin and hephaestin, are cuproenzymes required for the oxidation of iron to facilitate its cellular import (de Silva et al., 1997; Li et al., 2003; Vashchenko and MacGillivary, 2013). Importantly these enzymes also receive their copper cofactors within the Golgi. Therefore, in diseases characterized by copper deficiency, such as the Menkes, Occipital horn syndrome, and X-linked distal hereditary motor neuropathy, ES-Cu treatment could be useful in correcting iron homeostasis defect by facilitating copper transport to ceruloplasmin and hephaestin.

Future Directions

My work provides strong genetic and pharmacological evidence that directly implicates V-ATPase function in maintaining mitochondrial copper homeostasis. However, the biochemical mechanism(s) underpinning this observation has remained elusive. The recent report by Hughes et al. (Hughes et al., 2020) showing the role of V-ATPase in cellular cysteine homeostasis provides an important clue to address this mystery. Specifically, Hughes et al. showed that V-ATPase function is required for storing cysteine in the vacuole and when this function is disrupted, cytosolic cysteine levels rises, which in turn causes iron auxotrophy. This study linked V-ATPase activity to mitochondrial function but the mechanism by which elevated cysteine perturbed iron homeostasis was not addressed. Since cysteine can bind copper, one can envision a scenario where elevated cysteine in the cytosol sequesters copper, making it unavailable to the mitochondrial CcO as well as the iron import protein Fet3 in the Golgi

78

compartment. This situation could explain iron auxotrophy of the V-ATPase mutants as well as decreased copper levels in the mitochondria.

A prototrophic yeast strain where cellular cysteine levels can be easily manipulated could be useful in testing the above-described possibility. This is because the prototrophic strain can biosynthesize all amino acids and can be cultured in minimal media containing a carbon source, a nitrogen source (i.e., ammonium sulfate) and vitamin mix. The advantage of using this strain is that it does not require supplementation of any amino acids in the media for its growth, making it suitable to specifically test the role of cysteine in mitochondrial iron and copper homeostasis. By measuring mitochondrial respiration in prototrophic yeast cells with and without the addition of cysteine, we could determine if cysteine supplementation negatively impacts mitochondrial function. Additionally, V-ATPase inhibitor-sensitized respiratory growth could further consolidate the link between vacuolar pH, cysteine homeostasis, and mitochondrial respiratory chain function.

Importantly, in addition to identifying the link between vacuolar function and mitochondrial copper homeostasis, our copper-sensitized genomic screen has yielded a rich catalog of novel genes that were previously not linked to copper biology. We hypothesize that these genes are either broadly involved in the maintenance of cellular copper homeostasis or specifically involved in copper trafficking to mitochondrial CcO. In order to systematically study the role of these genes in copper metabolism, they can be prioritized using the following criteria: 1) The strongest rescue of respiratory growth

by copper supplementation, 2) evolutionary conserved nature of the hits, and 3) presence of the gene-product in the mitochondria. To distinguish between the roles of the putative hits in cellular versus mitochondrial copper homeostasis, one can measure cellular and mitochondrial copper levels in these mutants. If the mutant exhibits diminished mitochondrial copper and CcO activity but not total cellular copper levels, this would indicate a specific defect in mitochondrial copper import and should be investigated further.

Another major finding of my work is that ES/ES-Cu treatment can increase cellular iron levels by delivering copper to Fet3. To test the generality of this observation, this finding needs to be confirmed in higher eukaryotes. Future experiments using ES/ES-Cu treatment of human and murine cell lines and zebrafish models of systemic and mitochondrial specific copper deficiency could help address the question whether ES can stimulate increased iron absorption *in vitro,* in cell culture conditions and *in vivo,* in an intact organism.

REFERENCES

Ammann S, Schulz A, Krägeloh-Mann I, Dieckmann NM, Niethammer K, Fuchs S, Eckl KM, Plank R, Werner R, Altmüller J, Thiele H, Nürnberg P, Bank J, Strauss A, von Bernuth H, Zur Stadt, U, Grieve S, Griffiths, GM, Lehmberg K, Hennies HC, Ehl S. (2016). Mutations in AP3D1 associated with immunodeficiency and seizures define a new type of Hermansky-Pudlak syndrome. Blood. 127, 997-1006.

Askwith C, Eide D, Van Ho A, Bernard PS, Li L, Davis-Kaplan S, Sipe DM, Kaplan J. (1994). The FET3 gene of S. cerevisiae encodes a multicopper oxidase required for ferrous iron uptake. Cell. 76, 403-410.

Baertling F, A M van den Brand M, Hertecant JL, Al-Shamsi A, van den Heuvel LP, Distelmaier F, Mayatepek E, Smeitink JA, Nijtmans LG, Rodenburg RJ. (2015). Mutations in COA6 cause cytochrome *c* oxidase deficiency and neonatal hypertrophic cardiomyopathy. Hum Mutat. 36, 34-38.

Bagh MB, Peng S, Chandra G, Zhang Z, Singh SP, Pattabiraman, N, Liu, A, Mukherjee, AB. (2017). Misrouting of v-ATPase subunit V0a1 dysregulates lysosomal acidification in a neurodegenerative lysosomal storage disease model. Nat Commun. 8, 14612.

Banci L, Bertini I, Cefaro C, Ciofi-Baffoni S, Gallo A, Martinelli M, Sideris DP, Katrakili N, Tokatlidis K. (2009). MIA40 is an oxidoreductase that catalyzes oxidative protein folding in mitochondria. Nat Struct Mol Biol. 16, 198-206.

Berkenblit A, Eder JP Jr, Ryan DP, Seiden MV, Tatsuta N, Sherman ML, Dahl TA, Dezube BJ, Supko JG. (2007). Phase I clinical trial of STA-4783 in combination with paclitaxel in patients with refractory solid tumors. Clin Cancer Res. 13, 584-590.

Bingham MJ, Ong TJ, Summer KH, Middleton RB, McArdle HJ. (1998). Physiologic function of the Wilson disease gene product, ATP7B. Am J Clin Nutr. 67, 982s-987s.

Blaby-Haas CE, Merchant SS. (2014). Lysosome-related organelles as mediators of metal homeostasis. J Biol Chem. 289, 28129-28136.

Blackman RK, Cheung-Ong K, Gebbia M, Proia DA, He S, Kepros J, Jonneaux A, Marchetti P, Kluza J, Rao PE, Yumiko W, Giaever G, Nislow N. (2012).

Mitochondrial electron transport is the cellular target of the oncology drug elesclomol. PLoS ONE. 7, e29798.

Brett CL, Kallay L, Hua Z, Green R, Chyou A, Zhang Y, Graham TR, Donowitz M, Rao R. (2011). Genome-wide analysis reveals the vacuolar pH-stat of *Saccharomyces cerevisiae*. PLoS ONE. 6, e17619.

Calderone V, Dolderer B, Hartmann HJ, Echner H, Luchinat C, Del Bianco C, Mangani S, Weser U. (2005). The crystal structure of yeast copper thionein: the solution of a long-lasting enigma. Proc Natl Acad Sci USA. 102, 51-56.

Calvo SE, Mootha, VK. (2010). The mitochondrial proteome and human disease. Annu Rev Genomics Hum Genet. 11, 25-44.

Chambers A, Krewski D, Birkett N, Plunkett L, Hertzberg R, Danzeisen R, Aggett PJ, Starr TB, Baker S, Dourson M, Jones P, Keen CL, Meek B, Schoeny R, Slob W. (2010). An exposure-response curve for copper excess and deficiency. J Toxicol Environ Health B Crit Rev. 13, 546-578.

Chatterjee S, Kumari S, Rath S, Priyadarshanee M, Das S. (2020). Diversity, structure and regulation of microbial metallothionein: metal resistance and possible applications in sequestration of toxic metals. Metallomics. 12, 1637-1655.

Chen KL, Ven TN, Crane MM, Brunner MLC, Pun AK, Helget KL, Brower K, Chen DE, Doan H, Dillard-Telm JD, Huynh E, Feng YC, Yan Z, Golubeva A, Hsu RA, Knight R, Levin J, Mobasher V, Muir M, Omokehinde V, Screws C, Tunali E, Tran RK, Valdez L, Yang E, Kennedy SR, Herr AJ, Kaeberlein M, Wasko BM. (2020). Loss of vacuolar acidity results in iron-sulfur cluster defects and divergent homeostatic responses during aging in *Saccharomyces cerevisiae*. Geroscience. 42, 749-764.

Chen S, Sun L, Koya K, Tatsuta N, Xia Z, Korbut T, Du Z, Wu J, Liang G, Jiang J, Ono M, Zhou D, Sonderfan A. (2013). Syntheses and antitumor activities of N'1, N'3-dialkyl-N'1, N'3-di-(alkylcarbonothioyl) malonohydrazide: the discovery of elesclomol. Bioorg Med Chem Lett. 23, 5070-5076.

Chun CD, Madhani HD. (2010). Ctr2 links copper homeostasis to polysaccharide capsule formation and phagocytosis inhibition in the human fungal pathogen *Crytococcus neoformans*. PLoS. ONE. 5, e12503.

Cobine PA, Moore SA, Leary SC. (2020). Getting out what you put in: Copper in mitochondria and its impacts on human disease. Biochim Biophys Acta Mol Cell Res. 1868, 118867.

Cobine PA, Ojeda LD, Rigby KM, Winge DR. (2004). Yeast contain a non-proteinaceous pool of copper in the mitochondrial matrix. J Biol Chem. 279, 14447-14455.

Cobine PA, Pierrel F, Bestwick ML, Winge DR. (2006). Mitochondrial matrix copper complex used in metallation of cytochrome oxidase and superoxide dismutase. J Biol Chem. 2811, 36552-36559.

Colacurcio DJ, Nixon, RA. (2016). Disorders of lysosomal acidification-the emerging role of v-ATPase in aging and neurodegenerative disease. Ageing Res Rev. 32, 75-88.

Corrionero A, Horvitz HR. (2018). A C9orf72 ALS/FTD ortholog acts in endolysosomal degradation and lysosomal homeostasis. Curr Biol. 28, 1522-1535.

Dancis A, Haile D, Yuan DS, Klausner RD. (1994). The *Saccharomyces cerevisiae* copper transport protein (Ctr1p). J Biol Chem. 269, 25660-25667.

Dancis A, Klausner RD, Hinnebusch AG, Barriocanal JG. (1990). Genetic evidence that ferric reductase is required for iron uptake in *Saccharomyces cerevisiae*. Mol Cell Biol. 10, 2294-2301.

Dancis A, Yuan DS, Haile D, Askwith C, Eide D, Moehle C, Kaplan J, Klausner RD. (1994). Molecular characterization of a copper transport protein in *S. cerevisiae*: an unexpected role for copper in iron transport. Cell. 76, 393-402.

Danks DM, Campbell PE, Walker-Smith J, Stevens BJ, Gillespie JM, Blomfield J, Turner B. (1972). Menkes' kinky-hair syndrome. Lancet. 1, 1100-1102.

De Freitas J, Wintz H, Kim JH, Poynton H, Fox T, Vulpe C. (2003). Yeast, a model organism for iron and copper metabolism studies. Biometals. 16, 185-197.

de Silva D, Davis-Kaplan S, Fergestad J, Kaplan J. (1997). Purification and characterization of Fet3 protein, a yeast homologue of ceruloplasmin. J Biol Chem. 272, 14208-14213.

Dell'Angelica EC, Shotelersuk V, Aguilar RC, Gahl WA, Bonifacino JS. (1999). Altered trafficking of lysosomal proteins in Hermansky-Pudlak syndrome due to mutations in the beta 3A subunit of the AP-3 adaptor. Mol Cell. 3, 11-21.

Dell'Angelica EC. (2009). AP-3-dependent trafficking and disease: the first decade. Curr Opin Cell Biol. 21, 552-559.

Desai V, Kaler SG. (2008). Role of copper in human neurological disorders. Am J Clin Nutr. 88, 855S-858S.

Diakov TT, Tarsio M, Kane PM. (2013). Measurement of vacuolar and cytosolic pH *in vivo* in yeast cell suspensions. J Vis Exp. 19, 50261.

Diaz-Ruiz R, Uribe-Carvajal S, Devin A, Rigoulet M. (2009). Tumor cell energy metabolism and its common features with yeast metabolism. Biochim Biophys Acta. 1796, 252-265.

DiMauro S, Tanji K, Schon EA. (2012). The many clinical faces of cytochrome *c* oxidase deficiency. Adv Exp Med Biol. 748, 341-357.

Dix DR, Bridgham JT, Broderius MA, Byersdorfer CA, Eide DJ. (1994). The FET4 gene encodes the low affinity Fe(II) transport protein of *Saccharomyces cerevisiae*. J Biol Chem. 269, 26092-26099.

Dodani SC, Leary SC, Cobine PA, Winge DR, Chang CJ. (2011). A targetable fluorescent sensor reveals that copper-deficient SCO1 and SCO2 patient cells prioritize mitochondrial copper homeostasis. J Am Chem Soc. 133, 8606-8616.

Duncan C, White AR. (2012). Copper complexes as therapeutic agents. Metallomics. 4, 127-138.

Eden E, Navon R, Steinfeld I, Lipson D, Yakhini Z. (2009). GOrilla: a tool for discovery and visualization of enriched GO terms in ranked gene lists. BMC Bioinformatics. 10, 48.

Eide DJ, Bridgham JT, Zhao Z, James MR. (1993). The vacuolar H+-ATPase of *Saccharomyces cerevisiae* is required for efficient copper detoxification, mitochondrial function, and iron metabolism. Mol Gen Genet. 241, 447-456.

Eide DJ, Clark S, Nair TM, Gehl M, Gribskov M, Guerinot ML, Harper JF. (2005). Characterization of the yeast ionome: a genome-side analysis of nutrient mineral and trace element homeostasis in *Saccharomyces cerevisiae*. Genome Biol. 6, R77.

El-Chemaly S, Young LR. (2016). Hermansky-Pudlak Syndrome. Clin Chest Med. 37, 505-511.

Ferguson-Miller S, and Babcock GT. (1996). Heme/Copper terminal oxidases. Chem Rev. 96, 2889-2908.

Festa RA, Thiele DJ. (2011). Copper: an essential metal in biology. Curr Biol. 21, R877-883.

Flohe L, Otting F. (1984). Superoxide dismutase assays. Methods Enzymol. 105, 93-104.

Fogel S, Welch JW. (1982). Tandem gene amplification mediates copper resistance in yeast. Proc Natl Acad Sci USA. 79, 5342-5246.

Foster AW, Dainty SJ, Patterson CJ, Pohl E, Blackburn H, Wilson C, Hess CR, Rutherford JC, Quaranta L, Corran A, Robinson NJ. (2014). A chemical potentiator of copper-accumulation used to investigate the iron-regulons of *Saccharomyces cerevisiae*. Mol Microbiol. 93, 317-330.

Foster AW, Osman D, Robinson NJ. (2014). Metal preferences and metallation. J Biol Chem. 289, 28095–28103.

Franz KJ. (2013). Clawing back: broadening the notion of metal chelators in medicine. Curr Opin Chem Biol. 17, 143-149.

Freisinger P, Horvath R, Macmillan C, Peters J, Jaksch M. (2004). Reversion of hypertrophic cardiomyopathy in a patient with deficiency of the mitochondrial copper binding protein Sco2: is there a potential effect of copper? J Inherit Metab Dis. 27, 67-79.

Fu D, Beeler TJ, Dunn TM. (1995). Sequence, mapping and disruption of CCC2, a gene that cross-complements the Ca^{2+}-sensitive phenotype of *csg1* mutants and encodes a P-type ATPase belonging to the Cu^{2+}-ATPase subfamily. Yeast. 11, 283–292.

Gaxiola RA, Yuan DS, Klausner RD, Fink GR. (1998). The yeast CLC chloride channel functions in cation homeostasis. Proc Natl Acad Sci USA. 95, 4046-4050.

Georgatsou E, Alexandraki D. (1999). Regulated expression of the *Saccharomyces cerevisiae* Fre1p/Fre2p Fe/Cu reductase related genes. Yeast. 15, 573-584.

Ghosh A, Pratt AT, Soma S, Theriault SG, Griffin AT, Trivedi PP, Gohil VM. (2016). Mitochondrial disease genes COA6, COX6B, and SCO2 have overlapping roles in COX2 biogenesis. Hum Mol Genet. 25, 660-671.

Ghosh A, Trivedi PP, Timbalia SA, Griffin AT, Rahn JJ, Chan SS, Gohil VM. (2014). Copper supplementation restores cytochrome *c* oxidase assembly defect in a

mitochondrial disease model of COA6 deficiency. Hum Mol Genet. 23, 3596-3606.

Giles NM, Watts AB, Giles GI, Fry FH, Littlechild JA, Jacob C. (2003). Metal and redox modulation of cysteine protein function. Chem Biol. 10, 677-693.

Glerum DM, Shtanko A, Tzagoloff A. (1996). Characterization of COX17, a yeast gene involved in copper metabolism and assembly of cytochrome oxidase. J Biol Chem. 271, 14504-14509.

Gohil, VM. (2021). Repurposing elesclomol, an investigational drug for the treatment of copper metabolism disorders. Expert Opin Investig Drugs. 30, 1-4.

Gow PJ, Smallwood RA, Angus PW, Smith AL, Wall AJ, Sewell RB. (2000). Diagnosis of Wilson's disease: an experience over three decades. Gut. 46, 415-419.

Grimes A, Hearn CJ, Lockhart P, Newgreen DF, Mercer JF. (1997). Molecular basis of the brindled mouse mutant (Mo(br)): a murine model of Menkes disease. Hum Mol Genet. 6, 1037-1042.

Gupta A, Lutsenko S. (2009). Human copper transporters: mechanism, role in human diseases and therapeutic potential. Future Med Chem. 1, 1125-1142.

Guthrie LM, Soma S, Yuan S, Silva A, Zulkifli M, Snavely TC, Greene HF, Nunez E, Lynch B, De Ville C, Shanbhag V, Lopez FR, Acharya A, Petris MJ, Kim BE, Gohil VM, Sacchettini JC. (2020). Elesclomol alleviates Menkes pathology and mortality by escorting Cu to cuproenzymes in mice. Science. 368, 620-625.

Haas A. (1995). A quantitative assay to measure homotypic vacuole fusion *in vitro*. Methods Cell Sci. 17, 283-294.

Halliwell B, Gutteridge JM. (1984). Oxygen toxicity, oxygen radicals, transition metals and disease. Biochem J. 219, 1-14.

Halliwell B. (1992). Reactive oxygen species and the central nervous system. J Neurochem. 59, 1609-1623.

Hamer DH, Thiele DJ, Lemontt JE. (1985). Function and autoregulation of yeast copperthionein. Science. 228, 685-690.

Hassett R, Dix DR, Eide DJ, Kosman DJ. (2000). The Fe(II) permease Fet4p functions as a low affinity copper transporter and supports normal copper trafficking in *Saccharomyces cerevisiae*. Biochem J. 351, 477-484.

Holmes-Hampton GP, Jhurry ND, McCormick SP, Lindahl PA. (2013). Iron content of *Saccharomyces cerevisiae* cells grown under iron-deficient and iron-overload conditions. Biochemistry. 52, 105–114.

Horn N, Møller LB, Nurchi VM, Aaseth J. (2019). Chelating principles in Menkes and Wilson diseases: Choosing the right compounds in the right combinations at the right time. J Inorg Biochem. 190, 98-112.

Horn D, Al-Ali H, Barrientos A. (2008). Cmc1p is a conserved mitochondrial twin CX9C protein involved in cytochrome *c* oxidase biogenesis. Mol Cell Biol. 28, 4354–4364.

Huang Z, Chen K, Zhang J, Li Y, Wang H, Cui D, Tang J, Liu Y, Shi X, Li W, Liu D, Chen R, Sucgang RS, Pan X. (2013). A functional variomics tool for discovering drug-resistance genes and drug targets. Cell Rep. 3, 577-585.

Hughes AL, Gottschling, DE. (2012). An early age increase in vacuolar pH limits mitochondrial function and lifespan in yeast. Nature. 492, 261-265.

Hughes CE, Coody TK, Jeong MY, Berg JA, Winge DR, Hughes AL. (2020). Cysteine toxicity drives age-related mitochondrial decline by altering iron homeostasis. Cell. 180, 296-310.

Ishizaki H, Spitzer M, Wildenhain J, Anastasaki C, Zeng Z, Dolma S, Shaw M, Madsen E, Gitlin J, Marais R, Tyers M, Patton EE. (2010). Combined zebrafish-yeast chemical-genetic screens reveal gene-copper-nutrition interactions that modulate melanocyte pigmentation. Dis Model Mech. 3, 639-651.

Jaksch M, Ogilvie I, Yao J, Kortenhaus G, Bresser HG, Gerbitz KD, Shoubridge EA. (2000). Mutations in SCO2 are associated with a distinct form of hypertrophic cardiomyopathy and cytochrome *c* oxidase deficiency. Hum Mol Genet. 9, 795-801.

Jaksch M, Paret C, Stucka R, Horn N, Muller-Hocker J, Horvath R, Trepesch N, Stecker G, Freisinger P, Thirion C, Müller J, Lunkwitz R, Rödel G, Shoubridge EA, Lochmüller H. (2001). Cytochrome *c* oxidase deficiency due to mutations in SCO2, encoding a mitochondrial copper-binding protein, is rescued by copper in human myoblasts. Hum Mol Genet. 10, 3025-3035.

Janke C, Magiera MM, Rathfelder N, Taxis C, Reber S, Maekawa H, Moreno-Borchart A, Doenges G, Schwob E, Schiebel E, Knop M. (2004). A versatile toolbox for PCR-based tagging of yeast genes: new fluorescent proteins, more markers and promoter substitution cassettes. Yeast. 21, 947-962.

Jensen LT, Howard WR, Strain JJ, Winge DR, Culotta VC. (1996). Enhanced effectiveness of copper ion buffering by CUP1 metallothionein compared with CRS5 metallothionein in *Saccharomyces cerevisiae*. J Biol Chem. 271, 18514-18519.

Jo WJ, Kim JH, Oh E, Jaramillo D, Holman P, Loguinov AV, Arkin AP, Nislow C, Giaever G, Vulpe CD. (2009). Novel insights into iron metabolism by integrating deletome and transcriptome analysis in an iron deficiency model of the yeast *Saccharomyces cerevisiae*. BMC Genomics. 10, 130.

Jo WJ, Loguinov A, Chang M, Wintz H, Nislow C, Arkin AP, Giaever G. Vulpe CD. (2008). Identification of genes involved in the toxic response of *Saccharomyces cerevisiae* against iron and copper overload by parallel analysis of deletion mutants. Toxicol Sci. 101, 140-151.

Jomova K, Valko M. (2011). Advances in metal-induced oxidative stress and human disease. Toxicology. 283, 65-87.

Kaler SG. (2011). ATP7A-related copper transport diseases-emerging concepts and future trends. Nat Rev Neurol. 7, 15-29.

Kaler SG. (2013). Inborn errors of copper metabolism. Handb Clin Neurol. 113, 1745-1754.

Kaler SG. (2014). Neurodevelopment and brain growth in classic Menkes disease is influenced by age and symptomatology at initiation of copper treatment. J Trace Elem Med Biol. 28, 427-430.

Kayikci Ö, Nielsen J. (2015). Glucose repression in Saccharomyces cerevisiae. FEMS Yeast Res. 15, fov068.

Kim BE, Nevitt T, Thiele DJ. (2008). Mechanisms for copper acquisition, distribution, and regulation. Nat Chem Biol. 4, 176-185.

Kirshner JR, He S, Balasubramanyam V, Kepros J, Yang CY, Zhang M, Du Z, Barsoum J, Bertin J. (2008). Elesclomol induces cancer cell apoptosis through oxidative stress. Mol Cancer Ther. 7, 2319-2327.

Knight SA, Labbé S, Kwon LF, Kosman DJ, Thiele DJ. (1996). A widespread transposable element masks expression of a yeast copper transport gene. Genes Dev. 10, 1917-1929.

Kodama H, Fujisawa C, Bhadhprasit W. (2012). Inherited copper transport disorders: biochemical mechanisms, diagnosis, and treatment. Curr Drug Metab. 13, 237-250.

Kodama H, Murata Y, Kobayashi M. (1999). Clinical manifestations and treatment of Menkes disease and its variants. Pediatr Int. 41, 423-429.

Kodama H, Okabe I, Yanagisawa M, Kodama Y. (1989). Copper deficiency in the mitochondria of cultured skin fibroblasts from patients with Menkes syndrome. J Inherit Metab Dis. 12, 386-389.

Korvatska O, Strand NS, Berndt JD, Strovas T, Chen DH, Leverenz JB, Kiianitsa K, Mata IF, Karakoc E, Greenup JL, Bonkowski E, Chuang J, Moon RT, Eichler EE, Nickerson DA, Zabetian CP, Kraemer BC, Bird TD, Raskind WH. (2013). Altered splicing of ATP6AP2 causes X-linked parkinsonism with spasticity (XPDS). Hum Mol Genet. 22, 3259-3268.

Lamb AL, Torres AS, O'Halloran TV, Rosenzweig AC. (2000). Heterodimer formation between superoxide dismutase and its copper chaperone. Biochemistry. 39, 14720-14727.

Lamb TM, Xu W, Diamond A, Mitchell AP. (2001). Alkaline response genes of *Saccharomyces cerevisiae* and their relationship to the RIM101 pathway. J Biol Chem. 276, 1850-1856.

Lasserre JP, Dautant A, Aiyar RS, Kucharczyk R, Glatigny A, Tribouillard-Tanvier D, Rytka J, Blondel M, Skoczen N, Reynier P, Pitayu L, Rötig A, Delahodde A, Steinmetz LM, Dujardin G, Procaccio V, di Rago JP. (2015). Yeast as a system for modeling mitochondrial disease mechanisms and discovering therapies. Dis Model Mech. 8, 509-526.

Leary SC, Antonicka H, Sasarman F, Weraarpachai W, Cobine PA, Pan M, Brown GK, Brown R, Majewski J, Ha KC, Rahman S, Shoubridge EA. (2013). Novel mutations in SCO1 as a cause of fatal infantile encephalopathy and lactic acidosis. Hum Mutat. 34, 1366-1370.

Leary SC, Sasarman F, Nishimura T, Shoubridge EA. (2009). Human SCO2 is required for the synthesis of COXII and as a thiol-disulphide oxidoreductase for SCO1. Hum Mol Genet. 18, 2230-2240.

Lee JH, Yu WH, Kumar A, Lee S, Mohan PS, Peterhoff CM, Wolfe DM, Martinez-Vicente M, Massey AC, Sovak G, Uchiyama Y, Westaway D, Cuervo AM,

Nixon RA. (2010). Lysosomal proteolysis and autophagy require presenilin 1 and are disrupted by Alzheimer-related PS1 mutations. Cell. 141, 1146-1158.

Li L, Vulpe CD, Kaplan J. (2003). Functional studies of hephaestin in yeast: evidence for multicopper oxidase activity in the endocytic pathway. Biochem J. 375, 793-798.

Lin SJ, Culotta VC. (1995). The ATX1 gene of *Saccharomyces cerevisiae* encodes a small metal homeostasis factor that protects cells against reactive oxygen toxicity. Proc Natl Acad Sci USA. 92, 3784-3788.

Lin SJ, Pufahl RA, Dancis A, O'Halloran TV, Culotta VC. (1997). A role for the *Saccharomyces cerevisiae* ATX1 gene in copper trafficking and iron transport. J Biol Chem. 272, 9215-9220.

Little AG, Lau G, Mathers KE, Leary SC, Moyes CD. (2018). Comparative biochemistry of cytochrome *c* oxidase in animals. Comp Biochem Physiol B Biochem Mol Biol. 224, 170-184.

Llinares E, Barry AO, Andre B. (2015). The AP-3 adaptor complex mediates sorting of yeast and mammalian PQ-loop-family basic amino acid transporters to the vacuolar/lysosomal membrane. Sci Rep. 5, 16665.

Maeda, T. (2012) The signaling mechanism of ambient pH sensing and adaptation in yeast and fungi. FEBS J. 279, 1407-1413.

Maehara M, Ogasawara N, Mizutani N, Watanabe K, Suzuki S. (1983). Cytochrome *c* oxidase deficiency in Menkes kinky hair disease. Brain Dev. 5, 533-540.

Maghool S, La Fontaine S, Roberts BR, Kwan AH, Maher MJ. (2020). Human glutaredoxin-1 can transfer copper to isolated metal binding domains of the P_{1B}-type ATPase, ATP7B. Sci Rep. 10, 4157.

Maréchal A, Meunier B, Lee D, Orengo C, Rich PR. (2012). Yeast cytochrome *c* oxidase: a model system to study mitochondrial forms of the haem-copper oxidase superfamily. Biochim Biophys Acta. 1817, 620-628.

Meisinger C, Pfanner N, Truscott KN. (2006). Isolation of yeast mitochondria. Methods Mol Biol. 313, 33-39.

Mercer JF, Livingston J, Hall B, Paynter JA, Begy C, Chandrasekharappa S, Lockhart P, Grimes A, Bhave M, Siemieniak D, Glover TW. (1993). Isolation of a partial candidate gene for Menkes disease by positional cloning. Nat Genet. 3, 20-25.

Merz S, Westermann B. (2009). Genome-wide deletion mutant analysis reveals genes required for respiratory growth, mitochondrial genome maintenance and mitochondrial protein synthesis in *Saccharomyces cerevisiae*. Genome Biol. 10, R95.

Monty JF, Llanos RM, Mercer JF, Kramer DR. (2005). Copper exposure induces trafficking of the menkes protein in intestinal epithelium of ATP7A transgenic mice. J Nutr. 135, 2762-2766.

Mulligan C, Bronstein JM. (2020). Wilson disease: an overview and approach to management. Neurol Clin. 38, 417-432.

Nagai M, Vo NH, Shin Ogawa L, Chimmanamada D, Inoue T, Chu J, Beaudette-Zlatanova BC, Lu R, Blackman RK, Barsoum J, Koya K, Wada Y. (2012). The oncology drug elesclomol selectively transports copper to the mitochondria to induce oxidative stress in cancer cells. Free Radic Biol Med. 52, 2142-2150.

Nevitt T, Ohrvik H, Thiele DJ. (2012). Charting the travels of copper in eukaryotes from yeast to mammals. Biochim Biophys Acta. 1823, 1580-1593.

Nguyen M, Wong YC, Ysselstein D, Severino A, Krainc D. (2019). Synaptic, mitochondrial, and lysosomal dysfunction in parkinson's disease. Trends Neurosci. 42, 140-149.

Nguyen TQ, Dziuba N, Lindahl PA. (2019). Isolated *Saccharomyces cerevisiae* vacuoles contain low-molecular-mass transition-metal polyphosphate complexes. Metallomics. 11, 1298-1309.

Nixon RA, Yang DS, Lee JH. (2008). Neurodegenerative lysosomal disorders: a continuum from development to late age. Autophagy. 4, 590-599.

Nose Y, Kim BE, Thiele DJ. (2006). Ctr1 drives intestinal copper absorption and is essential for growth, iron metabolism, and neonatal cardiac function. Cell Metab. 4, 235-244.

O'Day S, Gonzalez R, Lawson D, Weber R, Hutchins L, Anderson C, Haddad J, Kong S, Williams A, Jacobson E. (2009). Phase II, randomized, controlled, double-blinded trial of weekly elesclomol plus paclitaxel versus paclitaxel alone for stage IV metastatic melanoma. J Clin Oncol. 27, 5452-5458.

O'Day SJ, Eggermont AM, Chiarion-Sileni V, Kefford R, Grob JJ, Mortier L, Robert C, Schachter J, Testori A, Mackiewicz J, Friedlander P, Garbe C, Ugurel S, Collichio F, Guo W, Lufkin J, Bahcall S, Vukovic V, Hauschild A. (2013). Final

results of phase III SYMMETRY study: randomized, double-blind trial of elesclomol plus paclitaxel versus paclitaxel alone as treatment for chemotherapy-naive patients with advanced melanoma. J Clin Oncol. 31, 1211-1218.

Ohya Y, Umemoto N, Tanida I, Ohta A, Iida H, Anraku Y. (1991). Calcium-sensitive cls mutants of *Saccharomyces cerevisiae* showing a Pet- phenotype are ascribable to defects of vacuolar membrane H(+)-ATPase activity. J Biol Chem. 266, 13971-13977.

Orij R, Urbanus ML, Vizeacoumar FJ, Giaever G, Boone C, Nislow C, Brul S, Smits GJ. (2012). Genome-wide analysis of intracellular pH reveals quantitative control of cell division rate by pH(c) in *Saccharomyces cerevisiae*. Genome Biol. 13, R80.

Pan X, Yuan DS, Xiang D, Wang X, Sookhai-Mahadeo S, Bader JS, Hieter P, Spencer F, Boeke JD. (2004). A robust toolkit for functional profiling of the yeast genome. Mol Cell. 16, 487-496.

Papadopoulou LC, Sue CM, Davidson MM, Tanji K, Nishino I, Sadlock JE, Krishna S, Walker W, Selby J, Glerum DM, Coster RV, Lyon G, Scalais E, Lebel R, Kaplan P, Shanske S, De Vivo DC, Bonilla E, Hirano M, DiMauro S, Schon EA. (1999). Fatal infantile cardioencephalomyopathy with COX deficiency and mutations in SCO2, a COX assembly gene. Nat Genet. 23, 333-337.

Peña MM, Lee J, Thiele DJ. (1999). A delicate balance: homeostatic control of copper uptake and distribution. J Nutr. 129, 1251-1260.

Peña MM, Puig S, Thiele DJ. (2000). Characterization of the *Saccharomyces cerevisiae* high affinity copper transporter Ctr3. J Biol Chem. 275, 33244-33255.

Pérez-Sampietro M, Herrero E. (2014). The PacC-family protein Rim101 prevents selenite toxicity in *Saccharomyces cerevisiae* by controlling vacuolar acidification. Fungal Genet Biol. 71, 26-85.

Polishchuck EV, Polishchuk RS. (2016). The emerging role of lysosomes in copper homeostasis. Metallomics. 8, 853-863.

Pope CR, De Feo CJ, Unger VM. (2013). Cellular distribution of copper to superoxide dismutase involves scaffolding by membranes. Proc Natl Acad Sci USA. 110, 20491-20496.

Portnoy ME, Schmidt PJ, Rogers RS, Culotta VC. (2001). Metal transporters that contribute copper to metallochaperones in *Saccharomyces cerevisiae*. Mol Genet Genomics. 265, 873-882.

Prohaska JR. (2008). Role of copper transporters in copper homeostasis. Am J Clin Nutr, 88, 826S–829S.

Rae TD, Schmidt PJ, Pufahl RA, Culotta VC, O'Halloran TV. (1999). Undetectable intracellular free copper: the requirement of a copper chaperone for superoxide dismutase. Science. 284, 805-808.

Read T, Richmond PA, Dowell RD. (2016). A trans-acting variant within the transcription factor Rim101 interacts with genetic background to determine its regulatory capacity. PLoS Genet. 12, e1005746.

Rees EM, Lee J, Thiele DJ. (2004). Mobilization of intracellular copper stores by the ctr2 vacuolar copper transporter. J Biol Chem. 279, 54221-54229.

Rees EM, Thiele DJ. (2007). Identification of a vacuole associated metalloreductase and its role in Ctr2-mediated intracellular copper mobilization. J Biol Chem. 282, 21629-21638.

Rigo A, Corazza A, di Paolo ML, Rossetto M, Ugolini R, Scarpa M. (2004). Interaction of copper with cysteine: stability of cuprous complexes and catalytic role of cupric ions in anaerobic thiol oxidation. J Inorg Biochem. 98, 1495-1501.

Robinson NJ, Winge DR. (2010). Copper metallochaperones. Annu Rev Biochem. 79, 537-562

Schlecht U, Suresh S, Xu W, Aparicio AM, Chu A, Proctor MJ, Davis RW, Scharfe C, St Onge RP. (2014). A functional screen for copper homeostasis genes identifies a pharmacologically tractable cellular system. BMC Genomics. 15, 263.

Serrano R, Bernal D, Simón E, Ariño J. (2004). Copper and iron are the limiting factors for growth of the yeast *Saccharomyces cerevisiae* in an alkaline environment. J Biol Chem. 279, 19698-19704.

Setty SRG, Tenza D, Sviderskaya EV, Bennett DC, Raposo G, Marks MS. (2008). Cell-specific ATP7A transport sustains copper-dependent tyrosinase activity in melanosomes. Nature. 454, 1142-1146.

Shoubridge EA. (2001). Cytochrome *c* oxidase deficiency. Am J Med Genet. 106, 46-52.

Smith AM, Heisler LE, Mellor J, Kaper F, Thompson MJ, Chee M, Roth FP, Giaever G, Nislow C. (2009). Quantitative phenotyping via deep barcode sequencing. Genome Res. 19, 1836-1842.

Soma S, Latimer AJ, Chun H, Vicary AC, Timbalia SA, Boulet A, Rahn JJ, Chan SSL, Leary SC, Kim BE, Gitlin JD, Gohil VM. (2018). Elesclomol restores mitochondrial function in genetic models of copper deficiency. Proc Natl Acad Sci USA. 115, 8161-8166.

Soma S, Morgada MN, Naik MT, Boulet A, Roesler AA, Dziuba N, Ghosh A, Yu Q, Lindahl PA, Ames JB, Leary SC, Vila AJ, Gohil VM. (2019). COA6 is structurally tuned to function as a thiol-disulfide oxidoreductase in copper delivery to mitochondrial cytochrome *c* oxidase. Cell Rep. 29, 4114-4126.

Soto, IC, Fontanesi F, Liu, J, Barrientos, A. (2012). Biogenesis and assembly of eukaryotic cytochrome *c* oxidase catalytic core. Biochim Biophys Acta. 1817, 883-897.

Spinazzi M, Casarin A, Pertegato V, Salviati L, Angelini C. (2012). Assessment of mitochondrial respiratory chain enzymatic activities on tissues and cultured cells. Nat Protoc. 7, 1235-1246.

Stearman R, Yuan DS, Yamaguchi-Iwai Y, Klausner RD, Dancis A. (1996). A permease-oxidase complex involved in high-affinity iron uptake in yeast. Science. 271, 1552-1557.

Stenger M, Le DT, Klecker T, Westermann B. (2020). Systematic analysis of nuclear gene function in respiratory growth and expression of the mitochondrial genome in *S. cerevisiae*. Microb Cell. 7, 234-249.

Stepien KM, Roncaroli F, Turton N, Hendriksz CJ, Roberts M, Heaton RA, Hargreaves I. (2020). Mechanism of mitochondrial dysfunction in lysosomal storage disorders: a review. J Clin Med. 9, 2596.

Taylor AB, Stoj CS, Ziegler L, Kosman DJ, Hart PJ. (2005). The copper-iron connection in biology: structure of the metallo-oxidase Fet3p. Proc Natl Acad Sci USA. 102, 15459-15464.

Timón-Gómez A, Nývltová E, Abriata LA, Vila AJ, Hosler J, Barrientos A. (2018). Mitochondrial cytochrome *c* oxidase biogenesis: Recent developments. Semin Cell Dev Biol. 76, 163-178.

Tsukihara T, Aoyama H, Yamashita E, Tomizaki T, Yamaguchi H, Shinzawa-Itoh K, Nakashima R, Yaono R, Yoshikawa S. (1995). Structures of metal sites of oxidized bovine heart cytochrome *c* oxidase at 2.8 A. Science. 269, 1069-1074.

Tümer Z, Møller LB. (2010). Menkes disease. Eur J Hum Genet. 18, 511–518.

Valnot I, Osmond S, Gigarel N, Mehaye B, Amiel J, Cormier-Daire V, Munnich A, Bonnefont JP, Rustin P, Rötig A. (2000). Mutations of the SCO1 gene in mitochondrial cytochrome *c* oxidase deficiency with neonatal-onset hepatic failure and encephalopathy. Am J Hum Genet. 67, 1104-1109.

Vashchenko G, MacGillivray RT. (2013). Multi-copper oxidases and human iron metabolism. Nutrients. 5, 2289-2313.

Vest KE, Leary SC, Winge DR, Cobine PA. (2013). Copper import into the mitochondrial matrix in *Saccharomyces cerevisiae* is mediated by Pic2, a mitochondrial carrier family protein. J Biol Chem. 288, 23884-23892.

Vest KE, Wang J, Gammon MG, Maynard MK, White OL, Cobine JA, Mahone WK, Cobine PA. (2016). Overlap of copper and iron uptake systems in mitochondria in *Saccharomyces cerevisiae*. Open Biol. 6, 150223.

Vögtle FN, Burkhart JM, Gonczarowska-Jorge, H, Kücükköse C, Taskin AA, Kopczynski D, Ahrends R, Mossmann D, Sickmann A, Zahedi RP, Meisinger C. (2017). Landscape of submitochondrial protein distribution. Nat Commun. 8, 290.

Voskoboinik I, Strausak D, Greenough M, Brooks H, Smith S, Mercer JF, Camakaris J. (1999). Functional analysis of the N-terminal CXXC metal-binding motifs in the human Menkes copper-transporting P-type ATPase expressed in cultured mammalian cells. J Biol Chem. 274, 22008-22012.

Vulpe C, Levinson B, Whitney S, Packman S, Gitschier J. (1993). Isolation of a candidate gene for Menkes disease and evidence that it encodes a copper-transporting ATPase. Nat Genet. 3, 7-13.

Weber RA, Yen FS, Nicholson SPV, Alwaseem H, Bayraktar EC, Alam M, Timson RC, La K, Abu-Remaileh M, Molina H, Birsoy K. (2020). Maintaining iron homeostasis is the key role of lysosomal acidity for cell proliferation. Mol Cell. 7, 645-655.

Winge DR, Nielson KB, Gray WR, Hamer DH. (1985). Yeast metallothionein. Sequence and metal-binding properties. J Biol Chem. 260, 14464-14470.

Wu L, Zhou L, Liu D Q, Vogt FG, Kord AS. (2011). LC-MS/MS and density functional theory study of copper(II) and nickel(II) chelating complexes of elesclomol (a novel anticancer agent). J Pharm Biomed Anal. 54, 331-336.

Wu X, Kim H, Seravalli J, Barycki JJ, Hart PJ, Gohara DW, Di Cera E, Jung WH, Kosman DJ, Lee J. (2016). Potassium and the K+/H+ exchanger kha1p promote binding of copper to apoFet3p multi-copper ferroxidase. J Biol Chem. 291, 9796-9806.

Xu W, Smith FJ, Subaran R, Mitchell AP. (2004). Multivesicular body-ESCRT components function in pH response regulation in *Saccharomyces cerevisiae* and *Candida albicans*. Mol Biol Cell. 15, 5528-5537.

Yadav AA, Patel D, Wu X, Hasinoff BB. (2013). Molecular mechanisms of the biological activity of the anticancer drug elesclomol and its complexes with Cu(II), Ni(II) and Pt(II). J Inorg Biochem. 126, 1-6.

Yambire KF, Rostosky C, Watanabe T, Pacheu-Grau D, Torres-Odio S, Sanchez-Guerrero A, Senderovich O, Meyron-Holtz EG, Milosevic I, Frahm J, West AP, Raimundo N. (2019). Impaired lysosomal acidification triggers iron deficiency and inflammation *in vivo*. Elife 8, e51031.

Yuan, DS, Dancis A, Klausner RD. (1997). Restriction of copper export in *Saccharomyces cerevisiae* to a late Golgi or post-Golgi compartment in the secretory pathway. J Biol Chem. 272, 25787-25793.

Yun CW, Bauler M, Moore RE, Klebba PE, Philpott CC. (2001). The role of the FRE family of plasma membrane reductases in the uptake of siderophore-iron in *Saccharomyces cerevisiae*. J Biol Chem. 276, 10218-10223.

Zulkifli M, Neff JK, Timbalia SA, Garza NM, Chen Y, Watrous JD, Murgia M, Trivedi PP, Anderson SK, Tomar D, Nilsson R, Madesh M, Jain M, Gohil VM. (2020). Yeast homologs of human MCUR1 regulate mitochondrial proline metabolism. Nat Commun. 11, 4866.

APPENDIX A

YEAST HOMOLOGS OF HUMAN MCUR1 REGULATE MITOCHONDRIAL

PROLINE METABOLISM*

I am a co-author in this work that was published in the journal *Nature Communications* (Zulkifli et al., 2020). In this project, I aided in the discovery that yeast proteins Put6 and Put7 are regulators of mitochondrial proline metabolism. I performed growth assays and enzyme assays utilizing the *PUT6* and *PUT7* yeast deletion strains. Specifically, I performed growth assays using 21 different nitrogen sources to uncover a proline-specific growth defect of *put6Δ* and *put7Δ* mutants (Figure A.1). I also developed a protocol for measuring aconitase activity to show that in the absence of Put6 and Put7, mitochondria exhibit enhanced oxidative stress (Figure A.2).

_____

* Reprinted from "Yeast homologs of human MCUR1 regulate mitochondrial proline metabolism." By Zulkifli M, Neff JK, Timbalia SA, Garza NM, Chen Y, Watrous JD, Murgia M, Trivedi PP, Anderson SK, Tomar D, Nilsson R, Madesh M, Jain M, Gohil VM. 2020. *Nat Commun*. 11:4866.
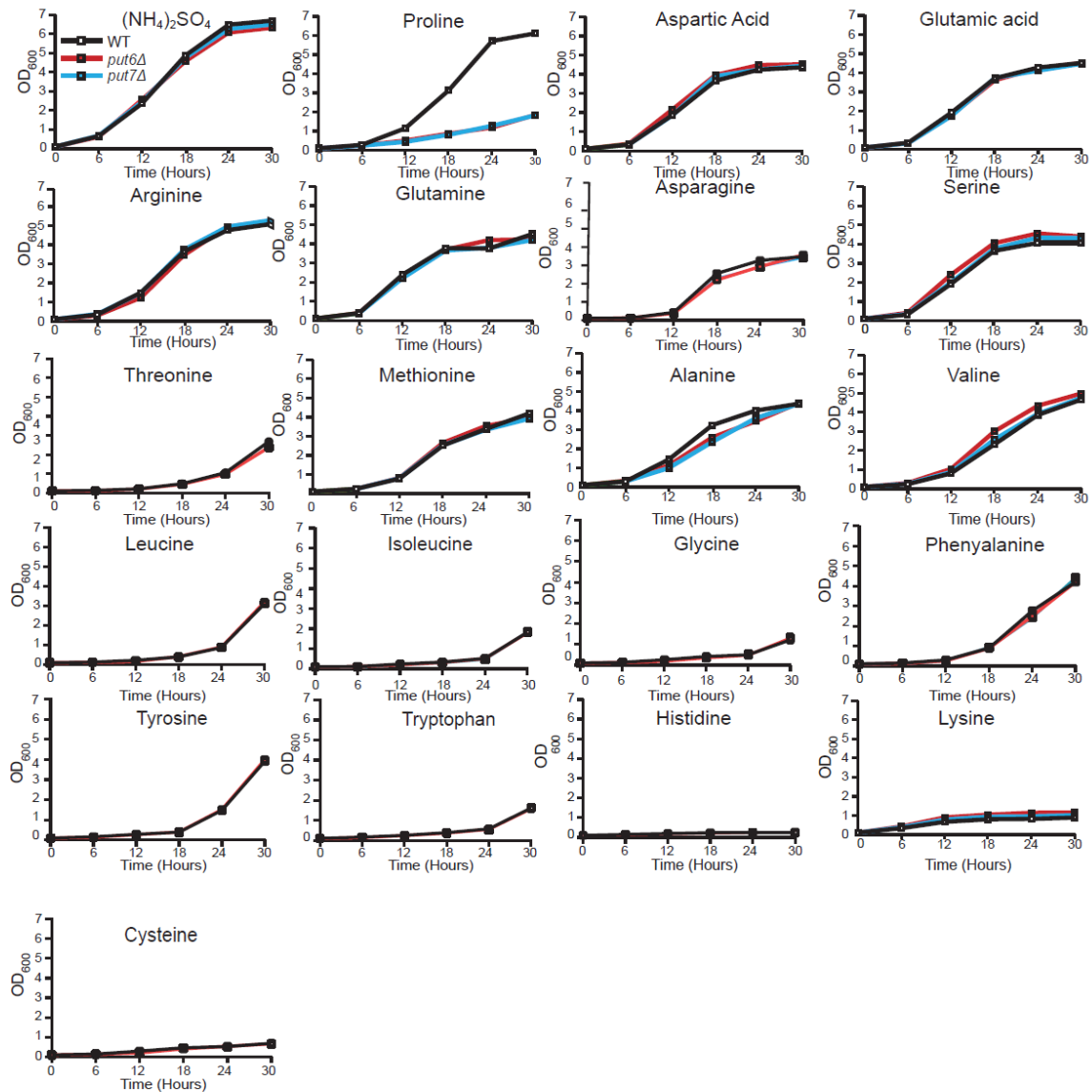
Figure A.1 Put6 and Put7 are specifically required for growth in proline

A) Prototrophic WT, *put6Δ*, and *put7Δ* yeast cells were cultured at 30°C in synthetic liquid media containing the indicated amino acids as the sole nitrogen source and galactose as the carbon source. Growth was monitored by measuring absorbance at 600 nm at the indicated time intervals. Ammonium sulfate was used as the most favored nitrogen source. (This figure adapted from Zulkifli et al., 2020).
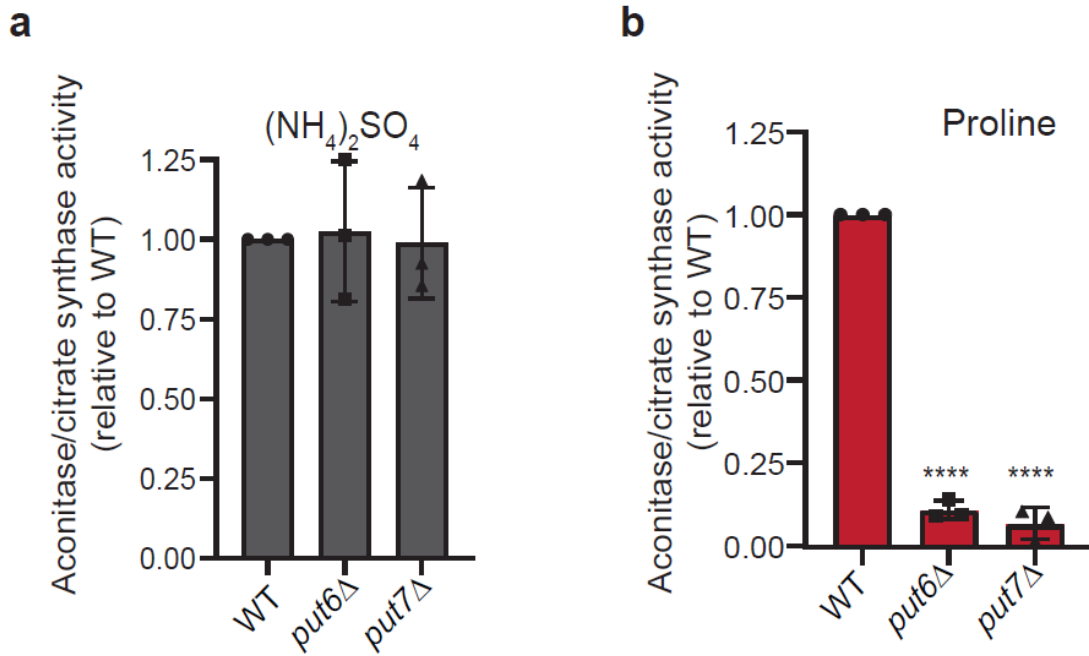
Figure A.2 Loss of Put6 and Put7 perturbs cellular redox homeostasis
Aconitase activity in isolated mitochondria from WT, *put6Δ*, and *put7Δ* yeast cells. Aconitase activity was normalized to citrate synthase activity and is expressed as mean ± SD relative to WT (n = 3 biologically independent experiments), p < 0.0001. (This figure adapted from Zulkifli et al., 2020).